Chair of Metal Forming

Department Product Engineering,

University of Leoben, Austria

DISSERTATION

Investigation of Friction in Closed-Die Warm Forging of Aluminium Alloys

A thesis submitted to the University of Leoben
in partial fulfillment of the requirements for the degree of
Doktor der Montanistischen Wissenschaften

Bernhard Buchner

January, 2008

Affidavit

I declare in lieu of oath, that I wrote this thesis and performed the associated research myself, using only literature cited in this volume.

Leoben, January 28th, 2008 Bernhard Buchner

Acknowledgements

First of all, I would like to thank my supervisor, Prof. Bruno Buchmayr for his support and his confidence in me and my work and Prof. Wilfried Eichlseder for the appraisal of this thesis.

Further I would like to thank the Chair of Metal Forming for letting me be a part of it's community. In countless entertaining talks and discussions I got new insights and found new friends. My thanks are especially aimed to Otto Harrer for proof-reading this work and Thomas Hatzenbichler, his technical advise in numerical simulation were an invaluable help during the work.

Special thanks are also owed to my scientific assistants Karl Markut, Gerhard Maderthoner, Andreas Umgeher and Andreas Weber. With their work, they considerably contributed to the success of this thesis. Furthermore, the technical assistance received from Andreas Berr and Ralph Ambrosch is highly appreciated.

I wish to express my gratitude to my wife and colleague Michaela Buchner for her love and patience during periods of hard work. I appreciate her emotional support and for lots of fruitful discussions inspiring me.

Moreover, I would like to thank my father, Gerhard Buchner, for his confidence and support in all my life. Further, I would like to thank all other members of my family, my friends and colleagues and all people that remain unnamed but contributed to where I stand now.

This work was made possible by the financial support from the federal province of Styria ("Zukunftsfonds Steiermark", Project 19) and the funding I received from Fuchs Schmiermittel GmbH.

Further I want to thank Lenze Antriebstechnik GmbH, Böhler Edelstahl GmbH and Rockmore International Inc. for the provision of materials and contributions in kind and Fuchs Schmiermittel GmbH and Acheson Industries for the provision of the lubricants.

Finally, I want to thank the Chair of Mechanical Engineering at the University of Leoben for the provision of the confocal laser scanning microscope.

Abstract

Aluminium forged parts play a significant role as components of light weight constructions in the automotive and aerospace industry. The fundamental knowledge of the friction behaviour at the tool-workpiece interface is necessary due to the fact, that it influences material flow, die filling, wear and workpiece quality.
In order to understand the tribological processes and interactions in the tool-workpiece interface systematically, basic experiments that allow an independent variation of influencing parameters are necessary. This thesis presents an investigation of friction in hot forging of aluminium by employing a modified ring-on-disc test. The experiments were performed with commercial graphite-based lubricants and at various loads, sliding velocities and specimen surface conditions. In addition, some tests were performed without lubrication. It was found, that dry sliding conditions result in sticking and – at low normal loads – in galling at the die-workpiece interface. Micrographs confirmed that at dry friction (most of) the relative motion was done by shearing in subsurface layers of the workpiece. When employing lubricants, the shearing was restricted to the graphite layer. In dependence on the used product and the normal load, the friction coefficients varied within narrow limits from 0.01 to 0.11. Generally, the friction coefficient decreased with increasing normal pressure at all investigated lubricants. In the observed range, the sliding velocity had no significant influence on the tests. However, the scatter of the friction coefficients at various velocities got smaller with increasing normal pressures. The results were compared to the results of a study employing a pin-on-disc test for lubricant evaluation, and good qualitative agreement was found in terms of friction coefficient and friction evolution during the tests.
In accurate finite element analysis, friction has to be faced by numerical models that consider the real conditions at the die-workpiece interface. In this context, physical approaches based on a contact model (for the determination of the real contact area) and a local friction law (applied to the real contact spots) allow the formulation of friction models that take the complexity of the tribosystem into consideration. This thesis presents a new contact model that takes the material properties and real asperity shapes into consideration, and simplification is achieved by making use of the statistical character of real surfaces. The main idea of the new concept was to obtain the real contact area-load relation by combining the bearing area curve and a model asperity with correct representation of the mean asperity slope. Experiments with aluminium specimens showed excellent correspondence with the numerical results.

Kurzfassung

Geschmiedete Aluminiumteile spielen als Leichtbaukomponenten eine wichtige Rolle in der Automobil-, Luft- und Raumfahrtindustrie. Ein Verständnis der Reibung in der Wirkfläche zwischen Werkzeug und Schmiedestück ist unerlässlich, da sie den Materialfluss, die Gravurfüllung, den Verschleiß und die Werkstückqualität beeinflusst.
Um die tribologischen Prozesse und Wechselwirkungen in der Wirkfläche systematisch untersuchen zu können, sind Experimente nötig, die eine unabhängige Variation der beeinflussenden Parameter erlauben. Diese Arbeit beschreibt die Untersuchung der Reibung beim Warmschmieden von Aluminium mittels eines modifizierten Ring-auf-Scheibe Versuchs. Die Versuche werden ohne Schmiermittel und mit kommerziellen grafithältigen Schmierstoffen bei unterschiedlichen Drücken, Geschwindigkeiten und Oberflächenzuständen durchgeführt. Die Ergebnisse zeigen, dass trockene Reibung zu Haften und – bei niedrigen Normalspannungen – zu starkem Materialübertrag führt. Metallographische Untersuchungen bestätigen, dass im Falle trockener Reibung die Relativbewegung (zum größten Teil) durch Abscherung im Inneren des Werkstückes erfolgt. Bei der Verwendung von Schmierstoffen hingegen bleibt die Scherung auf die Grafitschicht beschränkt. In Abhängigkeit des verwendeten Produktes und der Normalspannung variiert die Reibzahl innerhalb enger Grenzen von 0,01 bis 0,11. Grundsätzlich verringert sich bei allen getesteten Schmiermitteln die Reibzahl mit zunehmender Normalspannung. Die Reibgeschwindigkeit hat hingegen keinen signifikanten Einfluss auf die Ergebnisse. Allerdings kann mit steigender Normalspannung eine Abnahme der Streuung der Reibzahl bei unterschiedlichen Geschwindigkeiten beobachtet werden. Die Ergebnisse werden mit den Resultaten einer Untersuchung verglichen, die unterschiedliche Schmierstoffe mithilfe eines Stift-auf-Scheibe Versuchs charakterisiert, wobei eine gute qualitative Übereinstimmung in Bezug auf Reibzahl und Reibzahlverlauf festzustellen ist.
In Finite-Elemente Analysen wird die Reibung mithilfe numerischer Modelle berücksichtigt, die die realen Vorgänge in der Wirkfläche in Betracht ziehen. Eine Möglichkeit stellen hier physikalische Ansätze dar, die auf einem Kontaktmodell in Kombination mit einem lokalen Reibmodell basieren. Diese Arbeit stellt ein neues Kontaktmodell vor, das die Werkstoffeigenschaften und die Oberflächenstruktur berücksichtigt und Vereinfachungen aufgrund des statistischen Charakters von Oberflächen vornimmt. Die wahre Kontaktfläche wird durch die Kombination der Tragprofilkurve mit einer Modellrauheit in Abhängigkeit der Normalspannung bestimmt. Versuche mit Aluminiumproben zeigten eine exzellente Übereinstimmung mit numerischen Ergebnissen.

Contents

List of Symbols

symbol	unit	comment
A_a	µm^2	apparent contact area
A_b	µm^2	bearing area
A_r	µm^2	real contact area
a_j	%	contact area of bearing area curve and tool
α	1	relative contact area
b_j	%	contact area of Hansen profile and tool
β	°	asperity slope
$\overline{\beta}$	°	mean asperity slope
d_I	mm	inner diameter of the ring-shaped tool
d_O	mm	outer diameter of the ring-shaped tool
E	GPa	Young's modulus
F	N	force
F_n	N	normal force
F_f	N	friction force
F_H	N	force necessary to deform the Hansen profile
F_s	N	force supported by the load sensor
F_t	N	total force
f	Hz	sampling rate
γ	°	slope of the regression line
h	µm	height of a (deformed) asperity
$h_{a,i}$	µm	distance between actual and mean profile at increment i
h_f	µm	final height of a deformed asperity
i	1	control variable
j	1	control variable
φ	1	true strain
$\dot{\varphi}$	1/s	strain rate
k	MPa	shear yield stress
k_f	MPa	yield stress
l	µm	reference distance for surface characterisation
l_t	µm	bearing length
l_0	µm	base length of an undeformed asperity
l_1	µm	base length of a deformed asperity
m	1	shear factor (friction factor)

symbol	unit	comment
μ	1	friction coefficient
$\overline{\mu}$	1	mean friction coefficient (one measurement)
$\overline{\mu}_m$	1	mean friction coefficient (several measurements)
n	1	free variable
pfc	1	progression of regression line
p_l	MPa	pressure in entrapped lubricant
π	1	circular constant
R_a	µm	arithmetical mean height
R_p	µm	peak-to-mean-line height
R_t	µm	total profile height (peak-to-valley height)
R_z	µm	averaged peak-to-valley height
r	µm	radius of the base of a cone-shaped asperity
r_{cs}	µm	radius of a contact spot
r_x	µm	radius of a cone-shaped asperity at stroke x
r_{su}	µm	radius of curvature of summit
Δr	µm	change of radius at stroke x due to volume constancy
ρ_{rel}	1	relative density of porous lubricant
σ	1	standard deviation
σ_n	MPa	normal stress
$\sigma_{n,t}$	MPa	normal stress in the tool
$\sigma_{n,w}$	MPa	normal stress in the workpiece
$\sigma_{n,i}$	MPa	normal stress at increment i
$\overline{\sigma}_n$	MPa	mean normal stress (one measurement)
$\overline{\sigma}_{n,m}$	MPa	mean normal stress (several measurements)
σ'_n	MPa	normal stress at the limit of proportionality
T	Nm	torque
t_b	s	time at the begin of the stationary region
t_e	s	time at the end of the stationary region
t_p	%	profile bearing fraction
τ_I	MPa	flow strength of an interface layer
τ_f	MPa	friction stress
$\tau_{f,i}$	MPa	friction stress at increment i
$\overline{\tau}_f$	MPa	mean friction stress (one measurement)
$\overline{\tau}_{f,m}$	MPa	mean friction stress (several measurements)

symbol	unit	comment
τ'_f	MPa	friction stress at the limit of proportionality
u	1	maximum value of i
V_a	µm^3	volume of an asperity
$V_{a,d}$	µm^3	volume of a deformed asperity
V_f	µm^3	final total volume (asperity and lubricant)
$V_{l,in}$	µm^3	initial volume of a porous lubricant
$V_{l,f}$	µm^3	final volume of a porous lubricant
v	mm/s	velocity
v_i	mm/s	velocity at increment i
$\overline{v}_i$	mm/s	mean velocity at increment i (several measurements)
v_{ref}	mm/s	reference velocity
w	1	maximum value of j
x	µm	(horizontal) coordinate
x_f	mm	distance from center of rotation to contact area
x_s	mm	distance from center of rotation to load sensor
$\mathbf{x}$	-	vector of coordinate points $\{x_1 \dots x_?\}$
y	µm	(vertical) coordinate
$\mathbf{y}$	-	vector of coordinate points $\{y_1 \dots y_?\}$
y(j)	µm	height at section j
$y_{p,i}$	µm	distance between actual and reference profile at increment i

1 Introduction

1.1 Motivation of the Work

Aluminium is characterised by its low specific weight and its corrosion resistance. As a result of the general tendency to light weight constructions, aluminium alloys became important construction materials not only in aerospace applications but also in the automotive industry. Due to their ability to achieve high strength with certain alloying additions, aluminium alloys are not only used for shell elements but are also applied for structural, safety relevant components. For example, special alloys have been developed for high temperature applications as for aircraft engine elements. Due to the desired mechanical properties of such highly loaded components, these parts are typically manufactured by impression-die forging.

Because of global competition, the forging industry is confronted on the one hand with short product life cycles and on the other hand with higher demands on the product quality [1]. Due to cost pressure, increasing complexity of forgings and the demand on near-net-shape operations, the claims on forging processes are rising [2]. The application of modern computer technologies provides rapid, cost effective and proven methods to face these demands. In this context, the numerical simulation of forging processes plays a significant role as it allows an adequate optimisation of tool and workpiece, the design of safe and stable processes, the elimination of forging defects and the avoidance of premature tool-failure by an optimisation of the process parameters. Thus, the application of numerical simulation techniques provides an opportunity to substitute extensive and costly test series on real components. Commonly, the numerical simulation of forging processes aims in the determination of the material flow, the stress- and temperature distribution in the workpiece, the loads acting on the dies and of forging defects. Moreover, in some cases, it is possible to predict the microstructure and the properties of forgings [1].

However, the quality of the simulation depends on the accuracy of the input parameters (i.e. the material laws and the boundary conditions) and on the calculation method [3, 4]. The main parameters influencing forging processes are the flow curves of the specimen material, the heat transfer at the contact area and the friction in the die-workpiece interface [5–7]. The exact knowledge of the latter is paid much attention to as it affects power requirements, material flow, die filling, tool life and workpiece quality. Interface friction is taken into consideration in numerical simulation on the basis of friction models whose parameters have to be determined experimentally under similar conditions as those present in the real process. The main problem in the research area of forging and friction

is the provision of reliable material models and process data for numerical methods for forging simulations [8, 9].

1.2 State of the Art

Up to now, friction is considered in finite-element codes commonly in terms of simple, classical friction models as Amontons' friction law or the constant shear factor model. The corresponding friction coefficients or shear factors are identified by comparing the results of physical experiments with the results of equivalent numerical simulations. This is, the finite element analysis are calibrated to the real processes: The friction coefficients or shear factors loose their physical meaning and act as regulating quantities compensating all uncertainties of the numerical model [10, 11]. Of course, this approach is admissible in engineering practice, but it does not allow the detailed investigation of the tribological interactions in the tool-workpiece interface.

1.3 Tasks and Objectives

Until now, the interface friction in warm aluminium forging was only studied by means of the popular ring-compression test, where most of the parameters cannot be controlled independently from each other, and no stationary state is present. In contrast, the ring-on-disc test, where a ring-shaped tool is pressed against a flat specimen in relative motion around the ring's axis, allows an independent variation of interface pressure, relative velocity and movement. Thus, the first objective of this work was to utilise the ring-on-disc test for the estimation of friction under aluminium forging conditions and to design a cost-effective prototype machine to clarify the technical feasibility.
After verifying the applicability of the new device in examining friction at hot aluminium forging processes, the influence of the load collective and the surface conditions on friction had to be investigated systematically. The experiments had to be performed using a standard forging alloy for the automotive industry.
Finally, based on a physical approach, a new procedure to friction modeling under aluminium warm forging conditions should be developed. In contrast to present approaches, real materials and surface conditions should be considered by making use of finite element analysis, and simplification should be achieved by making use of statistical methods. However, the new model had to cope with the influence of a solid lubricant.

2 Tribological Background

2.1 Definitions

The German standard DIN 50 323-1 [12] defines *tribology*[1] as the science and technique of interacting surfaces in relative motion. It includes the complete area of friction, wear and lubrication. In addition to that, it contains the interactions at the interfaces between solid bodies as well as at the interfaces of solid bodies and fluids or gases. Tribology is an international established collective term for all questions of research and practical use in the technical areas of friction, lubrication and wear [14–17].

Tribological loads are defined as loads characterised by relative movement and interactions of surfaces under the influence of forces [12], and *tribological systems* (or *tribosystems*) are defined as the entirety of all material components and their properties as well as the characteristic processes and parameters participating in a tribological load [12, 18]; see Figure 2.1.

The bodies and media directly involved in the process are considered as the *elements* of the tribological system. With their tribological relevant properties they build the *structure* of the tribological system. The main tribological parameters of base- and counter body are their surface conditions, their chemical composition and their material properties. The chemical composition and the physical state of the intermediate layer (e.g. the lubricant) are decisive for the friction condition of the system, and the surrounding medium affects the system due to its chemical reactivity with the other elements [16].

The loads acting on the system are denoted as the *load collective*. This collective is composed of the normal force, the relative velocity, the temperatures of bodies and surrounding medium and the loading period.

In the analysis of tribological processes, the components of the tribosystem may not be regarded independently, but all parameters have to be considered in interrelation. The whole system can be strongly influenced by the change of just one of these components [14].

Friction is an interaction of mating material areas of bodies. It is a resistance against relative movement [19] and appears as *energy loss*. Kinetic energy gets transformed into other kinds of energy, mostly heat [14, 15]. *Outer friction* indicates the state when the contact regions are parts of different bodies, *internal friction* means the contact regions are parts of the same body [19].

In contrast to friction, *wear* is an undesired, continuously proceeding *material loss* from

[1] The term "tribology" (Greek: "teaching of friction") became widely used following a British study in 1966 (The Jost Report [13]).

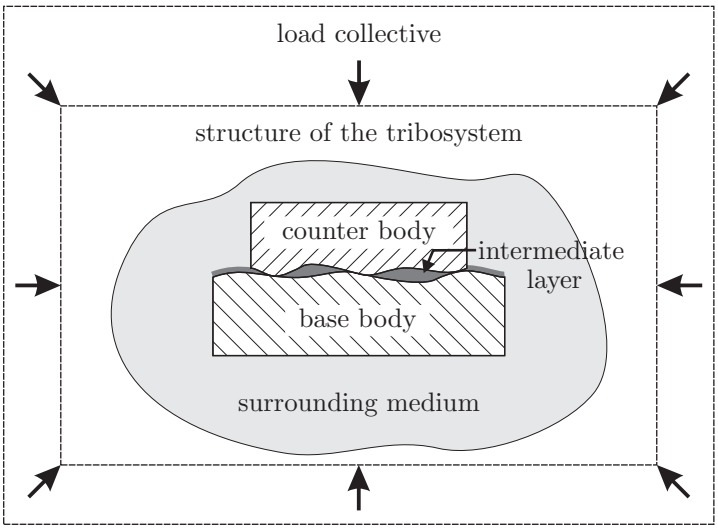

Figure 2.1: The structure of a tribological system (or tribosystem) defined by the German standards DIN 50 320 and DIN 50 323-1 [12, 18]. The whole system can be strongly influenced by the change of just one of these components [14].

the surface of a solid body, caused by mechanical reasons, i.e. contact and relative movement of a solid, liquid or gaseous counter body [18].
Friction and wear are both *tribological phenomena* which appear at the same time at identical tribological properties, but nevertheless, it is not possible to draw conclusions from the magnitude of one phenomenon to the magnitude of the other one. Experiments of Doege and Melching [20, 21] and Schneider [22] showed correspondingly that high wear rates may occur also in the presence of low friction. Furthermore, Westheide [23] and Fischer and Cron [24] concluded that there is no definite correlation between friction and wear. Finally, investigations by the author under dry sliding conditions resulted in high friction values where the amount of wear was quite small (see Section 3.4.3.1).

2.2 Dry Contact of Metallic Surfaces

In the following comments, the term *dry contact*, that describes a contact in the absence of lubricant, must not be confused with the term *clean contact*, that stands for a contact of oxide-free and uncontaminated surfaces.

2.2.1 Structure of Metallic Surfaces

In technical systems, the surfaces of metallic friction partners are never metallic clean. Usually surfaces are covered with boundary layers (see Figure 2.2), which develop by chemical or physical reaction of the base material in air, with humidity or with lubricants. Usually the boundary layer consists of more layers of different kind. The boundary

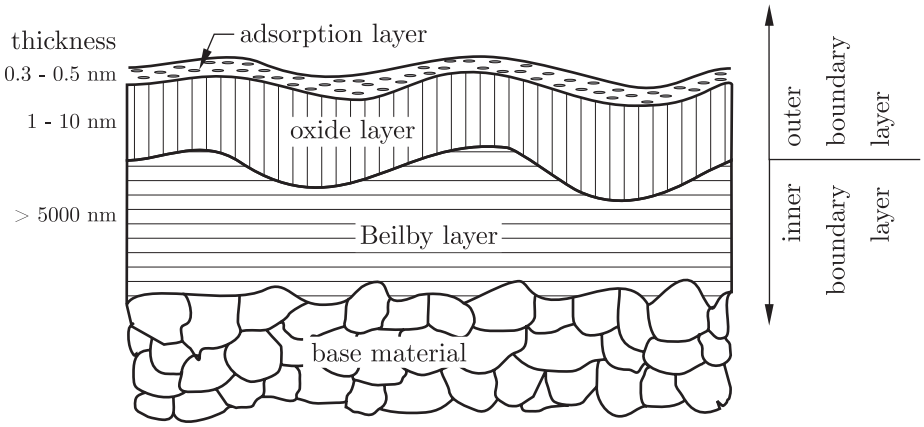

Figure 2.2: Structure of metal boundary layers [14].

layer of a technical metal surface can be divided into two regions, the inner and the outer boundary layer, which have different properties.
The *outer boundary layer* develops by the reaction of the inner boundary layer with the surrounding medium. It usually consists of an oxide layer and other thin layers which are developed by chemisorption and physical adsorption, respectively. The properties of the outer boundary layer can be very different compared to those of the base material and specify the wear behavior of the surface [16].
The *inner boundary layer* (the so called "Beilby-Layer") has the same chemical composition as the base material but has different mechanical and metallurgical properties caused by pre-deformation and shape cutting.

2.2.2 Microgeometry and Contact

Also the most carefully prepared surfaces are never perfectly plane but consists of hills and valleys. Concerning the surface effects, the surface conditions of tool and specimen are very important. It is responsible for size, allocation and orientation of the surface roughness and waviness, for the development of a lubricant film and for its ability of enduring surface extension of the specimen.

When two metallic bodies are brought in contact, the surfaces make first contact only at the highest points (the *summits* or *asperities*), and the real area of contact A_r is a small fraction of the apparent area of contact A_a (see Figure 2.3) [25]. If the contact

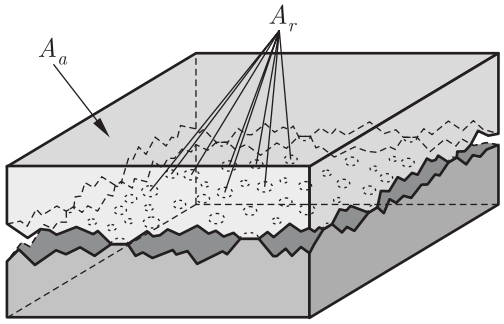

Figure 2.3: Contact points between two rough surfaces [25, 26]: The real area of contact A_r is a small fraction of the apparent area of contact A_a.

members are infinitely hard, the load cannot not bring them to touch each other in more than tree points. But since actual materials are deformable, the points become enlarged to small areas and simultaneously new contact points may set in [27]. The plastic deformation continues, until the real contact area A_r can support the normal pressure σ_n (see Figure 2.4). Finnie and Shaw [28] were among the first who assumed the real contact

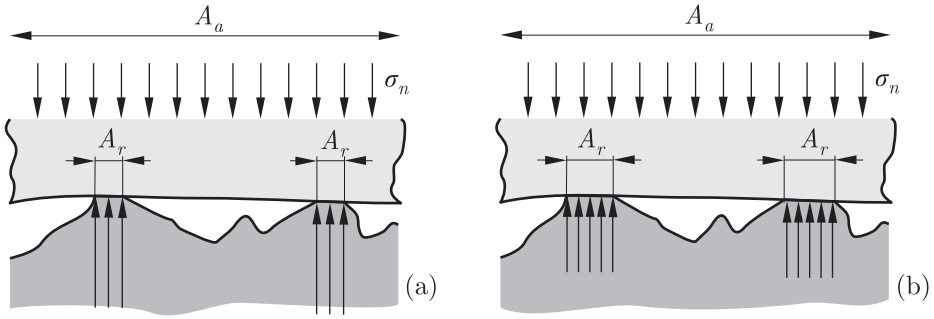

Figure 2.4: Contact between flat die and rough workpiece with plastic deformation of the asperities [25]: (a) The real contact area A_r is too small to support the pressure σ_n. This leads to a deformation, which results in an extend of the real contact area (b).

area to increase proportional to the applied normal pressure at light loads and to reach the apparent contact area asymptotically when the normal load is increased. The reason for this behaviour was seen to lie in the tendency for asperities to offer great resistance to flattening as flow occurs owing to strain-hardening and in the increasing material resistent to flow introduced by adjacent deformed peaks. Author's experiments, where ground and sandblasted AA6016 aluminium sheets were coined by a polished steel punch at different

load levels and subsequently observed by means of a laser confocal microscope[1], showed good correlation to Finnies and Shaws theory (see Figure 2.5). Further experimental work on measuring the real contact area was done by Dyson and Hirst [30], Pfestorf et al. [31] and Azushima et al. [32].

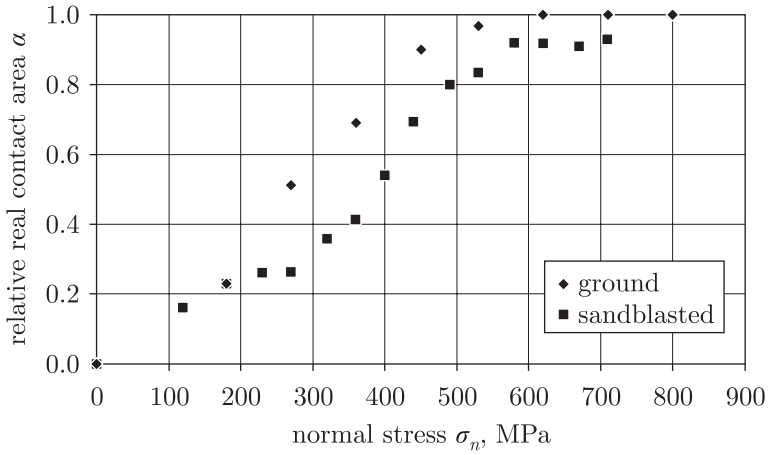

Figure 2.5: Experimental data on contact area evolution acquired for the compression of a ground and a sandblasted aluminium sheet (AA6016). The real contact area was determined with the method described in Section 4.3.3.2 and is expressed in terms of the relative contact area $\alpha = A_r/A_a$.

McFarlane and Tabor [33] found that the real area of contact is not only dependent on the normal pressure but is also affected by tangential stresses. They stated that when the real area of contact is just sufficiently large to bear the normal load, an infinitely small tangential stress is required to produce tangential flow, since the metal is already plastic (see Figure 2.6).

2.2.3 Characterisation of Surfaces

The analysis of technical surfaces plays an essential role in the description of tribological phenomena [11]. For the determination of the surface topography commonly tactile or optical techniques are employed.
Tactile methods make use of contacting instruments which allow the roughness to be determined in terms of the profile of a cross section of surface traced by a sharp stylus. A

[1] A description of the laser confocal microscope is given by Maass [29], and the determination of the real contact area is described in Section 4.3.3.2.

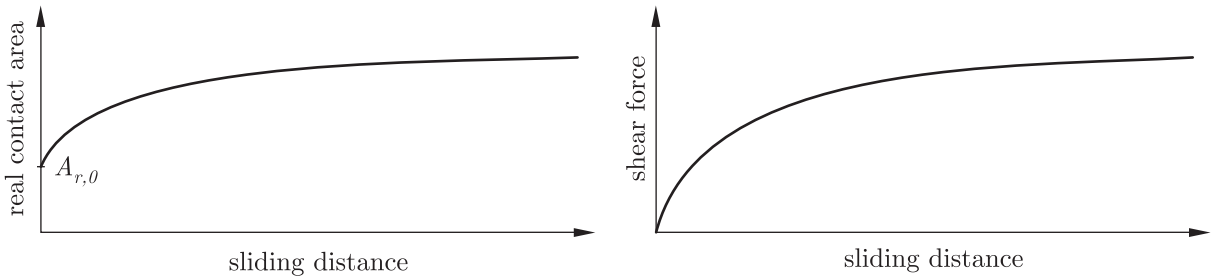

Figure 2.6: Variation of real contact area and of shear force with sliding distance [34]: When the real area of contact is just sufficiently large to bear the normal load ($A_{r,0}$), an infinitely small tangential stress is required to produce tangential flow, since the metal is already plastic [33].

three-dimensional surface representation can be achieved by recording a series of parallel profilometer traces.
Optical systems are based on confocal microscopy. A confocal microscope creates sharp images of a specimen that would otherwise appear blurred when viewed with a conventional microscope. This is achieved by excluding most of the light from the specimen that is not from the microscope's focal plane. The image has less haze and better contrast than that of a conventional microscope and represents a thin cross-section of the specimen. Thus, apart from allowing better observation of fine details it is possible to build three-dimensional reconstructions of a volume of the specimen by assembling a series of thin slices taken along the vertical axis [35].

The most popular way of quantitative surface characterisation is the use of roughness parameters as defined in the German standards DIN 4762 and DIN 4768. Therein, the actual surface is considered to include all its departures from a smooth reference plane that has a defined shape and fits the actual surface in a defined way. The parameters are determined from two-dimensional profile traces within a specified reference distance l, where vertical and horizontal parameters are distinguished.
Commonly, surface roughness is expressed in terms of the vertical parameters *total profile height* R_t, *arithmetical mean deviation* of the profile[1] R_a, *averaged peak-to-valley height* R_z or *peak-to-mean-line height* R_p. The total profile height is defined as the peak-to-valley height (see Figure 2.7 (a)), the arithmetical mean deviation is defined as

$$R_a = \frac{1}{l} \int_{x=0}^{x=l} |h_{a,i}| \, \mathrm{d}x, \tag{2.1}$$

[1] The arithmetical mean deviation is known as the *center line average CLA* in the Anglo-Saxon region.

with $h_{a,i}$ the distances between actual and mean profile, the averaged peak-to-valley height is calculated from the total profile heights of five adjacent, equally spaced surface sections, and the peak-to-mean-line height is defined as

$$R_p = \frac{1}{l} \int_{x=0}^{x=l} y_{p,i} \, \mathrm{d}x, \tag{2.2}$$

with $y_{p,i}$ the distances between actual and reference profile.
Horizontal surface parameters are the *roughness width* (the averaged horizontal distance between neighboring summits), the *bearing length* l_t (the sum of the sections $l'_{c1} \ldots l'_{cn}$ when the reference profile is shifted perpendicular to the ideal profile for a distance c, see Figure 2.7 (b)), and the *profile bearing fraction* t_p defined as

$$t_p = 100 \cdot \frac{l_t}{l}. \tag{2.3}$$

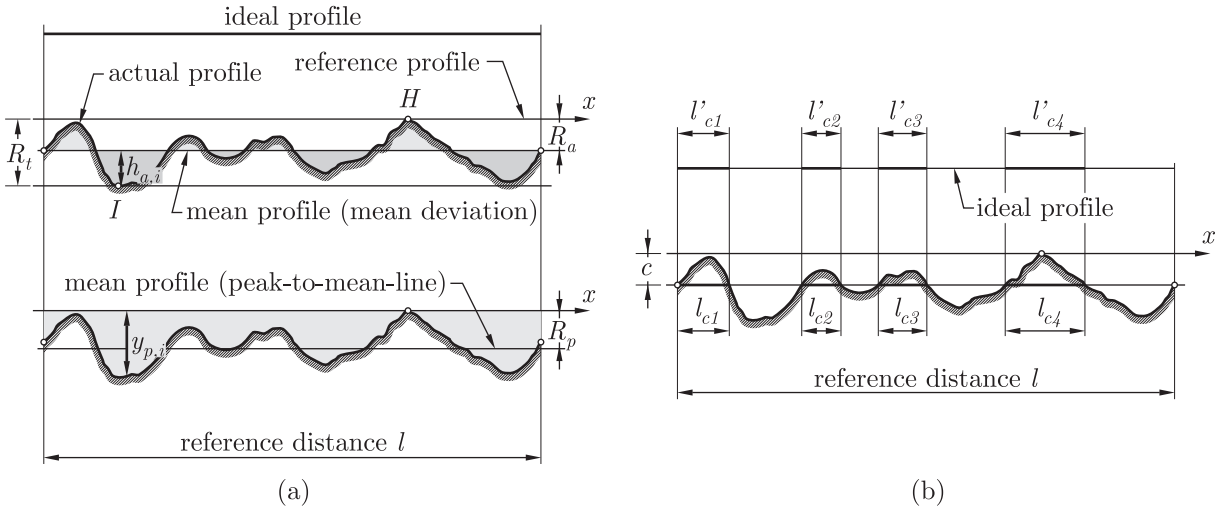

Figure 2.7: Vertical (a) and horizontal (b) surface parameters as defined in the German standards DIN 4762 and DIN 4768. These parameters are only defined for two-dimensional profile traces and are not suitable to describe the evolution of the real contact area under normal pressure.

However, none of these parameters is suitable to describe the evolution of the real contact area under normal pressure.
A distinctive characterisation for surfaces is the *bearing area curve* introduced by Abbott and Firestone [36] (see Fig. 2.8). Having the total load and strength characteristics of the

"rough" surface material, this curve gives a measure of the depth of plastic deformation required in a metallic contact before an adequate supporting area is generated for contacting a flat mating surface [37]. If a surface profile is represented by the vectors $\mathbf{x}$ and $\mathbf{y}$, the bearing area A_b at w equally spaced sections is approximated by:

$$A_{b,j} = \frac{1}{u} \sum_{i=1}^{u} \begin{cases} 1 & \text{for } y_{ij} \geq \mathrm{y}(j) \\ 0 & \text{for } y_{ij} < \mathrm{y}(j) \end{cases}, \qquad j = 0 \ldots w, \tag{2.4}$$

where u indicates the total number of points of the surface profile and $\mathrm{y}(j)$ is the height of the section j.

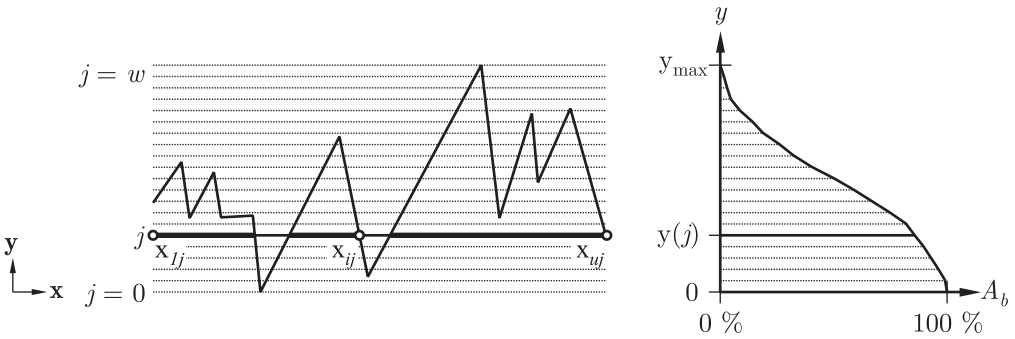

Figure 2.8: Numerical calculation of the bearing area curve (see Equation (2.4)).

Another significant representation of surfaces was given by Hansen [38] who proposed to model real topographies by calculating the mean asperity slope $\overline{\beta}$ at w equally spaced sections thereby determining the slope of a model asperity (see Fig. 2.9):

$$\overline{\beta_j} = \frac{1}{u} \sum_{i=1}^{u} |\beta_{ij}|, \qquad j = 0 \ldots w, \tag{2.5}$$

where u is the number of intersections at the height $\mathrm{y}(j)$.

2.2.4 Surface Modification in Metal Forming

In metal forming processes, the tool surfaces can be considered much smoother and harder than the workpiece surfaces. Thus, in the following section, the compression of a soft, rough surface by a hard, flat plate is discussed in order to identify the mechanism of surface conformation.

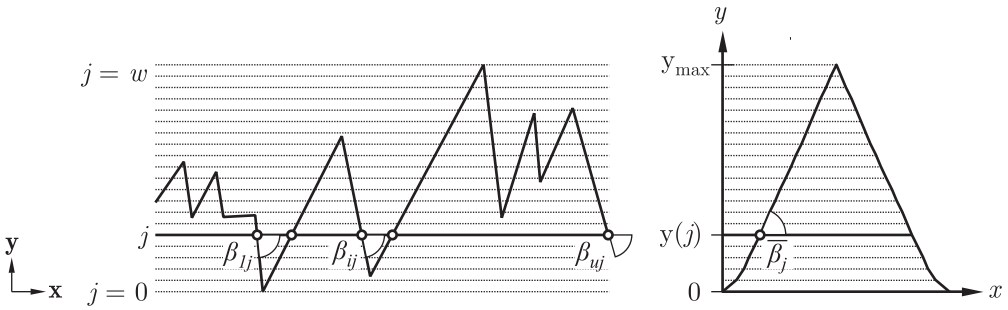

Figure 2.9: Numerical calculation of the average asperity slope as used for the model asperity proposed by Hansen [38] (see Equation (2.5)).

Butler [39] was the first who performed experiments where macroscopic model asperities were compressed with a flat punch. The model asperities were made of mild steel and the asperity slope was 5 °. Butler found, that in the absence of lubricant near 100 % of conformation of die and metal occurred.

Later, Heller [40] investigated the deformation of steel and aluminium model asperities with different asperity slops (15 °, 30 ° and 45 °). He found that the mode of asperity spreading had significant influence on surface conformation: When free spreading of the asperities base was allowed, the asperity slope remained constant during deformation and complete conformation was achieved, but when spreading was constrained, bulging of the asperities occurred and fine cracks were formed (see Figure 2.10). Heller concludes, that

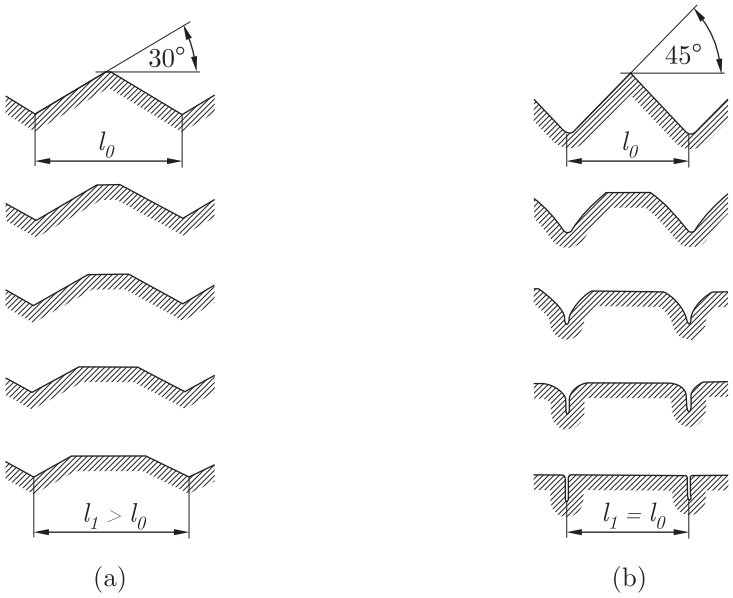

Figure 2.10: Free (a) and constraint (b) spreading of asperities as found by Heller [40].

in his experiments *"the final profile looked like the original profile where the amount of*

die stroke was removed". A rise of the valleys – as reported by other authors – was only observed when the spreading of the asperities was completely constrained.
Pullen and Williamson [41] analysed surface modification in the die-workpiece interface by compressing a glass blasted aluminium specimen in a closed die. The asperity slope of the specimen was determined by the present author as approximately 20 ° (see Equation (2.5)). Pullen and Williamson came to the conclusion, that the material displaced by the punch reappeared as uniform rise in the non-contacting surface, and that the valley floors began to rise even under the lightest loads. The asperity slopes were not found to change during the deformation.
Finally, Kienzle [42] and Mühlenweg [43] report on compression tests with lead specimen that showed that asperities with a slope lower than 45 ° could be completely conformed in compression tests, and asperities with larger slopes formed fine cracks due to bulging (comp. Heller [40]).
From the above findings and experiments by the author presented in Section 4.2.3, it can be summarised that the surface modification in the tool-workpiece interface is dependant on the mode of asperity spreading (free or constrained), the asperity slope, the radius in the floor of the valley and the material properties. This means that complete conformation with a strain-hardening material and under constrained spreading is only possible when the asperity slope is small (comp. Butler [39], Pullen and Williamson [41]). When the asperity slope gets larger, complete flattening can be only achieved in the presence of free spreading (comp. Heller [40]).

2.2.5 Surface Contact Models

Surface contact models allow the determination of the evolution of the real contact area in dependence on surface conditions, material properties and load. Basically, asperity-based models, profilometric theories, slip-line based techniques and numerical approaches can be distinguished.
Asperity-based models reduce the contact process of surfaces to the compression of geometrical simple model asperities by a smooth tool. Hertz [44, 45] was the first who considered the elastic contact of a sphere with a flat. Later, Bowden and Tabor [46] and Archard [47] studied the contact of single asperities with flat surfaces. Bowden and Tabor considered elastic as well as plastic contact: For elastic contact they used the following equation based on the Hertzian theory:

$$r_{cs} = \sqrt[3]{\frac{3 \cdot \sigma_n \cdot r_{su} \cdot n}{8 \cdot E}}, \tag{2.6}$$

with r_{cs} the radius of contact, σ_n the pressure, r_{su} the radius of curvature of spherical surfaces, n a numerical between 3–4 and E the Young's modulus. For the plastic contact they assumed

$$\sigma_n = r_{cs}^2 \cdot \pi \cdot k_f, \tag{2.7}$$

with σ_n the pressure, r_{cs} the radius of contact and k_f the yield stress of the asperity[1]. Archard concentrated on purely elastic contact assuming the asperities to be covered by smaller protuberances (thus introducing fractal surfaces).
All these theories are based on the assumption that when surfaces tough lightly, the contact spots will be well separated from each other and any interaction between them will be negligible. However, from their experiments, Pullen and Williamson [41] found the asperities to interact from the beginning of surface deformation. According to their *uniform rise hypotheses*, the material displaced by the flat reappears as rise in the non contacting surface. Under these conditions and the assumption of purely plastic contact, they obtained an approximate expression for the load-compliance-law. This model was further developed by Li and Sellars [48].

Higher sophisticated methods are based on the random process model: Following Longuet-Higgins [49], it is supposed that a surface can be described as a homogeneous, stationary, two-dimensional random process: The rough surface is assumed to consist of a mean plane with independent (i.e. not touching) hills and valleys randomly distributed on it. These models allow statements about the separation of mating surfaces, the real contact area and the number and sizes of individual contacts. Several authors have investigated statistically the shape of rough surfaces and their behaviour in elastic and plastic contact making simplifying assumptions.
Greenwood and Williamson [50, 51] assumed that the surface can be modeled by identical spherical asperities with either exponential or Gaussian height distributions. They considered elastic as well as plastic contact and described the change over. Bush et al. [52] and McCool and Gassel [53] constrained their research to elastic contact and replaced the cap of each asperity by a paraboloid having the same height and principal curvatures as the summit of the asperity. On the other hand, Tsukizoe and Hisakado [26] and Nayak [54] analysed the purely plastic contact of a rough surface and a hard, smooth flat.

Theories based on *profilometry* attempt to start from the real situation. The simplifying assumptions are made during the solution. The bearing area curve (as described in Section 2.2.3) can be used to study simple contact. The difficulty is to introduce the

[1] In fact, most of the asperity models are based on Equations (2.6) and (2.7), or similar expressions.

load. This can only be done simply for ideal plastic flow, when it is proportional to the area. The advantage over the corresponding derivation in the asperity-model theory is striking. The result now comes in two lines, and involves only the single assumption (other than ideal plastic flow), that the surface elements move vertically without pulling down their neighbors. Nothing has been found about the number and sizes of individual contacts, but equally nothing has been assumed about the number and size of individual asperities. When the contact area is an appreciable fraction of the apparent area, the whole concept of individual asperities fails. The profilometric approach can still deal with this situation [55].
Kragelsky and Demkin [56] investigated the contact of a wavy, rough surface in elastic and elastic-plastic contact with a flat where their concept was based on the bearing area curve approximated by an exponential and a parabolic function, respectively.

Hill [57] proposed a *slip-line field* for the compression of a wedge of infinite depth by a flat die (see Figure 2.11 (a)). As usual in slip-line theory, a plastic-rigid material was considered. His results are inconsistent with the experimental findings of Heller [40] and others that concluded that the slope angle would not change during upsetting. Hill's

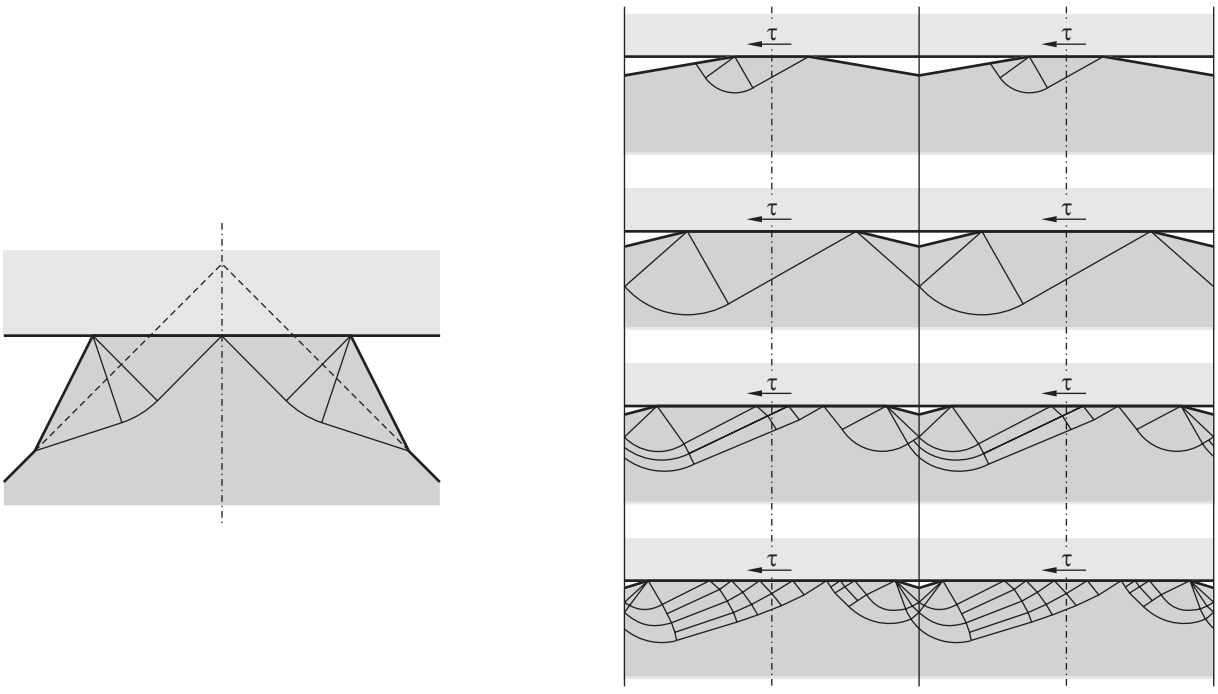

Figure 2.11: Slip-line fields for the compression of wedges of infinite depth by a flat die: (a) Hill's [57] and (b) Wanheim's [58] solution.

work was further developed by Ling and Troy [59] and Fogg [60]. All these analysis of asperity deformation are confined by the assumption of no plastic deformation of the bulk material.
A quite different slip-line solution was presented by Wanheim and his colleagues. For the case that no tangential stresses are present in the tool-workpiece interface, Wanheim [61] proposed the combination of three different slip-line fields: The starting point was Prandtl's solution of indenting a plane tool into a semi-infinite plate (modified to the compression of a symmetrical wedge). When the deformations started to interact ($\alpha = A_r/A_a \approx 0.33$), Hill's extrusion solution was assigned. Finally, when the boundary slip-line reached horizontal ($\alpha = 0.88$), a slip-line field proposed by Johnson was engaged. For the case of constant tangential stresses in the tool-workpiece interface, Wanheim et al. [58] proposed a solution based on the slip-line field developed by Johnson [62] for the extrusion through a perfectly smooth square die (see Figure 2.11 (b)). This allowed the determination of the load-conformation-law in dependence on the interface friction.

In order to asses the influence of temperature (the yield stress) on asperity flattening in cold, warm and hot forging, Neumaier [63] utilised a *numerical approach*. He modeled the real surface of the workpiece by taking profilometer traces and performed a finite element analysis of surface conformation in MSC.AutoForge assuming a flat tool and plane strain conditions. This method prevails over the previously mentioned in terms of real material properties and real surfaces. However, the problem ist still simplified: First, the real surfaces consists of asperities and not of wedges, and second, the material properties of the asperities may have significantly other character than these of the bulk material (comp. Section 2.2.1).
An interesting approach of integrating surface modification in finite element code without the necessity of modeling real surfaces is given by Doege and Kaminsky [11, 64] and Stupkiewicz and Mroz [65]: They propose to replace the surface asperities by a homogeneous, porous surface layer.

2.3 Dry Friction of Metallic Surfaces

In the following comments, the term *dry friction*, that describes friction in the absence of a lubricant, must not be confused with the term *clean friction*, that stands for a friction of oxide-free and uncontaminated surfaces.

2.3.1 Dry Friction Mechanisms

In this section an attempt of a systematical and complete description of dry friction mechanisms is made concentrating on the situation present in metal forming processes (thus ignoring elastic and molecular effects). It is generally agreed that surfaces in contact meet at asperities (comp. Section 2.2.2), and that frictional stresses can only be generated in the real contact area. The contributing friction mechanisms can be summarised as follows: adhesion, surface deformation and subsurface deformation (Figure 2.12 gives an overview on the friction mechanisms).

Adhesion is a denotation for cohesion forces between molecules of two distinct materials and the sticking of a body to another one, respectively. As described in Section 2.2.1, metallic surfaces are normally covered with oxides and contaminants that prevent mating surfaces from clean, metallic contact. However, when the surface layers are broken (e.g. as a result of plastic deformation of asperities), clean metallic contact will occur and adhesive bondings may be formed. Now, if the bodies move relative to each other, the adhesive connections have to be broken or, if the adhesive connection is stronger than the shear yield stress of the weaker body, they get sheared off. The therefore required energy is considered as the adhesive component of friction. The adhesion theory was put forward by Holm [66], Ernst and Merchant [67] and Bowden and Tabor [68, 69].

When discussing the effects of *surface deformation*, three different cases are to be distinguished:

1. Workpiece and tool roughness are of the same order (RWRT).
2. The workpiece surface is significantly smoother than the tool surface (SWRT).
3. The workpiece surface is significantly rougher than the tool surface (RWST).

In dependence on the surface conditions, the following mechanisms may occur:

- *plastic deformation*, *breaking* and *shearing* of interlocking asperities,
- *ploughing*, *micro-cutting* and the *formation of a plastic wave* in front of a tool asperity or wear particle.

When both, tool and workpiece surface are of the same order of roughness, the asperities will interlock and counteract relative sliding. Hence, when relative sliding is enforced, the interlockings have to be broken in terms of plastically deforming or breaking asperities

of the softer friction partner. An additional mechanism was introduced by Ming-Feng [70] who assumed the physical interlocking stronger than the shear yield stress of the softer material and therefore expected shearing of the weaker asperities beneath the zone work-hardened by interlocking.

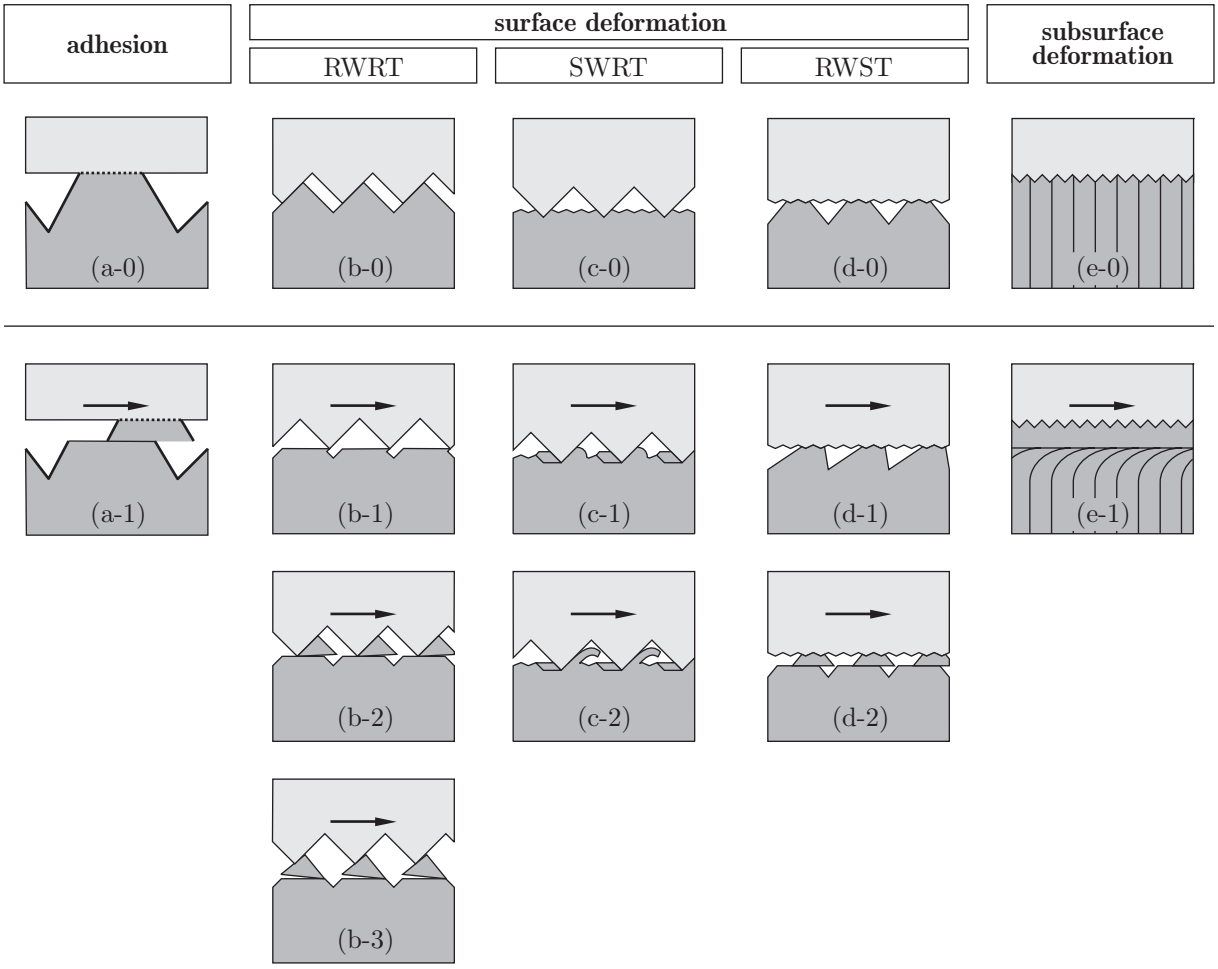

Figure 2.12: Mechanisms of dry friction ("0" indicates the static state): Adhesion occurs when the non-metallic surface layers are broken and metallic connections can form (a). Having a rough-workpiece-rough-tool (RWRT) interface, plastic deformation (b-1), shearing (b-2) and breaking of asperities (b-3) can be observed. Assuming a SWRT-interface, ploughing (c-1) and micro-cutting (c-2) can occur. In the case of a "smooth" tool (RWST), plastic deformation (d-1) and shearing (d-2) is observed. In the case of sticking friction, the subsurface layer is deformed (e-1).

When the workpiece is plane compared to the tool surface, the friction mechanisms are assumed to be quite different: The asperities of the tool will sink into the workpiece surface until the real contact area is able to bear the applied load. When now relative motion

is applied, the tool asperities will plough through the workpiece surface. In the case of ductile workpieces, a plastic wave will be formed in the front of and besides the indenters (see e.g. Kragelski [71], Avitzur and Nakamura [72]). If, however, the workpiece is of brittle material, the tool asperities will cut through the counter-body thereby forming chips. In further sliding, these chips can act on the workpiece surface in the same way as the tool asperities.
In the case of a comparable smooth tool and a rough workpiece (the situation commonly present in metalforming processes), the interlocking is restricted to the summits of workpiece asperities. In the presence of relativ motion, plastic deformation and shearing as proposed by Ming-Feng [70] can take place.
In tribological processes, plastic deformation is not constrained to the surface, but *subsurface deformation* is also present. In the case of sticking friction, the energy loss is completely caused by subsurface deformation.

In real metallic interfaces, commonly different mechanisms are superimposed. The presence of a mechanism is dependent on the surface conditions, the load and the material properties.

2.3.2 Influences on Dry Friction

As already mentioned in Section 2.1, friction is a tribological phenomenon und thus depends on the investigated tribosystem, i.e. its elements and the load collective. Parameters concerning the elements of the tribosystem (e.g. material properties, solubility of mating pairs, surface condition) are called *system related parameters*, parameters describing the load collective (e.g. temperature, load, velocity) are known as *process related parameters*. All these parameters have to be considered in interaction; the whole system can be significantly affected be the change of just one of these components.

The *material properties* of tool and workpiece influence the system in terms of hardness and yield stress, for example. These parameters determine the formation of the real contact area and are affected by temperature and stress.
Another factor that has been observed to influence the friction of sliding surfaces is the degree of *solid solubility* of the mating pairs depending on their chemical composition. Solubility of one friction partner in another is a condition for adhesion to take place. In order to minimise friction the metals must be insoluble in each other with neither metal dissolving in the other nor forming an alloy with it [37]. It is known that materials of similar strength are more readily soluble than materials with more distance in the elec-

trochemical series [73].
A very important system related parameter is the *surface condition* of tool and workpiece, respectively. On the one hand, the formation of the real contact area is strongly affected by the asperity shape as shown in Section 2.2.4, and on the other hand, the mode of surface deformation is dependent on the roughness of tool and workpiece (see Figure 2.12). Furthermore, boundary layers may prevent the friction partners from metallic contact.
The change in *atmosphere* influences the nature of the surface films. Accordingly, all the friction changes characteristic of surface layers can be brought about by sliding in different atmospheres.
The *temperature* can affect the physical and chemical behaviour of the surfaces and the bulk of sliding metals. Rising temperature causes a lower yield stress and increases the capacity of reaction, for example. In tribological systems, the temperature is not only determined by the load collective, but in sliding surfaces heat is generated due to friction (by energy dissipated in forming and breaking of junctions and in plastic deformation processes), and in turn the heat can affect friction. In the case that tool and workpiece are not at the same temperature, the heat transfer plays an important role [74].
The effect of *normal load* is determined primarily by the deformation of the asperities and thus by the evolution of the real contact area with load.
Surface heating and rate of shear are the factors that change with *velocity*, and investigations of Johnson et al. have shown that oxides can form at high velocities. Therefore, all the oxide film effects on friction must be considered [37].

2.4 Friction and Lubrication in Metal Forming

2.4.1 Tribology in Metal Forming

In analysis of the tribology of metal forming applications, especially the process related parameters differ significantly from these present in tribological processes of mechanical engineering.
In metal forming processes, the plastic deformation is caused by stresses transferred from the tool on the workpiece. Thus, the normal loads are commonly in a range of several times the yield stress of the workpiece material. Metal forming operations are frequently performed at elevated temperatures, and even in cold forming processes the temperatures can amount to several hundred degrees Celsius due to the heat generated by plastic deformation. Moreover, the sliding velocities are high in the most processes.
In contrast to many applications in mechanical engineering, both, the hardness and the

roughness of the friction partners are not of the same order, but the tool is much harder and smoother than the workpiece. Additionally, in bulk metal forming operations, the size of the workpiece surface is changed during the process (commonly it is enlarged). Due to the fact that the tool surface remains constant, this contributes to the relative velocity in the tool-workpiece interface. Another result of the permanent formation of new surfaces is that the tribological process in bulk metal forming equals the run-in behavior of mechanical components.

In contrast to wear, that is always an undesired phenomenon, the role of friction in metal forming is ambivalent: On the one hand, friction affects the forming loads (and thus energy consumption and tool life) and acts as energy loss, and on the other hand, friction is necessary to control the material flow [75]. The effect of material flow is not constrained to the outer shape of the part, it influences the mechanical properties of the workpiece and their distribution within the part [76, 77]. Thus, friction is beneficial in many forming operations. In rolling it allows the metal to be drawn into the gap between the rolls. In open-die forging it prevents the metal escaping from between the tools, and in closed die forging, it provides the back pressure in the flash to ensure filling of the die cavity [74, 78].

In metal forming processes, friction is controlled by the application of lubricants[1], this is, friction is reduced by transferring outer friction to inner friction (of the lubricant) and preventing direct metallic contact of tool and workpiece. In the presence of lubricant, the tool pressure is transmitted onto the material partly by pressurised lubricant entrapped in small valleys of the surface asperities and partly by the very thin film of lubricant squeezed between the tool and the material [79]. Thus, the pressure on the summits is significantly reduced and the asperities are stabilised by the hydrostatic pressure in the lubricant pockets (see Figure 2.13). As a consequence, the evolution of the real contact area is impeded.

As the lubricant acts as the intermediate layer in the tribosystem (see Section 2.1), there are numerous effects on and interactions with the other elements. Lubrication based influence parameters on the system are the viscosity, the shear stability and the pressure- and temperature durability of the lubricant, as well as its chemical and physical capacity of reaction within the system [73], and in the presence of surface expansion, the lubricant's ability to sustain the extension without breaking is important.
Moreover, the lubricant has an effect on the surface condition of the workpiece: When a

[1] *Lubrication* is the decrease of friction by using an adequate lubricant [14–17]. Under lubrication the specific use of lubricants and if necessary lubricants together with a lubricant carrier coating can be understood, which leads to the appearing of a good lubrication condition for a particular process.

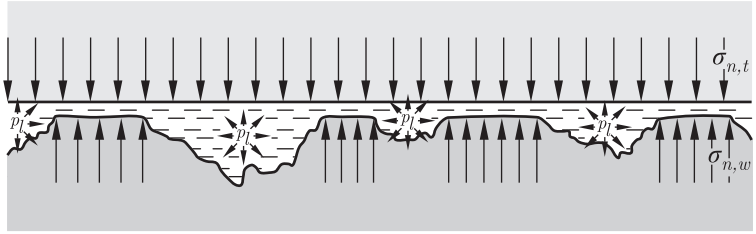

Figure 2.13: In the presence of lubricant, the tool pressure $\sigma_{n,t}$ is transmitted onto the workpiece partly by pressurised lubricant entrapped in small valleys of the surface asperities (p_l) and partly by the very thin film of lubricant squeezed between the tool and the workpiece ($\sigma_{n,w}$) [79]. As a consequence, the evolution of the real contact area is impeded.

metal mass is deformed plastically, the free surface of it will roughen itself from its initial texture due to the slip of crystalline grains. This is also the case when there exists an interposed film of a lubricant between tool and material [14, 79].

2.4.2 Liquid Metal Forming Lubricants

Mineral oils provide a basis for the most industrial applied lubricants. Oils and emulsions without polar or chemical reactive molecules are adsorbed at the mating surfaces by means of adhesion. The slipping effect of such lubricants is good but the separation effect is marginal, thus, additives are utilised [14].

Liquid lubricants are fluids which, under appropriate conditions, provide separation of tool and material surfaces over some of the contact area while allowing boundary contact at other places. Before such mixed-film lubrication can be discussed, it is necessary to examine the extreme case where the two surfaces are fully separated by a fluid film. Conditions in the interface are then governed by the bulk properties (such as viscosity[1]) of the lubricant. In the simplest case, the surfaces of the two bodies are separated by a film thick enough for surface roughness effects to be ignored. If a normal load is applied to the lubricant film, the film would collapse if it is not made load-bearing by one of the following measures [25]:

1. The lubricant may be supplied under sufficient pressure to balance the applied load over the bearing area. This is called *hydrostatic lubrication.*

[1] Viscosity has its roots in intermolecular attraction and is thus very sensitive to temperature. With increasing temperature, viscosity drops, increasingly so in lubricants of higher viscosities [25]. That is why the application of fluid lubricants is limited to cold forming temperatures.

2. The pressure may be generated in the lubricant film itself by creation of a converging gap in the direction of relative movement. Then, the moving surface drags the lubricant into the gap. If the fluid is incompressible and cannot leak out at the sides, it encounters resistance in the converging gap and generates an increasing pressure. This effect is called *hydrodynamic lubrication*.

When a forming load is applied to a lubricated workpiece surface, the asperities start to deform plastically, thus increasing the pressure of the lubricant, which is trapped in the roughness valleys in between or squeezed out. Roughness valleys that do have a connection to the edge of the surface cannot keep the lubricant. These are the so-called *open lubricant pockets*. With increasing normal pressure, the lubricant escapes and is not able to support or transmit the forming load. The forming load acts only on the asperities which results in a higher contact stress, a higher degree of surface flattening and thus, a higher fraction of real contact area. *Closed lubricant pockets* on the contrary do not have a connection to the edge of the surface. The lubricant gets trapped in those pockets and pressurised during forming. The developing hydrostatic pressure will take a part of the external load, thus reducing the normal pressure on the asperities [80]. These mechanisms are of great influence on friction and lubrication as well as on the resulting surface topography [81].

The basic idea of the mechanical-rheological concept developed by Sobis, Geiger and colleagues [31, 82–84] is to quantify the real contact area considering the lubrication controlled contact. It is assumed that any process of contact can be idealised by three contact mechanism: The first one is the solid contact, which is the main subject of contact mechanics. The earlier mentioned microscopic lubricant pockets represent the basis of the two next contact mechanism: a static lubricant pocket, which is a known mechanism of transmission of contact forces and a dynamic lubricant pocket, which should not be confound with self-acting hydrodynamic lubrication. The fundamental condition for any contact process is the equilibrium between the external force acting on the apparent contact area and the sum of the forces representing the three contact mechanisms.

2.4.3 Solid Metal Forming Lubricants

Solid lubricants are used in applications in which fluid lubricants can not meet the demands in terms of oxidation and decomposition phenomena. This is why the success of warm forging processes is based on the application of solid lubricants [24]. In solid film lubrication mechanical interaction between tool and workpiece asperities is prevented.

Due to its shear strength the film can take up high pressures without being squeezed out of the tool-workpiece interface [85].
In metal forming processes, the following types of solid lubricants are applied: layer-lattice compounds, conversion coatings with soaps, polymer-based lubricants, glasses and oxides, metal films and anorganic salts [24, 25, 86]. In this work, only layer-lattice compounds are discussed in more detail.
As their name implies, layer-lattice compounds possess a layered crystal structure. To serve as lubricants, the lamellae, which comprise strongly bonded atoms, must be held together by relatively weak forces. In practice, only graphite and molybdenum disulfide have gained wide application [24, 25].
Graphite has a lamellar hexagonal structure with individual layers held together with weak van der Waals forces. In metal forming application the temperature window is limited to a range of 500 °C to 600 °C in order to avoid oxidation. At temperatures less than 538 °C the lubrication of graphite in air is much better than in vacuum because graphite absorbs moisture or vapor in the air that can weaken the bonding force between the layer structure of the carbon atoms and reduce the shear strength within the lubricant film [87]. Graphite-based lubricants consist of fine dispersed graphite, additives that work as a binder, and a carrying agent. Lubricant breakdown is due to oxidation and thermal decomposition. Graphite-based lubricants are commonly sprayed onto the tools by means of a viscous carrier (mostly water or mineral oil). The time elapsed between lubricant application and contact with the workpiece play decisive roles in the evaporation of the carrier. It was found that the carrier fluid not only impaired the interlayer bonding but caused a squeeze film effect, if the contact time of the forging process was short enough [14, 24, 86].
Molybdenum disulfide (MoS_2) has a layered (lamellar) molecular structure with individual alternate layers of molybdenum and sulfur atoms. The low shear strength is explained by its anisotropy. The atomic arrangement in each layer is hexagonal, with each molybdenum atom surrounded by a trigonal prism of sulfur atoms. Thus, the force holding the atoms together in each group of S:Mo:S layers is the relatively strong covalent bonds, whereas the force between adjacent sulfur atoms is the relatively weak van der Waals force. Thermal stability in air is in the range of 350 °C to 400 °C. Unlike graphite, MoS_2 does not rely on adsorbed vapors or moisture, it has a greater load-carrying capacity and its manufacturing quality is better controlled. It can be applied to the surface by conventional methods in powder, grease, or spray form or by plasma spraying or sputtering [14, 24, 86].

2.4.4 Friction in Closed-Die Aluminium Forging

In closed-die forging the workpiece is placed in a die representing the negative of the shape of the final forging, and it is forced to fill the cavity by the application of pressure. The process is commonly performed at elevated temperatures (at approx. 80 % of the materials homologous temperature) and is – in contrast to rolling or extrusion – unsteady in terms of an unsteady forming zone. Compared to machined parts, the grain-flow pattern of forged components is not broken but optimised due to material flow. Especially in notches, that are critical to crack formation, forging results in a finer flow pattern thereby enhancing the fatigue strength of the workpiece (see Figure 2.14). Thus, forging results in stronger parts than cast or machined components and is used for safety relevant assemblies. Forgings are commonly used in automotive and aerospace applications, where a high strength-to-mass ratio is demanded.
The tribological loads in closed-die forging are characterised by very high contact pressures (up to several times the yield stress), high surface expansion and surface modification, high relative velocities and high temperatures and temperature gradients in the interface [88, 89]. However, the sliding distance of the material on the tool is comparably short.
The local conditions in the tool-workpiece interface are determined by the material flow. Melching [21] and Li [90] found three different zones in closed-die forging, that were verified by the author by means of a finite element analysis (see Figure 2.14): The *compression zone*, where minor relative motion is present, the *sliding zone* and the *shear-compression zone*, where surface expansion takes place. The most important parameters on the material flow are the geometry of workpiece and flash gap, the tribological system, forming speed and -temperature and the material properties. The material flow, on the other hand, influences die filling, forming loads and grain-flow pattern (and thereby the mechanical properties of the workpiece and their distribution within the part [76, 77]).

Aluminium alloys are important construction materials due to their low specific weight, their corrosion resistance and their ability to achieve high strength with certain alloying additions. Aluminium forged parts play a significant role as components of light weight constructions in the automotive and aerospace industry. In closed-die forging, aluminium is typically heated to 450–500 °C. The flow stress of aluminium during hot forming is known to be nearly independent on strain, but strongly dependent on strain rate [91]. This is, why special attention has to be payed to preventing the material escaping from the flash gap.

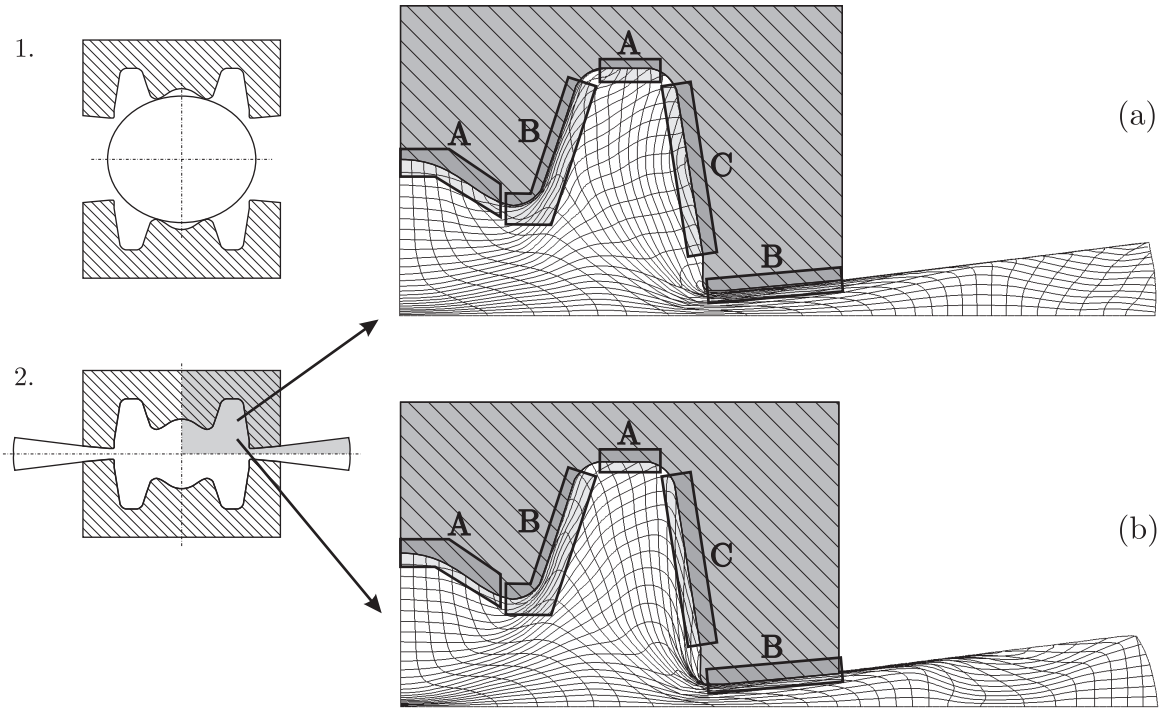

Figure 2.14: Material flow in closed-die forging in the case of no friction (a) and sticking friction (b): The *compression zone* **A**, where minor relative motion is present, the *shear-compression zone* **B**, where surface expansion takes place and the *sliding zone* **C**.

In warm forging operations, the lubricant is commonly applied onto the tool by means of an carrying agent due to the following reasons: On the one hand, the tool is usually cooler than the workpiece and the lubricant is exposed to the high temperature as short as possible, and on the other hand, the carrier has a cooling effect on the tool. Most extensively applied lubricants in aluminium hot forging are water-based graphite dispersions [24, 86]. Oil-based dispersions are also used in some cases, especially when the tool temperatures exceed 300 °C as in isothermal[1] operations. The oil components not only take over the carrier and cooling function, but make a considerable contribution to the reduction in friction and wear. A combination of the water and oil phase has been realised in water emulsions with oil containing graphite [86].

[1] In isothermal forging, the dies are heated up to approximately the same temperature as the workpiece to avoid die chilling. Usually, isothermal forging is performed with the help of low-velocity forging equipment like hydraulic presses [92].

2.5 Friction Models for Metal Forming

2.5.1 Review

The first systematical study on materials sliding on each other was performed by Leonardo daVinci. He found that *"friction produces double the effort if the weight be doubled"* and that *"friction made by the same weight will be of equal resistance at the beginning of movement although the contact be of different lengths and breadths"*. Later, Amontons mentioned that the force of friction was proportional to the load and independent on the apparent contact area. In 1779 Coulomb summarised the state-of-the-art investigations on friction. He concluded that friction was proportional to load and independent on sliding velocity or apparent contact area [37]. From these observations, the following relation commonly referred to as *Amontons friction law* or *Coulomb friction law* was formulated:

$$\tau_f = \mu \cdot \sigma_n, \tag{2.8}$$

where τ_f is the friction stress, σ_n is the normal stress and μ is the *friction coefficient*. The magnitude of this coefficient is between 0 and 1 (where 0 means no friction and 1 characterises sticking) and is assumed to be independent on sliding velocity and contact pressure. Up to now, the Amontons friction law is the most popular relation to calculate friction under low and moderate normal pressures as present in mechanical engineering. However, Bowden and Tabor [68, 69] showed that this assumption is only valid when the real contact area increases proportionally with the normal load.
In metal forming operations, the friction stress that can be transferred form the tool onto the workpiece is obviously limited by the shear yield strength of the workpiece material. When the normal load equals the yield stress of the workpiece, the maximum value of μ is given by:

$$k = \frac{k_f}{2} \quad \Rightarrow \quad \mu_{max} = 0.5 \qquad \text{(Tresca)}, \tag{2.9}$$

$$k = \frac{k_f}{\sqrt{3}} \quad \Rightarrow \quad \mu_{max} = 0.577 \quad \text{(von Mises)}, \tag{2.10}$$

where k_f is the yield stress and k is the yield shear stress calculated by the Tresca criterion and the von Mises criterion, respectively.
Nádai [93] was the first who suggested the assumption of a constant friction stress in

forming operations. Commonly, this is expressed in terms of the *constant shear factor model*[1]:

$$\tau_f = m \cdot k, \tag{2.11}$$

where τ_f is the friction stress, m is the *shear factor*[2] and k is the shear yield stress of the weaker friction partner. The magnitude of this factor is between 0 and 1 (where 0 means no friction and 1 characterises sticking) and is assumed to be independent on sliding velocity and contact pressure.

Orowan [101] proposed the combination of Amontons' law and the constant shear model: At loads lower than the yield strength, Amontons' law was applied, and at higher pressures, sticking was assumed:

$$\tau_f = \begin{cases} \mu \cdot \sigma_n & \text{for } \sigma_n < k_f \\ k & \text{for } \sigma_n \geq k_f \end{cases} . \tag{2.12}$$

This assumption was supported by experiment of Finnie and Shaw [28] in the analysis of friction in metal cutting: They found the friction stress to increase proportional to the applied normal pressure at light loads and to reach the shear yield strength asymptotically when the normal load was increased. In later investigations, Shaw et al. [102, 103] showed that in general tree regimes of friction exist depending on the ratio of the real to the apparent area of contact (see Figure 2.15): Region I corresponds to relatively lightly loaded sliders where Amontons' law holds. Region III, on the other hand, corresponds to the situation where there is no free surface (the real and apparent contact area are identical). Finally, region II is characterised by the bulk plastic flow of region III, but the incomplete contact area of region I. The transition from region I to region II was assumed to be given by the beginning interpenetration of the plastic zones of neighboring asperities. In Figure 2.15, the different friction models are compared.

2.5.2 State of the Art Friction Models for Metal Forming

Up to date, most popular friction models (besides of Amontons' law and the constant shear factor model) are based on the asymptotic model qualitatively described by Finnie and Shaw [28]. There are physical, mathematical and empirical approaches of describing

[1] This model is also referred to as *friction factor model* or *Siebel friction law* [92, 94–99]. However, this model was not found by the author in Siebel's article [100].

[2] This factor is also referred to as *friction factor*.

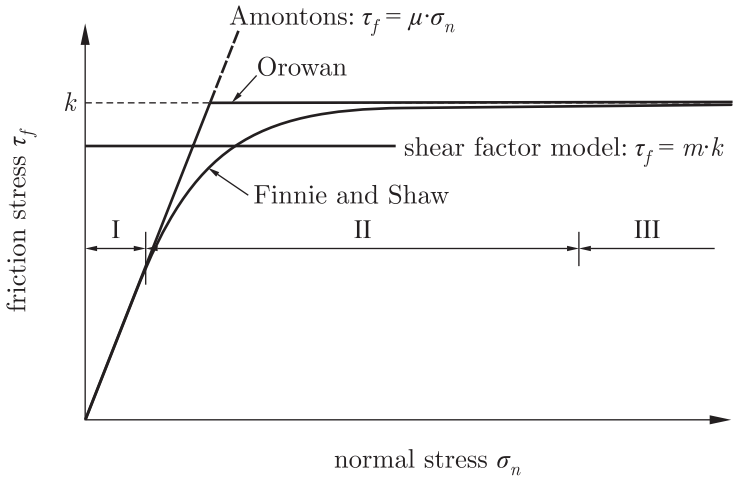

Figure 2.15: Comparison of friction models: Amontons assumed the friction stress to be proportional to the normal pressure, whereas a constant shear stress was postulated in the shear factor model. Orowan [101] combined both models, resulting in a sharp transition from one into the other. Finally, Finnie and Shaw [28] found the friction stress to increase proportional to the applied normal pressure at light loads and to reach the shear yield strength k asymptotically when the normal load was increased.

the experimental findings.

The *physical models* assume that friction can only take place in the real contact area and is therefore proportional to A_r. Thus, the evolution of the contact area has to be determined in dependence on the applied normal load. In the real contact area, friction is mostly described by the constant shear factor model. The friction stress τ_f in the system is then expressed by:

$$\tau_f = m \cdot k \cdot \alpha, \tag{2.13}$$

with m the shear factor, k the shear yield strength of the weaker friction partner and α the relative contact area $\alpha = A_r/A_a$. In most models, m has to be determined experimentally, where the load-compliance-law is calculated either by means of the slip-line theory or by employing numerical simulation methods. Both approaches take material properties and asperity shape (asperity slope) into consideration. However, the analysis are mostly constrained to plain-strain problems.

The most popular physical model based on a slip-line solution is the *general friction law* developed by Wanheim, Bay and colleagues [58, 61, 104–106]. For the deformation of surface asperities, taking friction into consideration by assuming a constant friction stress, the slip-line fields shown in Figure 2.11 were suggested. To determine the real area of contact and the friction stress as functions of the normal pressure and the friction factor, slip-line fields were drawn for various shear factors and compression levels. From measuring the resulting slip-line fields and using geometrical relations, the corresponding

values of α, m and σ_n were calculated assuming ideal plastic material behaviour. Their results are shown in Figure 2.16. Additionally, Wanheim [61] and Nellemann et al. [107]

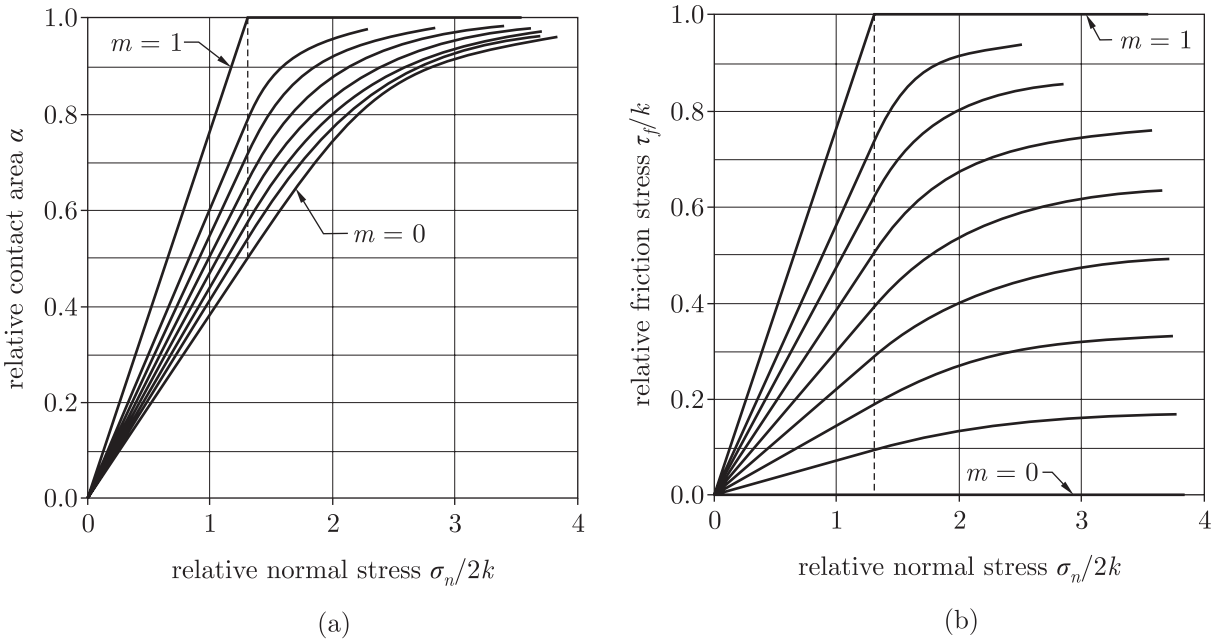

Figure 2.16: Evolution of the contact area (a) and the friction stress (b) in dependence on the normal stress and the friction factor m as determined by means of the general friction law [61].

made approaches to take the role of trapped lubricant into consideration. Later, Bay [106] reports an analytically approximated expression for the graphically estimated friction curves. The limit of proportionality (τ_f', σ_n') is expressed by [108]:

$$\frac{\tau_f'}{k} = 1 - \sqrt{1-m} := A, \tag{2.14}$$

$$\frac{\sigma_n'}{k_f} = \frac{1 + \frac{\pi}{2} + \arccos(m) + \left(1 - m^2\right)^{\frac{1}{2}}}{\sqrt{3} \cdot \left(1 + \sqrt{1-m}\right)} := B, \tag{2.15}$$

where k is the shear yield stress, k_f is the yield stress and m is the shear factor. The region where the friction stress τ_f is proportional to the normal stress σ_n is given by:

$$\frac{\tau_f}{k} = \left(1 - \sqrt{1-m}\right) \cdot \frac{\sigma_n}{B \cdot k_f}\ , \tag{2.16}$$

and the transition from a linear τ_f-σ_n - dependency to a constant friction shear stress is expressed by:

$$\frac{\tau_f}{k} = A + \left(m - A\right) \left[1 - \exp\left(\frac{A \cdot \left(1 - \frac{\sigma_n}{B \cdot k_f}\right)}{m - A}\right)\right]. \tag{2.17}$$

Neumaier [63] determined the load-compliance relation by means of numerical simulation: He modeled the real surface of the workpiece by taking profilometer traces and performed a finite element analysis of surface conformation in MSC.AutoForge assuming a flat tool and plane strain conditions. From his results, Neumaier parameterised an equation proposed by Li and Sellars [48] for the description of the load-compliance relation[1]:

$$\alpha = \left[1 - \exp\left(-1 \cdot \frac{\sigma_n}{k_f}\right)\right]^{1{,}5}. \tag{2.18}$$

For the estimation of the friction stress, an equation suggested by Kaminsky [11] was engaged leading to:

$$\tau_f = m \cdot k \left[1 - \exp\left(-1 \cdot \frac{\sigma_n}{k_f}\right)\right]. \tag{2.19}$$

However, this relation holds only true for the specific tribosystem investigated in [63]. Neumair's approach prevails over the Wanheim model because the real mechanical properties of the friction partners as well as their real surface conditions are considered.

Approaches based on a smoothing of Orowan's model [101] (see Figure 2.15) without any physical justification are classified as *mathematical models*. For example, Doege et al. [110] utilised an equation originally developed by Betten [111] for the characterisation of the behaviour of linear-elastic non-hardening materials. For the application as friction model, Betten's relation is given by:

$$\tau_f = k \cdot \sqrt[n]{\tanh\left[\left(\frac{\mu \cdot \sigma_n}{k}\right)^n\right]}, \tag{2.20}$$

where n is a parameter regulating the transition from Amontons' friction law to the constant shear model.

[1] Similar relations were proposed by Levanov et al. and Stephenson [109].

Empirical friction models are based on empirical equations, whose parameters are identified by friction tests. Representatives of this group are Hemyari [112], who formulated constitutive equations based on dimensional analysis, Ceretti and Giardini [113] who based their relations on surface roughness and Doege et al. [3, 4, 89, 114].

2.5.3 Comparison of Friction Models in Bulk Metal Forming

For the mixed lubrication condition often prevailing in metalworking, the coefficient of friction μ is a useful measure because it relates the properties of the interface to the local or average normal stress, although this representation is not physically exact [14, 115]. However, when the normal pressure exceeds the yield strength and completely sticking of an ideal plastic material is assumed, the workpiece shears-off in its bulk and the shear stress (and therefore the friction stress) remains constant. In oder to meet equation (2.8), the friction coefficient has to decrease although the friction condition does not change and the model fails.
When Amontons' friction law is applied in numerical simulation of forming processes, the friction stresses (and therefore the loads) are overestimated [116], this is, the result of the simulation is on the safe side. On the other hand, when this law is used in the evaluation of friction tests performed under forming conditions, friction is easily underestimated.

The concept of a constant interface shear factor m refers the friction behaviour to the shear strength of the weaker friction partner, what is physically plausible only in the case of sticking ($m = 1$) [14, 115]. Generally, interface films are best described by their flow strength τ_I, but in the case of an interface composed of a softer metal or solid lubricant, the shear factor model is often preferable for simplicity of analysis. However, when τ_I depends on the interface pressure or the forming velocity, m becomes meaningless.
In metal forming operations the constant shear factor model prevails over Amontons' friction law because of its better representation of the friction conditions under severe loads [117]: Löwen [118] performed cylinder compression tests without lubrication and with solid lubricants and found no proportionality of normal stress and friction stress, respectively. From this observations, he concluded, that Amontons' law is not suited to describe friction in forging processes and the shear factor model should be applied. Similar results are reported by Male [119] who performed ring-compression tests with graphite-lubrication.

Several authors compared different friction models with regard to their applicability in numerical simulation. Petersen et al. [116] compared the experimentally determined ma-

terial flow during upsetting aluminium specimen under dry friction and that predicted by finite-element simulation. In their analysis, the law of constant friction and the general friction law were applied. They concluded, that the latter is more adequate for modeling the boundary conditions at the tool-workpiece interface when the nominal surface pressure over a considerable part of the contact area assumes values smaller than the yield stress.
In order to examine five different friction models (including Amontons' law, the shear factor model and the general friction law), Tan [99] performed upsetting tests on aluminium specimen and carried out finite-element analysis. By comparing the results of simulation and experiments, friction parameter values for the regarded process were obtained. Tan found, that all of the chosen friction models worked with no significant difference. In fact, the chosen friction models were very dissimilar; calibration curves applying each of the models in finite-element calculations, however, were obtained to agree with experimental data by adjustment of the friction factor magnitude. Based on these observations, it was hard to tell which friction model was of higher accuracy in finite-element simulations.
Hayhurst and Chan [120] correspond with Tan stating that the precise choice of friction model does not dominate, instead, the important feature is the accurate calibration of the model for the correct conditions.

2.6 Friction Tests for Forging Operations

In the experimental determination of friction in metal forming, direct and indirect methods are distinguished: In *direct testing methods*, the friction stresses are acquired by using measurement pins locally in the tool-workpiece-interface, whereas friction is determined via a deduced quantity such as force or deformation and thus averaged on the entire tool-workpiece-interface in *indirect experiments* [121]. Due to the character of the tests, Bederna [122] speaks of *local* and *integral* procedures. Detailed overviews on friction testing under metal forming conditions are given by Bühler and Löwen [121], Schey [25] and Dannenmann et al. [14]; Figure 2.17 shows a classification of state-of-the-art friction tests for forging processes.

2.6.1 Direct Testing Methods

Commonly, local contact stresses in the tool-workpiece interface are acquired by means of measurement pins that are mounted in the tool (see Figure 2.17 (a-c)). Van Rooyen

and Backofen [123, 124] were the first who proposed the use of measurement pins in the analysis of friction in rolling processes by applying separate pins for acquiring normal and tangential stresses, respectively (a). State-of-the-art methods mostly employ combined pins that allow the determination of normal and tangential stresses at the same place. The main disadvantage of method (b) is the falsification of results by workpiece material penetrating the gap between pin and tool, the different stiffness of pin and tool and thus the impact on the material flow at the measuring point [125]. At least the problem with penetrating material can be counteracted by engaging the assembly (c), where the cylindrical top of the pin, that has to be surrounded by a gap in order to allow tangential deflection, is replaced by a sphere, that is rotated and not deflected by tangential stresses. Löwen [118] and Bernhardt [75] employed such pins in their investigations.

2.6.2 Indirect Testing Method

The group of indirect testing techniques can be subdivided in methods, where friction is determined by specimen deformation and methods, in which friction is determined by force or torque measurements.

In testing methods, where friction is estimated by the specimen's deformation, the final shape of the workpiece is determined for the decided process and various friction conditions by means of theoretical or numerical analysis. From these results, nomograms are drawn relating a characteristic dimension of the deformed workpiece to a friction condition (commonly expressed in terms of the friction coefficient μ or the shear factor m). Then, the experiments are simply evaluated by measuring the characteristic dimension and identifying the corresponding friction value by look up in the nomogram.
These methods are very popular in industrial practice. The tests are easy to perform and represent the real process very well. However, most of the parameters can not be controlled independently from each other, and no stationary state is present. Moreover, sliding distances are quite short. Due to this, these kinds of tests are usually used in comparative investigations (e.g. assessment of different lubricants) or in the calibration of numerical simulation (i.e. to make the simulation result look like the experimental result by the calculation of a "friction coefficient" that compensates all uncertainties of modeling).
The simplest test in this category is the barreling compression test proposed by Ebrahimi and Najafizadeh [126], where friction is determined by the maximum diameter after upsetting (see Figure 2.17 (d)), while the most popular method is the ring-compression test.

This test was developed by Kunogi [127, 128] and Male and Cockcroft [129]; friction is determined by the change of the inner diameter of a compressed ring[1] (see Figure 2.17 (e)). This method was further developed and applied by numerous authors [8, 92, 131–136]. Another approach was made by Schey and Lonn [134], Wilson and Lak [137] and other authors: they determined friction by means of plain-strain compression tests[2] (see Figure 2.17 (f)).
In Figure 2.17 (g), the spike test utilised for lubricant characterisation e.g. by Sheljaskow [139], Sofuoglu and Gedikli [140] and Kok and Gankema [141], is presented. Here, friction is related to the height of the extruded pin. Figure 2.17 (h) shows the double-cup-extrusion test as depicted by Kim et al. [142] and Gariety et al. [143], where friction is estimated by calculating the height ratio of the cups.

Indirect experiments, in which friction is determined from force or torque measurements, allow a physical interpretation of the tribological interactions in the tool-workpiece interface [17]. Moreover, the parameters can be set and varied independent on each other. This group of experiments can be subdivided in tests with instrumented toolkits and tests where the tools perform a normal and a tangential movement (upsetting sliding tests).
Bederna [122] performed cylinder compression tests where the lower tool was equipped with strain gauges in order to measure the friction stress in the tool-workpiece interface; the normal load was acquired by means of a load cell (see Figure 2.17 (i)). Later, this approach was further developed by Doege et al. [3, 4, 89, 114]: They designed a model experiment to determine friction and heat transfer in backward-can-extrusion by means of a lower punch equipped with strain gauges and thermocouples (see Figure 2.17 (j)). Finally, Wang and Ramaekers [144] estimated friction in plain-strain upsetting by measuring the compression force and the force at the section plane by load cells (see Figure 2.17 (k)).

The group of upsetting sliding tests can be further subdivided in *shift compression tests*, where tool and specimen are not in contact over the entire sliding surface at the same time, and *twist compression tests*, where contact over the entire sliding surface at the same time is achieved.
The simplest shift compression tests is the pin-on-disc test as usually used to investigate tribological interactions at low normal pressures (see Figure 2.17 (l)). However, Kawai and Dohda [145], Attanasio et al. [146] and Ceretti and Giardini [113] have performed pin-on-disc experiments under forming conditions and Vergne et al. [147] performed pin-

[1] A detailed description of the test and a historical review is given by Male [119, 130].

[2] The determination of friction by means of plain-strain compression tests is discussed and reviewed by Uyyuru [138].

on-disc tests to measure friction under hot rolling conditions. Hemyari [112] and Groche and Kappes [2] utilise a sliding-upsetting test, in which at first a cylindrical specimen is compressed with a special tool in order to obtain a homogenous surface expansion on the bottom side of the specimen and then the lower tool is moved and the sliding force is measured (see Figure 2.17 (m)). Lately, two different research teams [148, 149] evaluated lubricants by performing a sliding-upsetting test proposed by Guérin et al. [150], where relative motion is applied on an indenter penetrating a cylindrical billet (see Figure 2.17 (n)). This is, in principle, similar to strip-drawing as utilised by Pawelski [151] and Ngaile et al. [152] (see Figure 2.17 (o)).

The simplest twist compression test is the ring-on-disc test as introduced by Schey and Lonn [134], where the torque transferred from the tool to the specimen is measured (see Figure 2.17 (p)). This test was further developed and applied by several other authors [97, 153–156]. An interesting version of the ring-on-disc test was proposed by Hansen and Bay [157]: They performed backward-can-extrusion followed by a rotation of the container, thus taking surface expansion into account (see Figure 2.17 (q)).

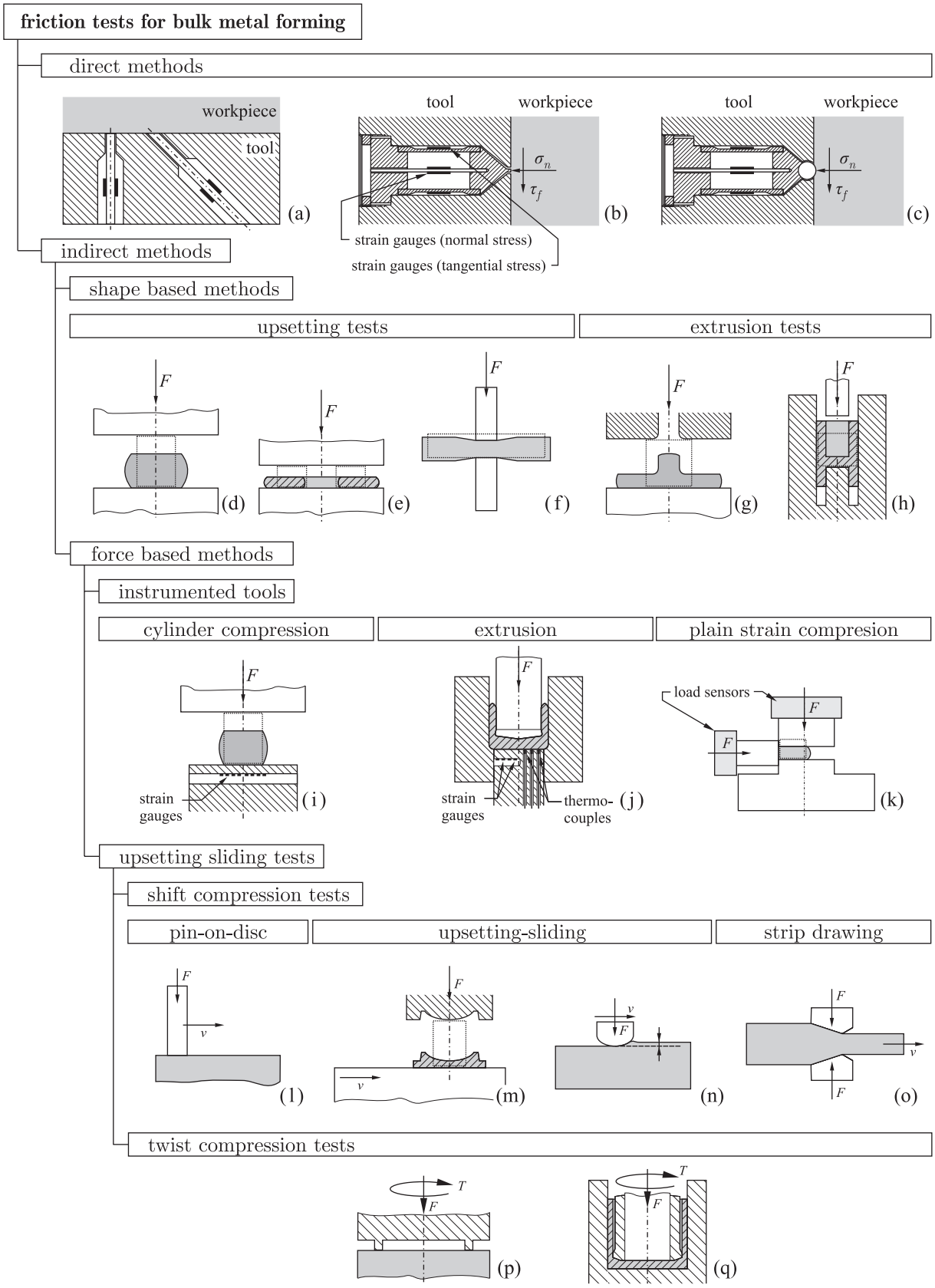

Figure 2.17: Classification of friction tests for bulk metal forming.

3 Experimental Work

3.1 Conceptional Aspects of the New Testing Device

The tribological conditions in forging operations are characterised by high contact pressures (many times over the workpiece yield stress), high surface enlargement and -modification and high relative velocities as well as high temperatures and temperature gradients. However, the sliding distances are comparatively short.
The main criterion for each model experiment is that its results are transferable to the real process. Thus, besides the friction partners also the loads and contact conditions have to represent the real process. An ideal device for friction determination simulates pressures, temperatures, sliding velocities and contact time of the real process. Moreover, the surface expansion of the plastic friction partner is realised [78, 117].
Doege et al. [158] compared state parameters of model experiment (cylinder compression) and real process (precision forging). They found, that under the same initial conditions, the state parameters of cylinder compression were of significantly lower range than these of precision forging. In particular, the relative velocities in the tool-workpiece interface varied considerably from each other. From their findings, the authors concluded that a modeling of the "outer parameters" as materials, temperatures and tool velocity is not sufficient in order to represent the real process.
An independent setting of the process-related parameters has to be ensured due to the wide range of contact conditions present in the forging of complex components [79]. Furthermore, the contact area has to be large and homogeneous enough to allow reliable measurements and should not change during the test. Finally, steady lubrication conditions (no lubricant exchange, etc.) in the die-workpiece interface are required.
Concerning a physical interpretation of tribological phenomena, Messner et al. [17] advice the performance of friction tests that allow a measurement of normal and tangential forces in the plane of the tool-workpiece interface. In all tests of these category, relative motion of tool and workpiece is enforced and regions of sticking, that are typical for impression forging processes, can not be formed. In contrast to Bühler and Löwen [121], Melching [21] assumes the friction conditions to be not seriously affected by enforced sliding (and prevention of sticking) because friction is of importance only in areas of relative movement.

The ring-on-disc test commonly applied in the analysis of friction under low normal pressures was found to meet most of the stated demands properly. It allows an independent variation of interface pressure, relative velocity and movement as well as temperatures.

Due to the simplicity of the test principle, it was decided to utilise this method for the actual investigation. However, surface enlargement is not considered in the original configuration (see Figure 2.17 (p)), and although the specimen deforms plastically under sufficiently high pressures, the operation has the character of hardness testing and the surface roughness remains almost unchanged [159]. A method to overcome this problem was presented by Hansen and Bay [157] by combining backwards can-extrusion with twist-compression in oder to characterise lubricants for cold forging of steel (see Figure 2.17 (q)).

The new testing device to be developed should allow investigations under cold forging, warm forging and isothermal forging conditions of aluminium alloys, and to model the real process as exact as possible the usually disposed graphite-based lubricants should be also applied in the model experiments. This means that the construction had to withstand high temperatures, high forces, high torques and rough environmental conditions. In order to enable reproducible results, the testing sequences (i.e. heating, application of lubricant and testing) should be controlled automatically. Last but not least a cost-effective prototype machine should be designed to clarify the technical feasibility.

3.2 Experimental Setup

3.2.1 The Rotary Forging Tribometer

Figure 3.1 (a) shows the Rotary Forging Tribometer (RFT) that was designed and manufactured at the Chair of Metal Forming under direction of the author [160]. The apparatus consists of a press, a rotational device, the friction facility, a lubricant spraying device, an inductive heating system and a smoke venting system.

The *press* supplies the normal force for the tests. Its frame is made of an upper and a lower cross-head connected by two side columns. The working space of the press is restricted by a safety gate in the front and guard plate in the back of the frame. The upper cross-head houses a hydraulic cylinder, whose force is controlled manually by means of a relief valve, and the lower cross-head mounts the rotational device and the friction facility.
The *rotational device* supplies the circular motion for the tests. It consists of a servo motor controlled by a servo inverter and a bevel gear system flanged to the lower press cross-head.
Figure 3.1 (b) shows the *friction facility* which is mounted in the working space of the press. Its bottom plate is connected to the lower cross-head, where the circular motion is

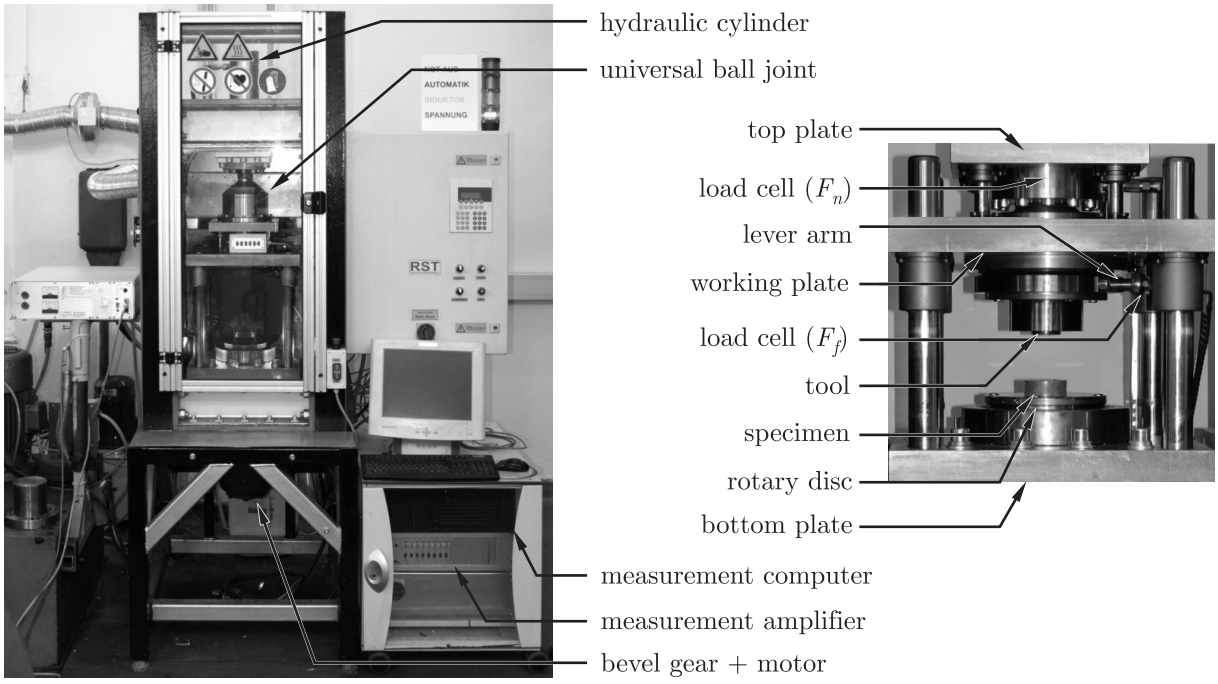

Figure 3.1: The apparatus used in the investigations: (a) The Rotary Forging Tribometer (RFT) and (b) friction facility with their main components.

supplied from the bottom side by means of a shaft connected to the bevel gear. The top plate is linked to the push rod of the hydraulic cylinder via a universal ball joint. Bottom plate and working plate are supported torsionally stiff by four guide rods that transfer the frictional torque from the working plate onto the bottom plate. The specimen (workpiece) is mounted on a rotary disc and transmits the frictional torque to the pivot-mounted ring-shaped tool. The tool is supported by a load cell via a lever arm which enables an accurate measurement of the frictional torque. The acquisition of the compression force is realised by another load cell, the rotational speed of the specimen is calculated from the speed of the servo motor. Frictional speed as well as interface pressure are dependent on the tool geometry. The specimen is brought to forging temperature by means of an inductive heating system, whereas the tool is heated by a heating sleeve.

The *inductive heating system* consists of a frequency generator and the heating station that takes up the induction coil. The heating station is mounted on a lifting table at the back side of the press. It can be lifted for insertion and removal of specimen.

The lubricant is applied onto the tool by an automatic *lubricant spraying device* that allows a reproducible dosage. The device is equipped with a storage tank and an agitator for continuous mixing.

The testing device is controlled by a programmable logic control unit (PLC); the data

acquisition is realised by a measurement amplifier that is connected to a commercial personal computer[1].

The tribometer has a maximum upsetting force of approximately 150 kN and provides a maximum torque of more then 800 Nm on the rotary disc. The rotational speed can be up to 1.7 s^{-1} and the sliding distance itself is not constrained by the testing device. The maximum temperature of the specimen is 1200 °C, the maximum temperature of the tool is 450 °C. The temperatures can be kept constant in an interval of ± 2.5 °C.

3.2.2 The Data Acquisition System

Following the concept of the new device, primarily normal and tangential forces have to be acquired. As described in Section 3.2.1, the normal force is measured directly at the working plate, whereas the tangential force is acquired by means of the configuration shown in Figure 3.2. From the force F_s supported at the distance x_s from the center of

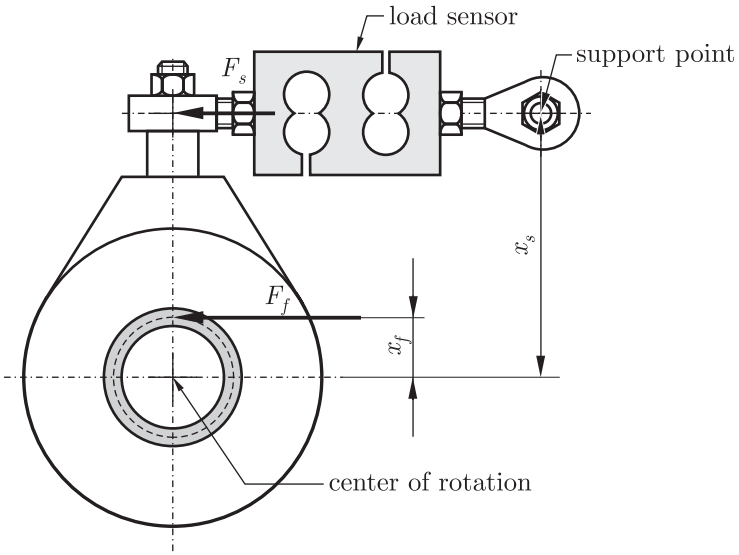

Figure 3.2: Measurement of the friction force.

rotation, the averaged frictional force F_f at a distance x_f is calculated as:

$$F_f = F_s \cdot \frac{x_f}{x_s} \; . \tag{3.1}$$

[1] The data acquisition system is described in more detail in Section 3.2.2.

Additionally to the forces, the acquisition of the sliding distance was demanded. Due to the fact that the servo motor is already equipped with a resolver, and the engine speed can be obtained as analog output directly from the servo inverter, no additional angular sensor was necessary.

The cycle time of the PLC's highest task class was 10 ms (corresponding to a clock rate of 100 Hz). This was decided to be sufficient for the control of the RFT because the time critical parameters normal force and sliding speed were controlled externally by means of a pressure relive valve and the servo inverter[1], respectively. However, for data acquisition, a sampling rate of 100 Hz was too low regarding the fact that the contact time of forging processes is commonly short and friction in the beginning of sliding is of interest. Due to these considerations, the measurement chain was realised using an external data acquisition system as shown in Figure 3.3. The engaged measurement system[2] had a total

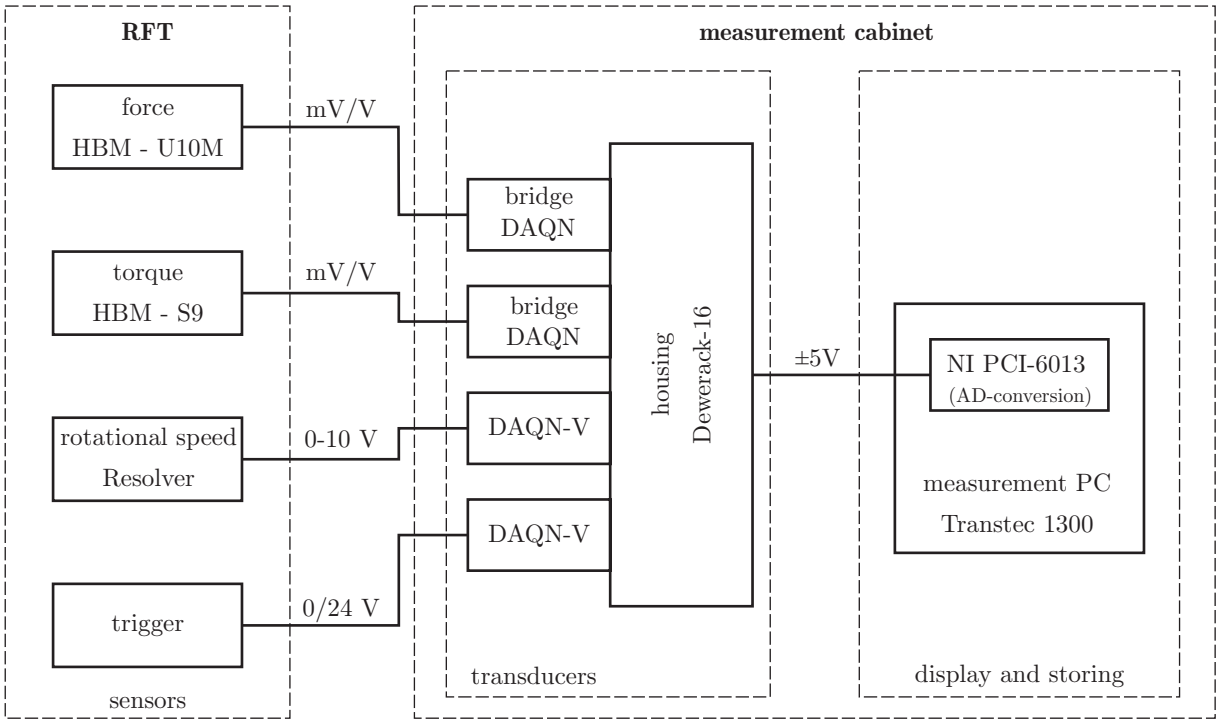

Figure 3.3: Measurement chain.

sampling rate of 200 kS/s corresponding to a sampling rate of 66.7 kHz per channel when

[1] The cycle time of the servo inverter was 1 ms.

[2] A *DEWE-Rack 16* in combination with *DAQN-Bridge* and *DAQN-V* transducer modules (all DEWETRON, Austria) was used as measurement amplifier. The data were acquired by means of a *NI PCI-6013* measurement board (National Instruments, USA) with a resolution of 16 bit.

three channels were active. However, exact triggering was required in order to minimise the amount of data and thus, a forth channel had to be engaged to start and stop the data acquisition, resulting in a maximum sampling rate of 50 kHz per channel. The trigger was realised by means of a mechanical switch at the bottom plate and an adjustable activator at the working plate of the friction facility. The activator was adjusted in a way that the switch was pushed and started the measurement short before the tool contacted the specimen.

For the documentation, visualisation and storage of the data and the control of data acquisition, a LabVIEW^{TM}-routine was developed by the author. When the measurement was activated in the routine, the system waited for the trigger signal. After triggering, the force channels were reset to zero and data acquisition was started. The data were online stored to the specified destination and visualised in graphs as function of the elapsed time.

3.3 Preliminary Tests

3.3.1 Cold Forging Tests

In a first trial the functionality of the tribometer was tested by performing classical ring-on-disc experiments under cold forging conditions. The aim of the investigation was to determine the limits of the new apparatus in terms of pressure and speed control, and to assess its applicability in the acquisition of reliable and reproducible data. Moreover, a suitable test procedure had to be found regarding the order of the sliding and the upsetting phase.

3.3.1.1 Toolkit and Specimen Geometry

Figure 3.4 shows the toolkit and specimen geometry used in the cold forging tests. The outer ring diameter of the tool was $d_O = 40$ mm and an inner ring diameter was $d_I = 36$ mm. The specimen had cylindrical shape and was placed on the rotary disc by means of a centering pin and an eccentric actuator pin. The workpieces were manufactured of extruded aluminum alloy AA6082, where the tool was made of stainless martensitic chromium steel 1.4122, which had good wear resistance and friction properties.

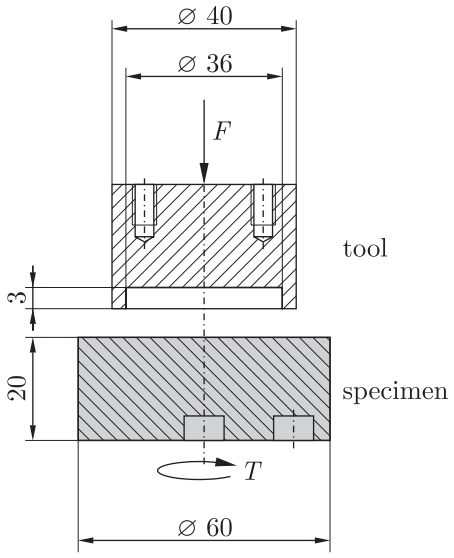

Figure 3.4: The toolkit used in the preliminary cold forging tests.

3.3.1.2 Execution of the Tests

As already stated, a suitable test procedure had to be found regarding the order of sliding and upsetting phase. Basically, two different test procedures can be performed with the rotational forging tribometer:

1. The specimen is upset at the beginning of the test and then the rotation is applied while the normal pressure is kept constant (upsetting-sliding).

2. The rotation is started at the beginning of the test and then upsetting is performed while the sliding velocity is kept constant (sliding-upsetting).

In upsetting-sliding experiments, the role of normal pressure control is of minor importance; when set in the beginning of the test, it is almost constant during sliding. The sliding velocity, in contrast, has to be adjusted as quickly as possible in order to enable friction estimation at stationary conditions. To determine the influence of the sliding velocity on upsetting-sliding tests, four experiments were executed at constant normal pressure where the friction velocity was set to different levels in the range between 22.5 and 180 mm/s.
On the other hand, normal stress is the dominating parameter acting on sliding-upsetting experiments. In order to evaluate this influence, four experiments were performed at constant friction velocity, and the pressure was raised in steps from 30 MPa up to 430 MPa. In addition, upsetting-sliding was also executed at different pressures, and sliding upsetting was performed at different sliding speeds. The parameters for the experiments are

illustrated in Table 3.1. For the lubrication a commercial lubricant based on mineral oil was used. The friction length was 80 mm and all experiments were performed at room temperature. Two specimens were tested for each parameter set.

Table 3.1: Parameters used in the preliminary cold forging tests.

no.	series	program	normal pressure [MPa]	velocity [mm/s]
1	1	1. upsetting 2. sliding	430	22.5
2				45.0
3				90.0
4				180.0
5	2	1. upsetting 2. sliding	30	90.0
6			175	
7			340	
8			430	
9	3	1. sliding 2. upsetting	30	90.0
10			175	
11			340	
12			430	
13	4	1. sliding 2. upsetting	430	22.5
14				45.0
15				90.0
16				180.0

3.3.1.3 Evaluation and Results

The experiments revealed, that the intentional function of the testing device could be completely met and the system served its purpose. The tests were evaluated by comparing their measurement curves. Figure 3.5 shows the developing of sliding speed and normal pressure in upsetting-sliding and sliding-upsetting experiments, respectively. From these data, the test procedure for further investigations had to be decided. Additionally, Figure 3.6 gives the friction stress as function of the sliding distance and the normal pressure for upsetting-sliding.

The decision on the test procedure was based on two major demands: On the one hand, the test should allow an exactly physical interpretation of the tribological interactions in the tool-specimen interface, and on the other hand, the control system had to cope with the procedure. In fact, at very low sliding speeds, both versions of the test are equal. However, at higher velocities, the intrinsic differences become visible (see Figure 3.5): In

the case of upsetting-sliding, different normal loads have no effect on the control mode of the servo inverter, the curves are congruent for all stress levels (Figure 3.5 (a)).

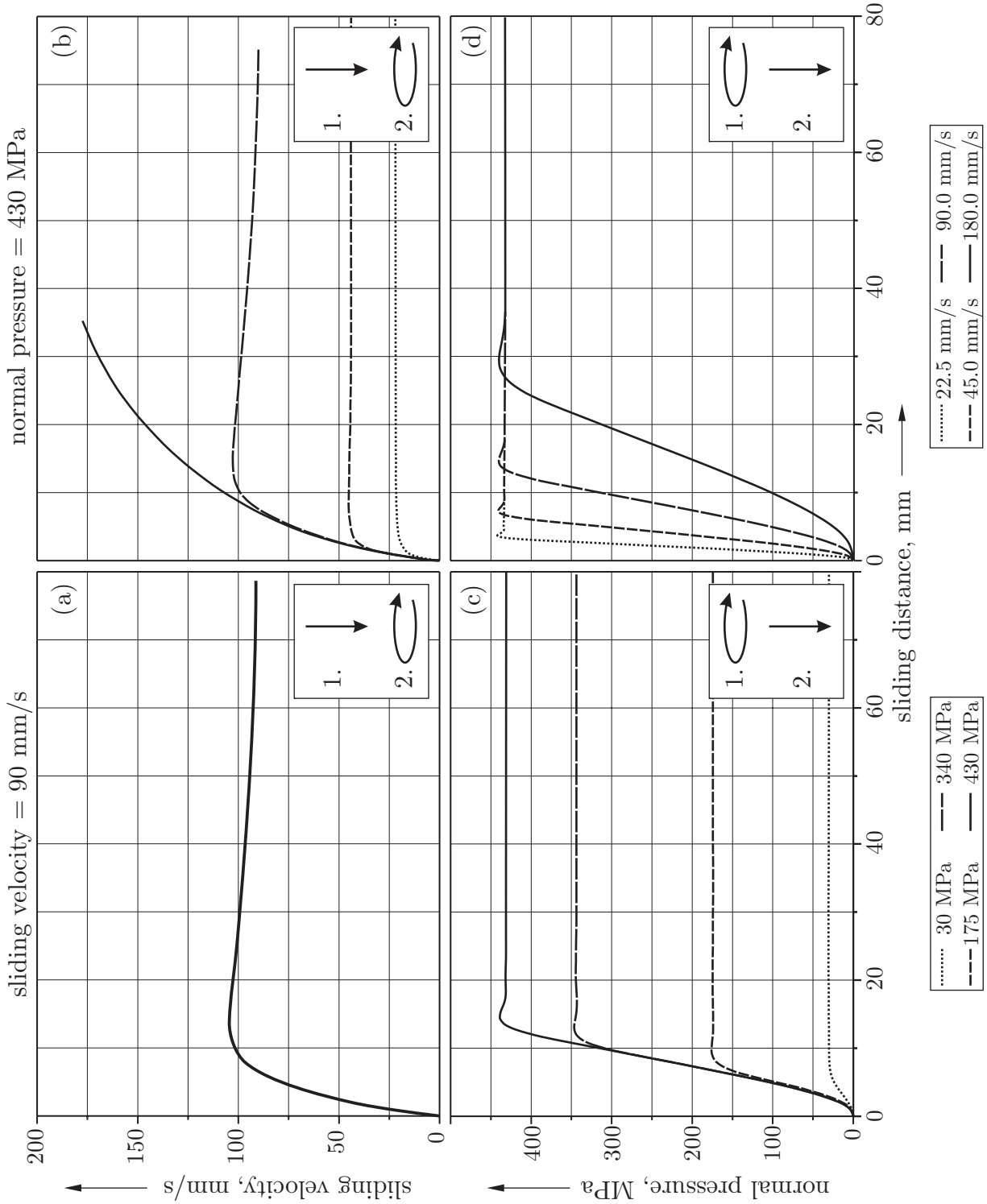

Figure 3.5: Results of the preliminary cold forging tests. The test procedure is indicated by pictographs. From these data, the test procedure for further investigations had to be decided.

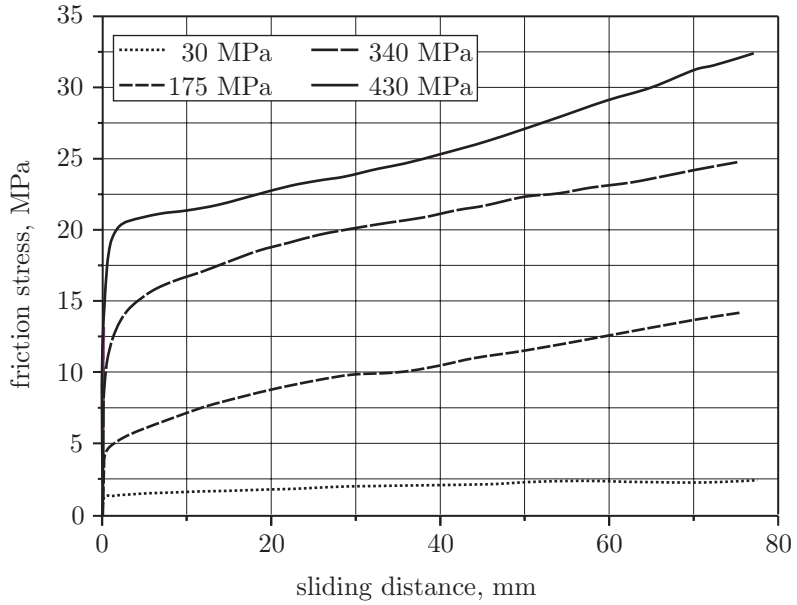

Figure 3.6: The friction stress of the preliminary cold forging tests as function of the sliding distance and the normal pressure for upsetting-sliding.

However, one has to note that the desired velocity is not obtained during the sliding distance due to initial overshooting. Regarding Figure 3.5 (b), it is seen that the amount of overshooting depends on the desired sliding velocity. While there is no overshooting found at speeds of 22.5 and 45 mm/s, the velocity of 180 mm/s can not be reached in the test. Under this consideration, the influence of the inertia of the engine on the sliding velocity is significant and can lead to wrong measurements, especially at short sliding distances and high speeds.

Figure 3.5 (d) is the equivalent of sliding-upsetting to Figure 3.5 (a) in upsetting-sliding. It is easily seen that the desired pressure is adjusted very well, but the single curves are not congruent. This is due to the control behaviour of the pressure relief valve: It takes always the same time to adjust the pressure. Thus, if the sliding velocity is enhanced, the decided stress is obtained at higher sliding distances. The behaviour at different normal loads (Figure 3.5 (c)) is comparable to that shown in Figure 3.5 (b), however, in sliding-upsetting the desired stress is exactly achieved also under high loads.

Regarding the physical interpretability of the experiments, at most one – if any – parameter should vary during the test. This condition can be only met with upsetting-sliding experiments, that are only dependent on the desired velocity (in contrast sliding upsetting tests are dependent on desired pressure and velocity). Moreover, it was shown that the influence of the normal pressure on friction is more pronounced than the influence of sliding velocity [161].

Due to these considerations it was decided to perform upsetting-sliding experiments in the further investigation thereby restricting the maximum rotational speed to approx. 0.75 s^{-1} (corresponding to 90 mm/s with the toolkit shown in Figure 3.4).

3.3.2 Warm Forging Tests With Classical Ring-on-Disc Configuration

3.3.2.1 Toolkit and Specimen Geometry

Figure 3.7 shows the toolkit and specimen geometry used in the preliminary warm forging tests. The outer ring diameter remained the same as in the cold forging tests (d_O = 40 mm), but the inner ring diameter was set to d_I = 32 mm because of the lower yield stress of heated aluminium. The specimen had the same shape and was made

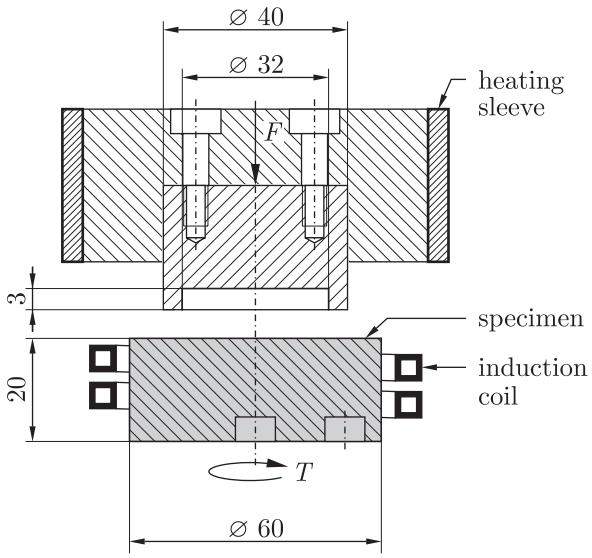

Figure 3.7: The toolkit used in the preliminary warm forging tests with classical ring-on-disc configuration.

of the same extruded aluminium bar as in the cold forging tests. The tool was made of hot work tool steel steel 1.2344 and hardened to 55 HRC.

3.3.2.2 Execution and Results of the Tests

The specimen were heated to 200, 300 and 400 °C, respectively, and the tool temperature was 250 °C. The normal pressure was varied from 95 MPa up to 230 MPa, the average

velocity was set to 5 mm/s and a zinc compound was applied as lubricant.
It was observed that the tool sank into the specimen at workpiece temperatures greater than 300 °C after short sliding distances (10–20 mm) due to frictional heating in the contact zone and the specific flow curve of warm aluminium alloys (see Section 2.4.4 and Figure 3.8). From these experiments it emerged that warm forging experiments with aluminium alloys have to be performed with entrapped specimen in order to ensure constant conditions during the tests.

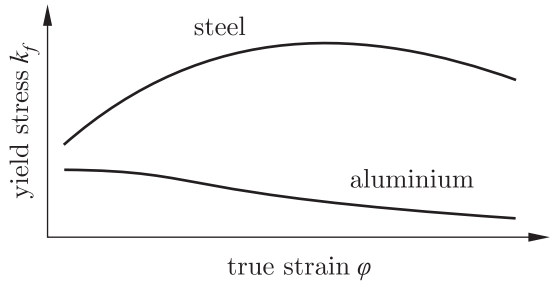

Figure 3.8: Qualitative flow curves for hot forging of steel and aluminium: In contrast to the flow stress of steel, the flow stress of aluminium during hot forming shows no strain hardening.

3.3.3 Warm Forging Tests With Entrapped Specimen

3.3.3.1 Toolkit and Specimen Geometry

Figure 3.9 (a) shows the new developed toolkit with entrapped specimen used in the further investigations. The ring-shaped workpiece is placed in the cavity of a container and compressed by an annular tool with the same inner and outer diameter as the specimen ($d_O = 40$ mm, $d_I = 30$ mm). Sliding on the bottom face of the workpiece is prevented by preparing the bottom of the cavity with radial ridges, and the container is split in order to allow easy removal of the tested specimen. The temperatures of die and workpiece are measured via thermo couples. As in the previous tests, tool and specimen are made of hot work tool steel 1.2344 and AA6082, respectively.
This toolkit was also modified in a similar way as proposed by Hansen and Bay [157] in order to give a defined surface expansion (see Figure 3.9 (b)), but it revealed that this configuration did not work with hot aluminium due to the problems discussed above.

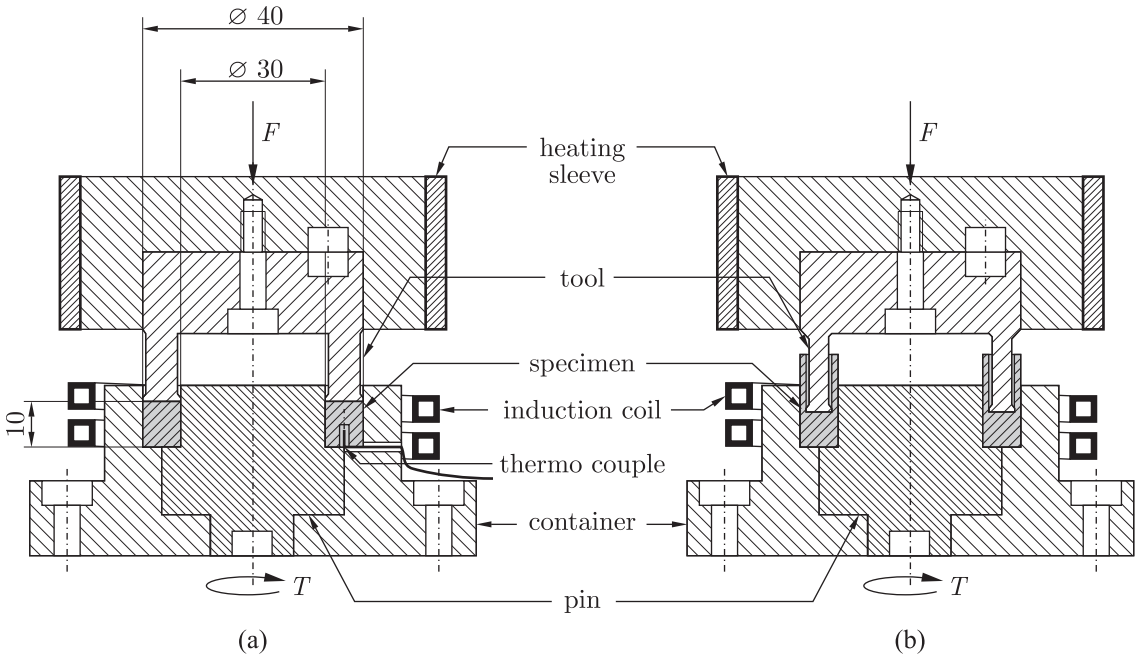

Figure 3.9: Toolkit used in the preliminary warm forging tests with entrapped specimen (a) and modification for defined surface expansion (b). It revealed that configuration (b) did not work with hot aluminium due to unsteady conditions during the test.

3.3.3.2 Execution of the Tests

First trials with the closed-die toolkit verified the principal functionality of the device, however, preliminary test series had to be performed to control the tests properly even under warm forging conditions. Therefore, the evolution of friction stress with increasing normal pressure with different lubricants was analysed in the following way: Sand-blasted specimen were compressed by a polished tool at 10 different load levels starting from 20 MPa to 180 MPa, were the pressure was increased without changing the workpiece.
In order to investigate differences of the lubricants given in Table 3.2, two test series were performed applying the lubricants in their recommended dilution ratio. In addition, a third series was conducted using lubricant diluted a week before to analyse the effect of aging.

Table 3.2: Lubricant test matrix for preliminary warm forging tests.

	lubricant type	rec. dilution ratio
A	dispersion of graphite in water	1:15
B	dispersion of graphite in water	1: 7

Tool and workpiece temperature were set to 250 °C and 450 °C, respectively, sliding was performed at 40 mm/s and the relative displacement was 70 mm. The series were repeated three times. For each new specimen, the tool was prepared with grit 800 sandpaper and 3 µm polishing suspension.

The experiments were performed in the following way: First, the tool was brought to operating temperature. When the testing sequence was started by the PLC, the specimens were heated, and the final temperature was kept constant for 180 s in order to allow for temperature equalisation. Then, the lubricant was applied by the automatic spraying device. It was found that the application should be done in several steps (e.g. 4×0.3 s) to give the carrier enough time for evaporation. In the real process, the dies are very massive, thus the cooling effect of the lubricant is limited and carrier evaporation is ensured. However, in the experiments, the cooling effect on the tool is significant due to its exposed position, and time is needed for temperature equalisation. After lubricating, the execution of the test itself was started employing the upsetting-sliding sequence.

3.3.3.3 Evaluation and Results

The evaluation of the experiments was performed in two steps (see Figure 3.10):

1. First, the stationary region of the experiment was determined from the velocity curve: Constant conditions were assumed in the interval $[t_b$–$t_e]$ where the actual velocity at time step i was equal to or greater then the reference velocity ($v_i \geq v_{ref}$).

2. In the stationary region, the mean values of normal pressure σ_n, friction stress τ_f and friction coefficient μ were calculated by the following equations:

$$\overline{\sigma}_n = \frac{1}{f \cdot (t_e - t_b)} \sum_{i\,=\,t_b}^{t_e} \sigma_{n,i} \ , \tag{3.2}$$

$$\overline{\tau}_f = \frac{1}{f \cdot (t_e - t_b)} \sum_{i\,=\,t_b}^{t_e} \tau_{f,i} \ , \tag{3.3}$$

$$\overline{\mu} = \frac{\overline{\tau}_f}{\overline{\sigma}_n}. \tag{3.4}$$

   Herein, t_b and t_e indicate the begin and the end of the stationary region and f is the sampling rate of data acquisition. $\sigma_{n,i}$ and $\tau_{f,i}$ are the normal pressure and friction stress at time increment i, respectively.

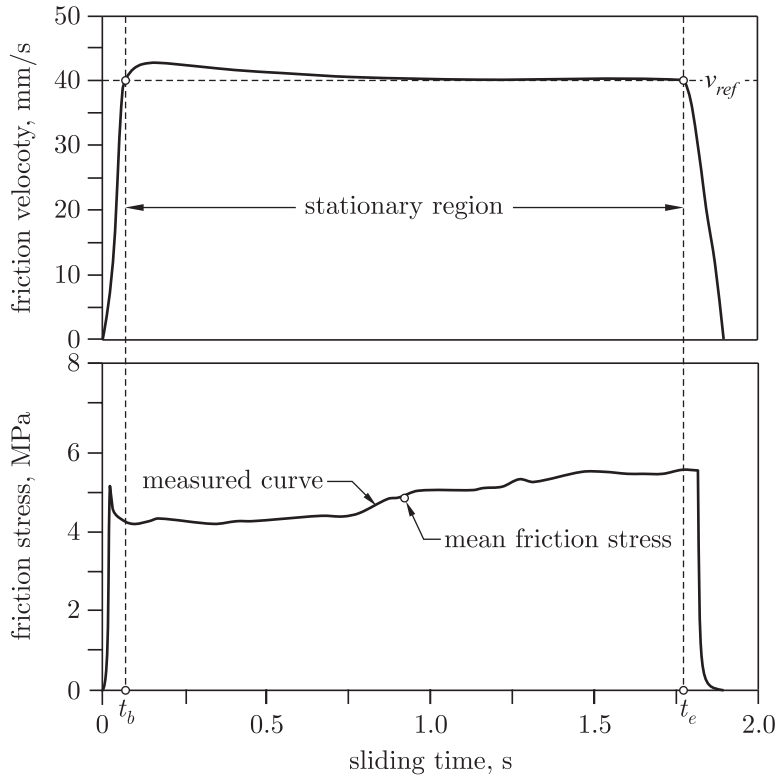

Figure 3.10: Evaluation of the ring-on-disc tests: In the stationary region of the experiment, the mean values of normal pressure, friction stress and friction coefficient were calculated.

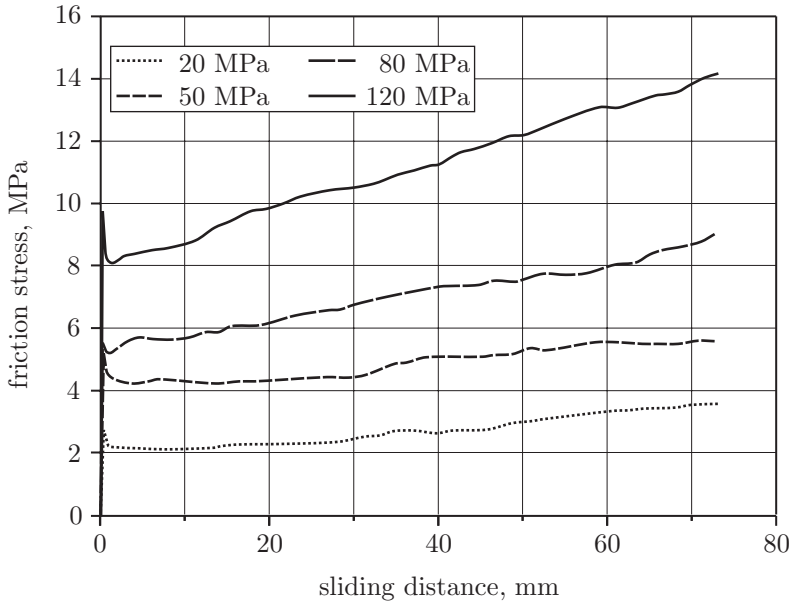

Figure 3.11: The friction stress of the preliminary warm forging tests performed in closed dies as function of the sliding distance and the normal pressure. The tests were carried out with lubricant **B**.

Figure 3.11 shows some friction curves as function of the sliding distance and the normal pressure obtained with lubricant **B**. In contrast to the results of the cold forging tests, sticking friction is well pronounced in the beginning of sliding.
In Figures 3.12 and 3.13, the evolution of friction stress and friction coefficient with increasing normal pressure is compared for fresh lubricants **A** and **B**. When regarding the development of the friction stresses, an asymptotic behaviour can be determined with both lubricants (the friction stresses at 175 MPa normal pressure are due to material extruded in the tool-container interface). However, these behaviour must not be mixed up with the asymptotic friction model that assumes dry sliding and shearing of the weaker friction partner. In fact, the shear yield stress of AA6082 at an interface temperature of approximately 350 °C is about 40–50 MPa what is far from the maximum of 17 MPa observed in the tests. Obviously, the shear stress of lubricant **B** is lower than that of **A**.

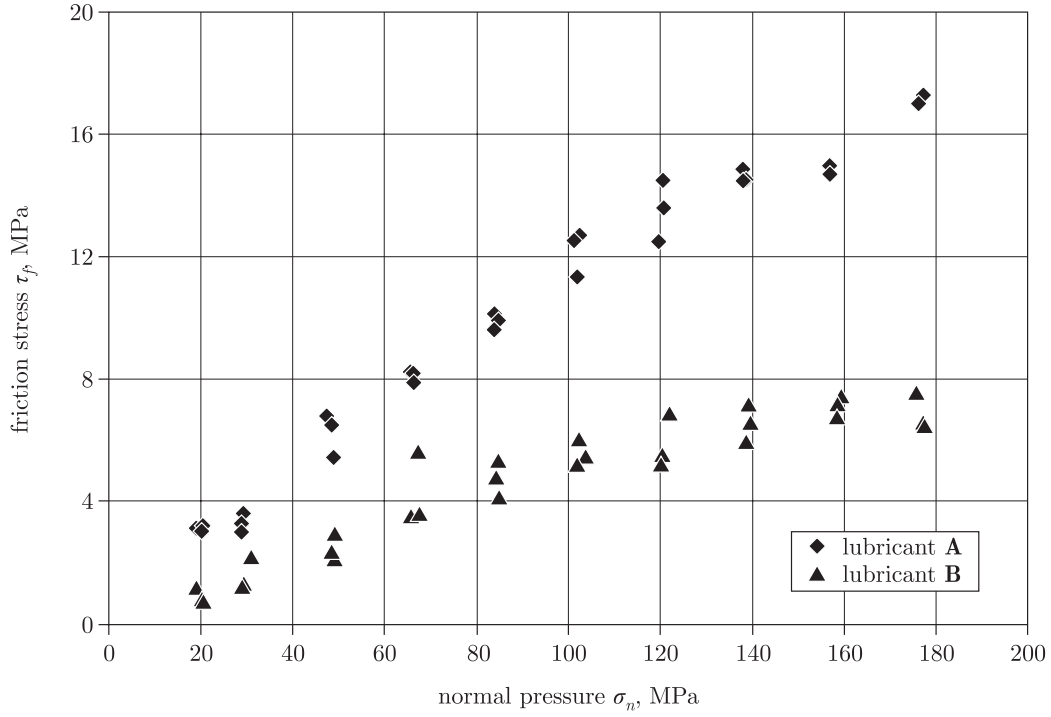

Figure 3.12: Friction stresses of fresh lubricants **A** and **B** in the preliminary warm forging tests. In both cases, an asymptotic behaviour is observed (the friction stresses with lubricant **A** at 175 MPa normal pressure are due to material extruded in the tool-container interface). Obviously, the shear stress of lubricant **B** is lower than that of **A**.

When comparing the evolution of friction coefficients with increasing normal load, lubricant **A** shows a monotonic decreasing behaviour. In contrast, the application of lubri-

cant **B** results in a slight rise of the friction coefficient at low pressures until a maximum value is reached at $\sigma_n = 65$ MPa. If the normal stress is further increased, the friction coefficient shows a decreasing behavior.

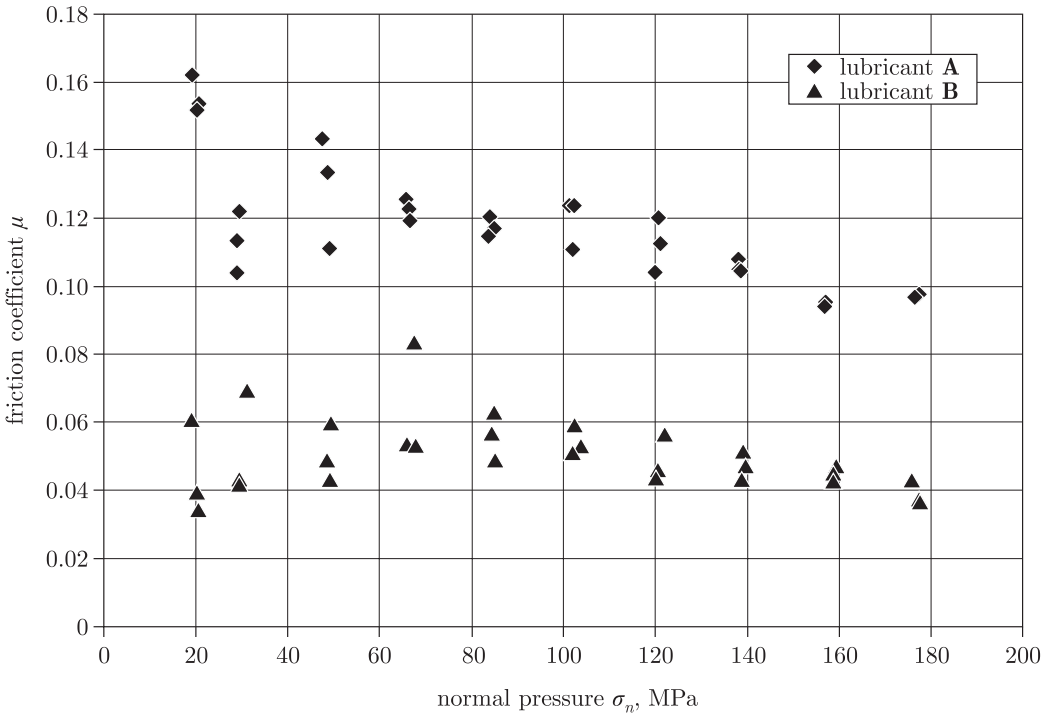

Figure 3.13: Friction coefficients of fresh lubricants **A** and **B** in the preliminary warm forging tests. In contrast to lubricant **A**, that shows a monotonic decreasing behaviour, the friction coefficient rises at low normal pressures and falls at elevated pressures when applying lubricant **B**.

The results of fresh diluted and old lubricant are compared in Figures 3.14 and 3.15. The fact that the old lubricant was loaded only up to 140 MPa was not due to the lubricant but was caused by technical problems with the hydraulic power pack. Obviously, fresh lubricant gives significantly lower friction and more reproducible conditions at the interface, what enables more stabile forging processes. However, the basic behaviour of fresh and old lubricant are the same: The friction stress shows asymptotic increase and the friction coefficient rises at low normal pressures, reaches a maximum value at 50 MPa and falls at higher pressures. From these results it was decided, that in all further experiments the lubricant had to be diluted directly before the execution of the tests.

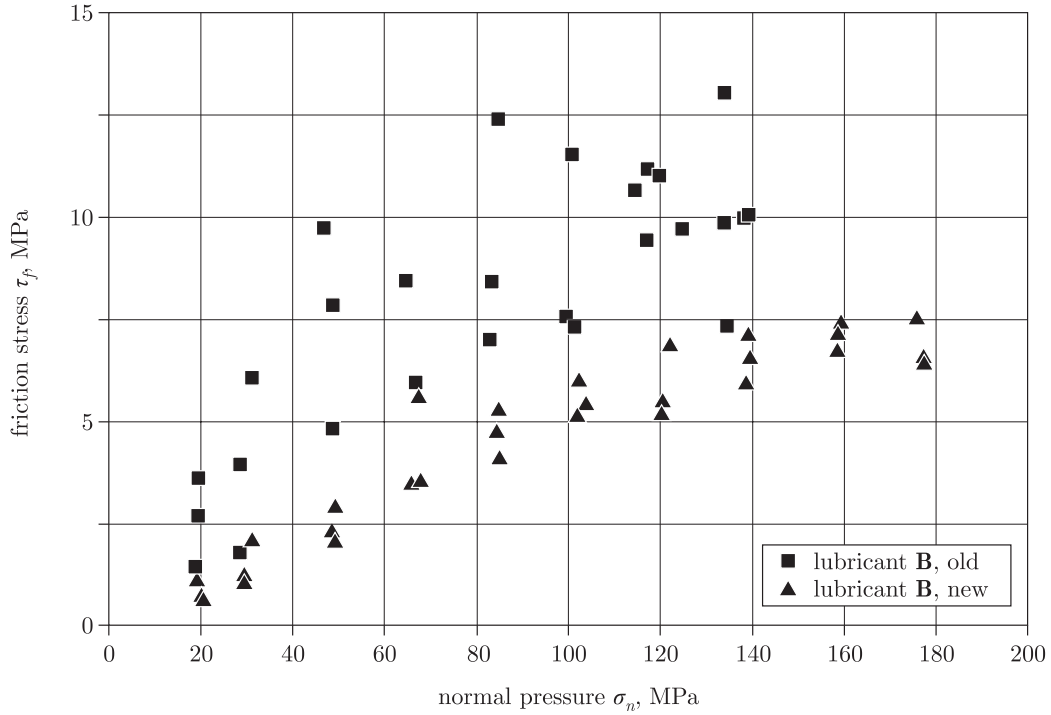

Figure 3.14: Friction stresses of fresh and old lubricant **B**. Obviously, fresh lubricant gives lower friction and more reproducible conditions at the interface. This leads to more stabile processes.

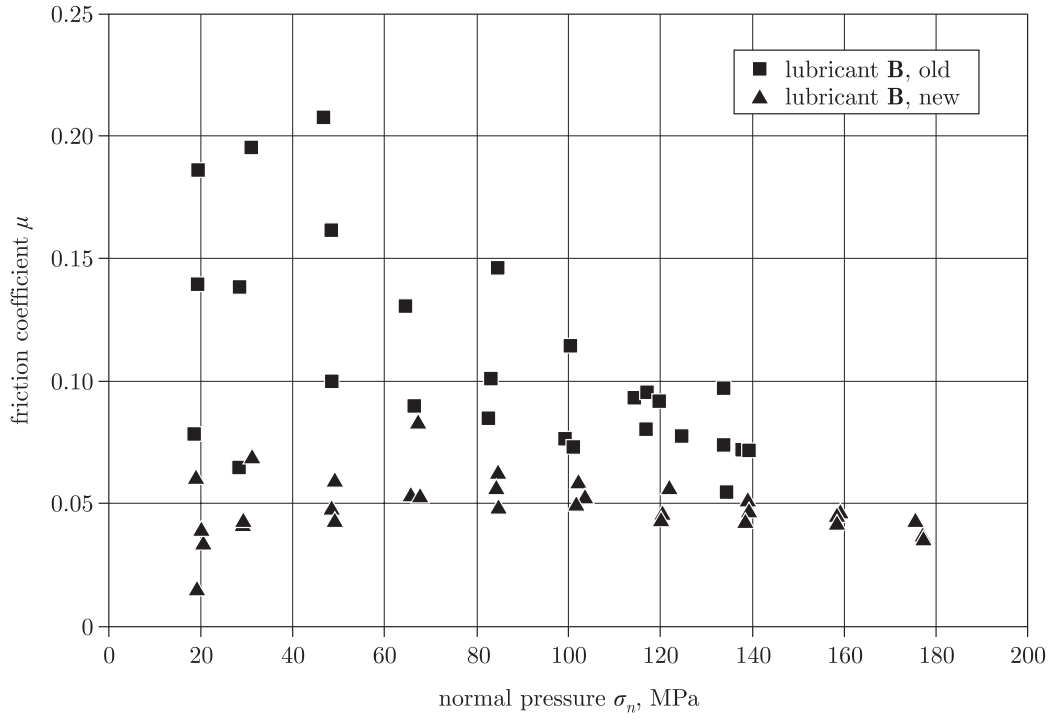

Figure 3.15: Friction coefficients of fresh and old lubricant **B**.

3.4 Ring-on-Disc - Tests

After verifying the applicability of the new developed toolkit (see Section 3.3.3.1) in examining friction at hot aluminium forging processes, the influence of the load collective and the surface conditions on friction was investigated systematically. As in the preliminary tests, the specimen were made of AA6082, which is a standard forging alloy in automotive engineering, mechanical engineering and in naval architecture, and the tool material was hot work tool steel 1.2344 hardened to 55 HRC.

3.4.1 Execution of the Tests

The experiments were performed with three different commercial graphite-based lubricants (see Table 3.3) and at various loads (20–150 MPa), sliding velocities (10–100 mm/s) and specimen surface conditions (turned, sand blasted). In addition, some tests were performed without lubrication. The changing parameters of the test series are summarised in Table 3.4.

Table 3.3: Lubricant test matrix for ring-on-disc tests.

	lubricant type	rec. dilution ratio
A	dispersion of graphite in water	1:15
B	dispersion of graphite in water	1: 7
C	emulsion of a dispersion of graphite in water and mineral oil	2: 1

On the one hand, the sliding velocities were varied at the same interface conditions (series 1–4), and on the other hand, the interface conditions were changed at constant sliding speeds (series 5–9). In all test series, experiments were performed at 50, 100, 130 and 150 MPa normal pressure[1]; additionally, tests without lubricant were also carried out at $\sigma_n = 20$ MPa. Tool and workpiece temperature were set to 250 °C and 450 °C, respectively, and the relative displacement was 70 mm. For each parameter set and when pick-up occurred, the tool was prepared with grit 800 sandpaper and 3 µm polishing suspension. Within a parameter set, seven tests were performed with exception of series 9, where just

[1] Due to the fact that the normal pressure was adjusted by means of a pressure relive valve, the exact values differed slightly from the stated values.

Table 3.4: Parameters used in the ring-on-disc tests.

no.	series	lubricant	surface condition	pressure levels	sliding velocity, mm/s
1–4	1	**B**, 5 × 0.3 s	sand-blasted	4	10
5–8	2	**B**, 5 × 0.3 s	sand-blasted	4	40
9–12	3	**B**, 5 × 0.3 s	sand-blasted	4	70
12–16	4	**B**, 5 × 0.3 s	sand-blasted	4	100
17–20	5	**B**, 4 × 0.3 s	sand-blasted	4	40
21–24	6	**B**, 4 × 0.3 s	turned	4	40
25–28	7	**A**, 4 × 0.3 s	sand-blasted	4	40
29–32	8	**C**, 4 × 0.3 s	sand-blasted	4	40
33–37	9	without	sand-blasted	5	40

two experiments were carried out per load level due to heavy wear at some stages.
The experiments were carried out in the following way: First, the tool was brought to operating temperature. When the testing sequence was started by the PLC, the specimen was heated, and the final temperature was kept constant for 180 s in order to allow temperature equalisation. Then, the lubricant was applied by the automatic spraying device (series 1–8). After lubricating, the execution of the test itself was started employing the upsetting-sliding sequence.

3.4.2 Evaluation of the Tests

The experiments were evaluated similar as described in Section 3.3.3.3:

1. First, the stationary region of the experiment was determined from the velocity curve (see Figure 3.10).

2. In the stationary region, the mean values of normal pressure σ_n, friction stress τ_f and friction coefficient μ were calculated by Equations (3.2), (3.3) and (3.4).

3. For easier illustration, the $\overline{\sigma}_n$-, $\overline{\tau}_f$- and $\overline{\mu}$-values of each parameter set were averaged to the mean values $\overline{\sigma}_{n,m}$, $\overline{\tau}_{f,m}$ and $\overline{\mu}_m$ and the standard deviations were calculated. In order to avoid falsified results, apparent outliers were not considered in this calculation.

3.4.3 Results and Discussion

3.4.3.1 Results of Tests Without Lubricant

The friction stresses and friction coefficients obtained from the experiments without lubrication are presented in Figure 3.16. Even at the lowest load level, the asymptotic behavior of the friction stress is well pronounced; at normal loads higher than 65 MPa, a more or less steady state is reached. When regarding the friction coefficient, a decrease from an initial value of $\mu = 1.83$ (!) to a final value of $\mu = 0.34$ is observed. As a friction

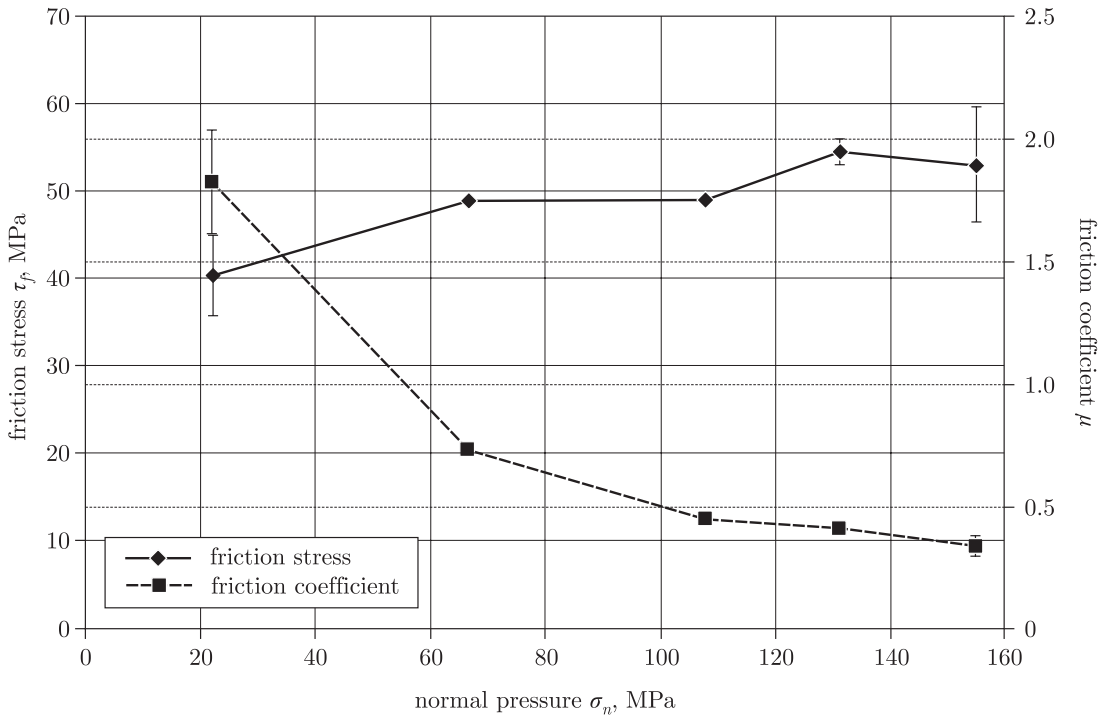

Figure 3.16: Friction stress and friction coefficient of the tests without lubrication.

coefficient higher than 1 can only be explained by the adhesion theory, extensive welding in the tool-workpiece interface had to be assumed. This assumption was verified by a visual inspection of the surfaces and by a comparison of the lifting forces of the friction facility after the tests. Dull (and worn) surfaces were found at low normal pressures (20 and 50 MPa), whereas bright surfaces were observed at higher loads (see Figure 3.17). Moreover, at 20 MPa normal pressure, a force of 14 kN was necessary to open the device, at 65 MPa normal pressure, the lifting force was 10 kN and at higher pressure levels, the lifting force was about 3.5–4 kN [1].

[1] The lifting force in the absence of welding was approximately 0.5 kN.

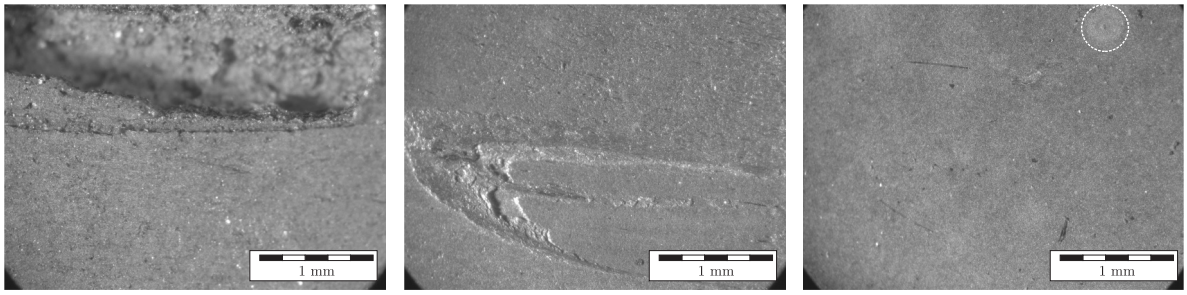

(a) (b) (c)

Figure 3.17: Surfaces of specimens tested without lubricant at normal pressures of (a) 20 MPa, (b) 65 MPa and (c) 105 MPa. At high pressures, the surfaces are bright and shiny with the exception of small spots (see e.g. at the right of the upper border in (c)).

The yield stress of AA6082 at 350 °C (what is a realistic temperature at the tool-specimen interface) was determined to be $k_f = 90$ MPa [1]. This corresponds with a shear yield stress of $k = 45$ MPa according to the Tresca criterion or to $k = 52$ MPa when the von Mises criterion is applied. From the performed experiments, shearing of the specimen (and therefore sticking friction) can be presumed at normal pressures equal to or greater than 65 MPa.

From these observations, the following hypotheses was developed: At low normal pressures, relative motion is present in the tool-specimen interface at the beginning of the test. However, friction is high and the oxide layer of the specimen is worn off after a short sliding distance thereby enabling direct metallic contact of aluminium and steel. As a consequence, extensive welding takes place due to the high affinity of both materials to each other. Sticking is established, the specimen shears off in its bulk, and heavy wear occurs resulting in dull surfaces and material transfer from the specimen onto the tool (see Figure 3.17 (a)).

In contrast, at heavy loads, relative motion in the tool-specimen interface is prevented due to heavy interlocking of the asperities and the specimen shears in its bulk from the beginning of the test. The oxide layer of the specimen is not damaged and separates the friction partners. Thus, the surfaces are bright after the experiments although sticking took place. Hence, the low friction values presented in Figure 3.16 are due to the inadequacy of Amontons' friction law discussed in Section 2.5.3 and do not represent a state of sliding.

In order to validate this hypotheses, metallographic specimen were prepared from workpiece cuts perpendicular to the contact surface and parallel to the sliding direction. The

[1] Flow curves of AA6082 were determined at different temperatures for a strain rate of $\dot{\varphi} = 1\ \mathrm{s}^{-1}$ by means of a thermo-mechanical treatment simulator (Servotest, UK).

results are shown in Figure 3.18, where the case of heavy material loss is compared to the case of unworn surfaces. In both images, the plastic deformation is clearly indicated by the deformed microstructure. This characteristic texture qualitatively described by Rigney and Hirth [162] is present at all load levels irrespective of the surface appearance. From this investigation, it can be concluded that the friction mechanism is always that of sticking friction independent on the normal pressure, however, at low contact loads, heavy wear is present due to the destruction of the oxide layer.

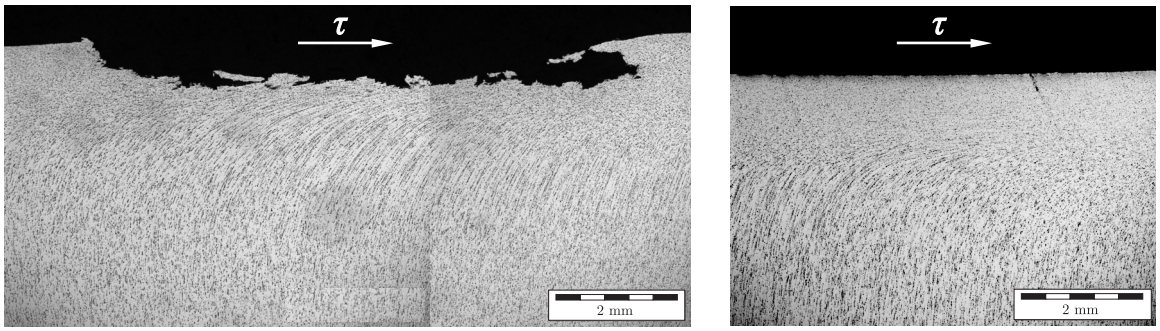

(a) (b)

Figure 3.18: Metallographic specimen of the workpiece: The cuts were performed perpendicular to the contact surface and parallel to the sliding direction. (a) shows the specimen in the presence of heavy material loss ($\sigma_n = 20$ MPa), (b) shows the specimen in a region without heavy wear ($\sigma_n = 20$–150 MPa). In both cases, the plastic deformation of the bulk material is evident (comp. with Figure 2.12 (e)).

3.4.3.2 Results of Tests With Lubricant

In Figure 3.19, the friction stress is plotted in dependence on the sliding velocity. A formation of groups is clearly visible: The curves at the both lower as well as the curves at the both higher velocities are qualitatively similar to each other. In contrast to the friction stresses of the tests at lower speeds, that start with a minimum value, the experiments at higher velocities reach a minimum at 100 MPa normal pressure. Except of series 1, all curves have a maximum value at $\sigma_n = 130$ MPa. However, the high friction stress of series 1 at a normal pressure of 150 MPa was due to material extruded in the gap between tool and container and did not indicate another tendency. At higher sliding velocities, this extrusion did not occur.

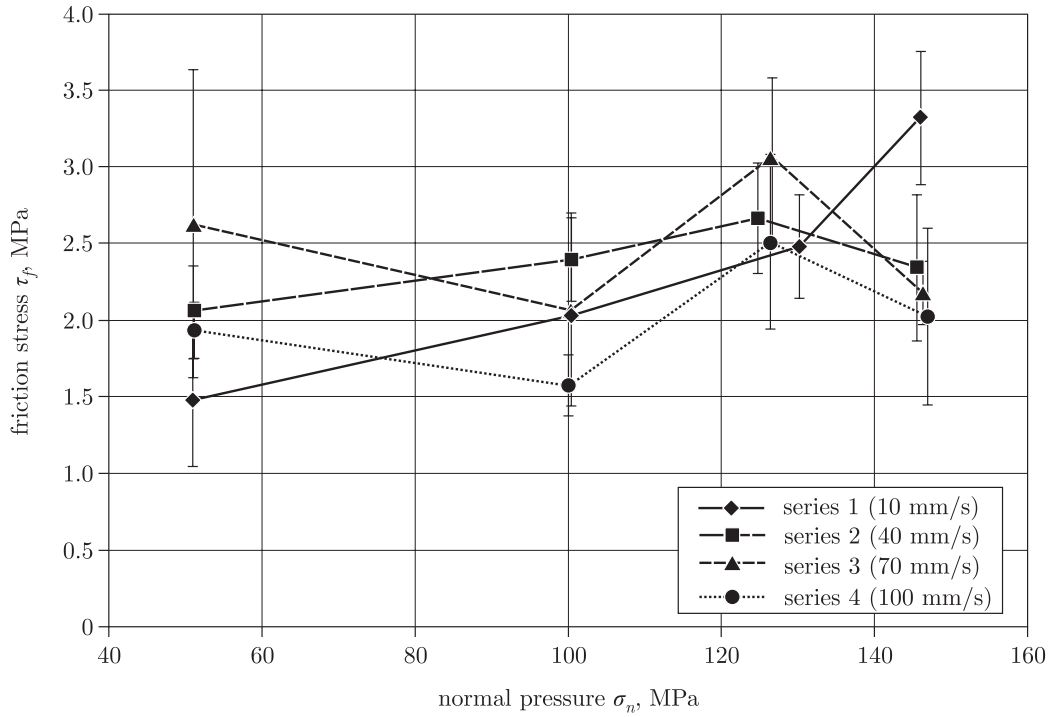

Figure 3.19: Friction stresses in dependence on the sliding velocity. The curves at the both lower as well as the curves at the both higher velocities are qualitatively similar to each other.

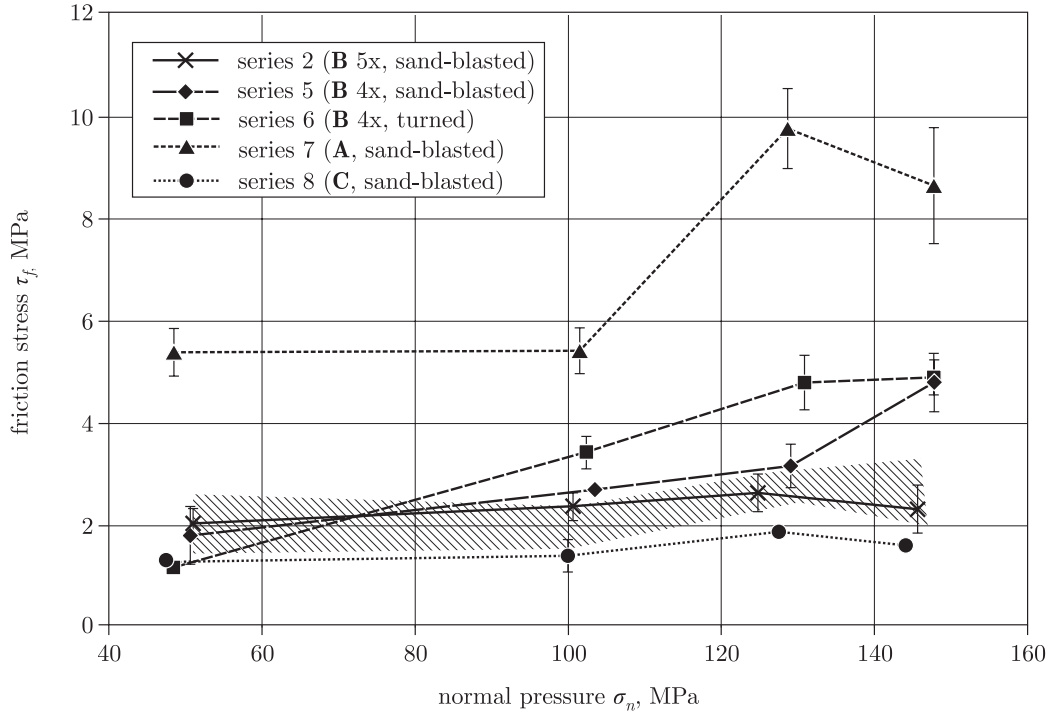

Figure 3.20: Friction stresses in dependence on the interface conditions. For comparison, the region of the velocity dependent curves is indicated hatched.

Figure 3.20 presents the friction stress in dependence on the surface condition. For comparison, the region of the velocity dependent curves is indicated hatched. Except of series 5, that shows a behaviour as series 1, all series have a maximum value at a normal stress of 130 MPa and have similar or lower values at contact loads of 150 MPa. In contrast to the other curves, the series 7 shows a sharp rise from $\sigma_n = 100$ to $\sigma_n = 130$ MPa. When comparing the sand-blasted with the turned surface, the curve of the untreated specimen rises significantly steeper than that of the sand-blasted workpiece. The lowest friction stresses are obtained with lubricant **C** (series 8), whereas the highest friction stresses are caused by the conditions present in series 7 (lubricant **A**).
In Figure 3.21, the friction coefficients are evaluated in dependence on the sliding velocity. Again, a formation of groups can be observed for the two lower and the two higher normal loads. At all conditions, the friction coefficient falls significantly in the range of $\sigma_n = 50$–100 MPa and does not change very much in the interval of $\sigma_n = 100$–150 MPa. Generally, the lowest friction coefficients are observed at the highest normal pressure (the inconsistency of series 1 was already discussed above). In all series, both, the deviation of the single values of one test condition as well as the deviation of the mean values of different series decreases with increasing normal pressure.
Finally, Figure 3.22 shows the friction coefficients in dependence on the surface conditions. In general, the friction coefficient increases significantly at low normal pressures and stays approximately constant or shows a light decrease at elevated contact stresses. Lubricant **A** has a well pronounced local maximum at $\sigma_n = 130$ MPa, and the friction coefficient rises at high normal pressures in series 5 as it has the same characteristics as series 1. However, the behavior of series 6 is contrary: Here, the friction coefficient rises from the beginning, reaches a maximum at a normal pressure of 130 MPa, and decreases slightly at $\sigma_n = 150$ MPa. The lowest friction coefficients are achieved with lubricant **C** (series 8), whereas the highest values are caused by lubricant **A** (series 7).

In the assessment of the lubricants, it has to be stated that all products investigated reduced friction significantly compared to the dry friction condition. In fact, lubricant **A** that showed the poorest lubricating effect reduced the friction stress about 80 %, and lubricant **C** reduced friction about more than 90 %. Moreover, all lubricants prevented the tool from wear. Micrographs confirmed that shearing was restricted to the graphite layer and the asperities; the bulk material of the specimen was not affected.
When comparing the lubricants regarding to their lubricating effect, it was found that the product with the highest recommended dilution ratio of 1:15 gave the poorest results and the product with the lowest dilution ratio of 2:1 gave the best results.

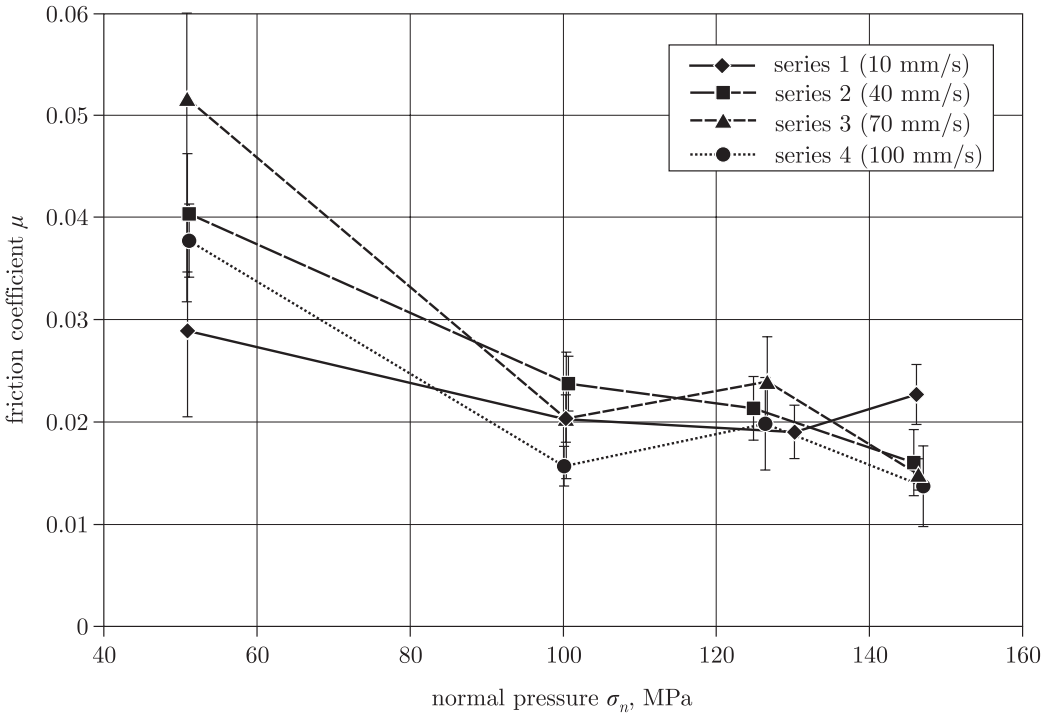

Figure 3.21: Friction coefficient in dependence on the sliding velocity. Again, a formation of groups can be observed (comp. with Figure 3.19).

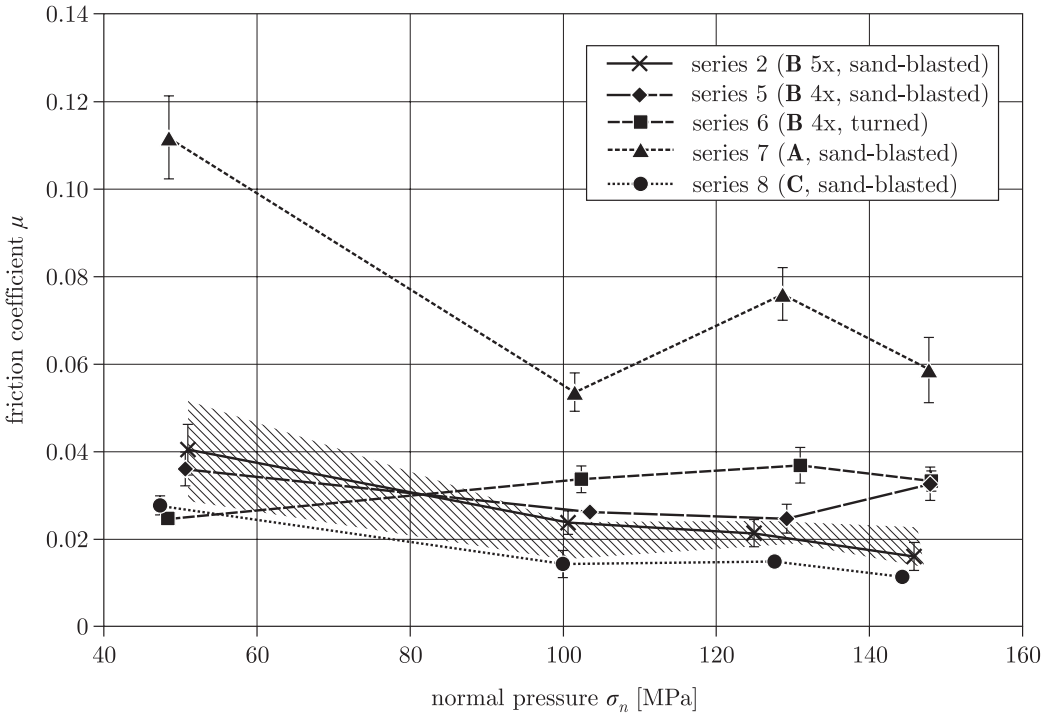

Figure 3.22: Friction coefficient in dependence on the interface conditions. For comparison, the region of the velocity dependent curves is indicated hatched.

However, the present analysis aimed in the characterisation of the load collective and the interface conditions on friction and not in the assessment of different lubricants. From this point of view, especially two conclusions could be made:

1. The effect of surface conditions on friction was significantly more pronounced than the influence of the load collective.

2. When regarding the load collective, the effect of normal pressure was in the observed range more significant than the influence of the sliding velocity.

As in solid lubricated interfaces (nearly) all shearing is done in the lubricant layer, the lubricant itself and the surface conditions of the friction partners are the dominating parameters of the tribological system. The change of the specimens surface from a random surface to an orientated surface, for example, had a significant effect on the resulting friction stress due to the changed behavior in retaining the lubricant.
The influence of the normal pressure in general has two effects: On the one hand, the lubricant's behaviour can be affected, and on the other hand, the real contact area and the lubricant pockets are governed.
In solid lubrication, the effect of the sliding velocity on friction is expressed by a physical or thermal decomposition of the lubricant layer. However, the sliding velocities in the investigations were not high enough to cause these effects.

3.5 Pin-on-Disc - Tests

In the scope of a research cooperation with a forging plant, that aimed in the characterisation of lubricants with respect to their lubricating effect and their applicability in the production of parts with long flow paths, experiments with a representative selection of commercial lubricants had to be performed.
As the ring-on-disc test did not meet the demands on long flow paths (80 mm) and on the sliding at virgin lubricant layers, an appropriate toolkit was developed. The sliding at virgin lubricant layers can only be realised when tool and specimen are not in contact over the entire sliding surface at the same time. This eliminates a ring-shaped geometry. Furthermore, the active surface of the tool had to be plane in order to avoid additional plastic specimen deformation leading to wrong measurements during sliding.
The only possibility to meet these demands was to perform a kind of ring-on-disc test as used by Attanasio et al. [146], Vergne et al. [147] and Ceretti and Giardini [113]. In all their investigations, the pin represented the tool and the disc represented the workpiece.

In the present analysis, the role of pin and disc was exchanged to avoid additional tangential stresses due to plastic interlocking. Furthermore, two pins were used instead of one in order to load the device symmetrically. Long sliding distances could be achieved by adjusting the distance between contact areas and axis of rotation.

3.5.1 Toolkit and Specimen Geometry

Figure 3.23 shows the toolkit used in the reported investigation, where tool and specimen were made of hot work tool steel 1.2344 (hardened to 52 HRC) and AA2618, respectively. AA2618 is a heat treatable Al-Cu-Mg-Fe-Ni forging alloy developed for high temperature applications, especially for aircraft engine components [163]. A very important point

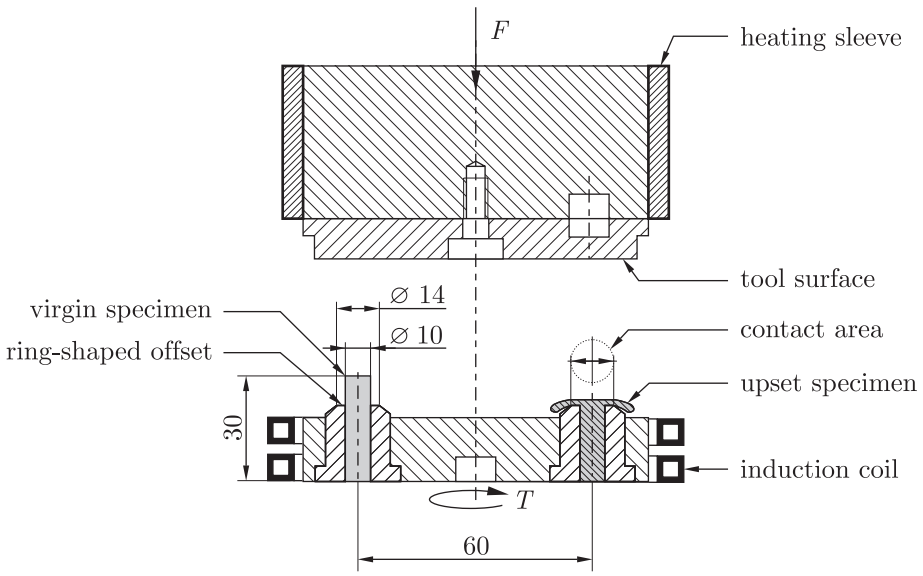

Figure 3.23: Toolkit for the pin-on-disc experiments.

was that the tool-workpiece contact area should remain constant during the analysis independent on the compression force. This demand was met by placing a ring-shaped offset around the specimen, making the contact area constant to 154 mm^2.

3.5.2 Execution of the Tests

The four investigated lubricants are listed in Table 3.5 and the parameter matrix for the tests is shown in Table 3.6. In all experiments, the tool temperature was 250 °C and the specimen were heated up to 450 °C. The sliding velocity was 150 mm/s and the sliding

distance was set to 80 mm. Three tests were executed for each parameter set, and each experiment was performed with virgin specimens, whereas the tool was changed only when a new lubricant was applied. In order to maximise the effects on a tool surface modification, all tests were started at the same tool position.

Table 3.5: Lubricant test matrix for pin-on-disc tests.

	lubricant type	rec. dilution ratio
A	dispersion of graphite in water	1:15
B	dispersion of graphite in water	1: 7
C	emulsion of a dispersion of graphite in water and mineral oil	2: 1
D	dispersion of graphite in mineral oil	1: 5

The experiments were performed in the following way: First, the tool was brought to operating temperature and well lubricated. When the testing sequence was started by the PLC, the specimens were heated, and the final temperature was kept constant for 60 s in order to allow temperature equalisation. After this, the execution of the test itself was started automatically. In order to avoid an interaction of different influences, the specimens were compressed in a first step and thereafter the rotation began. The data acquisition was started by the mechanical trigger. After the test, tool and specimen were inspected.

It has to be stated that the specimen's surface was enlarged during upsetting in dependence on the compression force, e.g. different forces led to different amounts of surface expansion. However, the influence of surface enlargement was restricted to the start of the test, thereafter virgin lubricant layers were present independently on the normal force.

3.5.3 Evaluation of the Tests

As already mentioned, the main focus of the investigations was the characterisation of different lubricants with respect to their lubricating effect and their applicability in the production of parts with long flow paths. Hence, an adequate assessment was performed on the basis of the acquired measurement curves and on the basis of the inspection of the sliding surfaces after the tests.

Table 3.6: Parameters used in the pin-on-disc tests.

no.	series	lubricant	dilution ratio	normal pressure [MPa]
1			1: 7	
2	1	**A**	1:15	210
3			1:22	
4			1: 7	
5	2	**A**	1:15	330
6			1:22	
7			1: 3	
8	3	**B**	1: 7	210
9			1:15	
10			1: 3	
11	4	**B**	1: 7	330
12			1:15	
13			1: 0	
14	5	**C**	2: 1	210
15			1: 1	
16			1: 0	
17	6	**C**	2: 1	330
18			1: 1	
19			1: 2	
20	7	**D**	1: 5	210
21			1:10	
22			1: 2	
23	8	**D**	1: 5	330
24			1:10	

3.5.3.1 Evaluation of the measurement curves

During each experiment, the normal force, F_n (compression force), the friction force, F_f (tangential force), and the rotational speed, v, were measured (see section 3.2.2). By means of the known contact area, A_a, both the normal stress, σ_n, and the friction stress, τ_f, could be calculated:

$$\sigma_n = \frac{F_n}{2 \cdot A_a}, \tag{3.5}$$

$$\tau_f = \frac{F_f}{2 \cdot A_a}. \tag{3.6}$$

The evaluation of the measurements was carried out in several steps similar to the procedure described in Section 3.4.2 (see Figure 3.24):

1. All data were acquired with a fixed sampling rate, i.e. the time intervals between the sampling were kept constant. However, for the comparison of measurements, a constant stroke interval is preferable. Thus, in a first step, all the data were transferred from equal time spacing to equal stroke spacing.

2. For all three tests representing the same parameter set, average measurement curves were determined by calculating the mean σ_n-, τ_f-, and v-values for each stroke increment, i:

$$\overline{\sigma}_{n,i} = \frac{\sigma_{n,i1} + \sigma_{n,i2} + \sigma_{n,i3}}{3}, \tag{3.7}$$

$$\overline{\tau}_{f,i} = \frac{\tau_{f,i1} + \tau_{f,i2} + \tau_{f,i3}}{3}. \tag{3.8}$$

$$\overline{v}_i = \frac{v_{i1} + v_{i2} + v_{i3}}{3}. \tag{3.9}$$

3. The begin of the stationary region of the experiment was identified as the stroke s_i at which the average velocity became equal to or greater than the reference velocity ($\overline{v}_i \geq v_{ref}$).

4. For each average curve, the regression line was determined in the interval corresponding to the stationary region of the experiment.

5. From these regression lines, the values characterising the lubricants were derived. The friction coefficient, μ, which was calculated in the center of the regression line, is well-established in depicting the friction-reducing effect of lubricants:

$$\mu = \frac{F_f}{F_n}, \tag{3.10}$$

where F_n is the normal force and F_f is the friction force. The characterisation of the physical stability of lubricant layers in dependence on the sliding distance is a less common task. In the scope of the present work, the following two values have been considered suitable to describe the durability of lubricant layers: the slope, γ, of the regression line and the standard deviation, σ, of the mean curve.

3.5.3.2 Surface Inspection

After each test, the tool and the specimen surface were assessed optically. Furthermore, after the completion of the test series, the surface roughness of all tools was measured

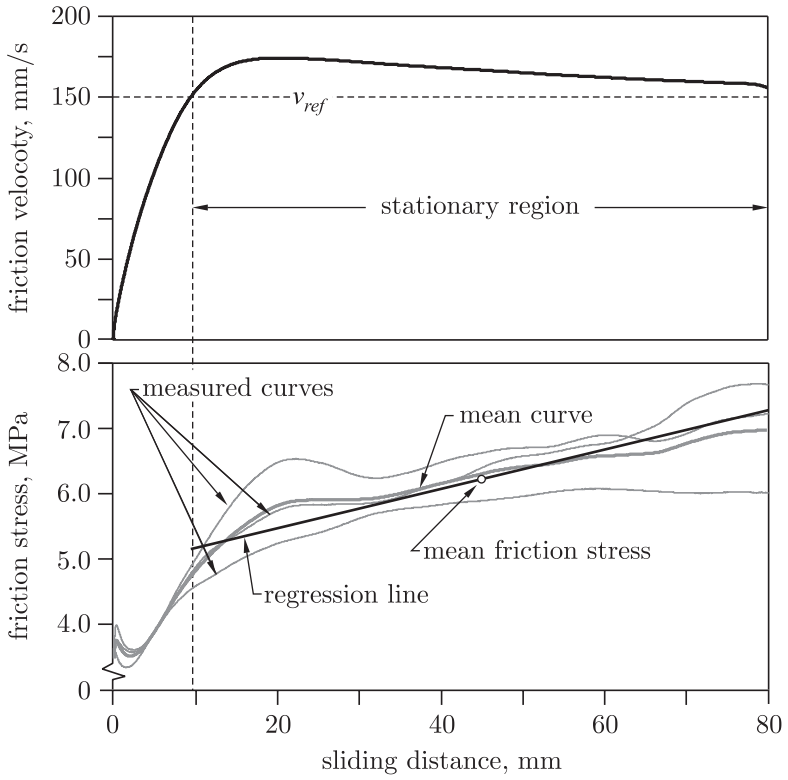

Figure 3.24: Evaluation of the measurement curves. The mean friction stress divided by the mean normal stress gives the mean friction coefficient.

in order to get further information on the tribological interactions in the tool-workpiece interface. This was done by measuring roughness profiles in and perpendicular to the sliding direction at 20, 50 and 80 mm sliding distance and by calculating the averaged values.

3.5.4 Results and Discussion

Figure 3.25 presents mean curves of the four lubricants listed in Table 3.5 at the same testing conditions. Lubricant **A** seems to be not affected by the surface expansion in the upset area (corresponding to the first 14 mm of the sliding track). The sticking friction stress is high (about twice) compared to the other lubricants and it is larger than the sliding friction stress which decreases slightly with increasing distance. Regarding the lubricants **B-D**, the sliding friction stress exceeds the static friction stress and increases until it reaches a maximum at a distance of about 14–20 mm. However, the maximum sliding friction stress of lubricants **B** and **C** is in the range of that of lubricant **A**, but the sliding friction stress of lubricant **D** is about twice this value. At sliding distances larger

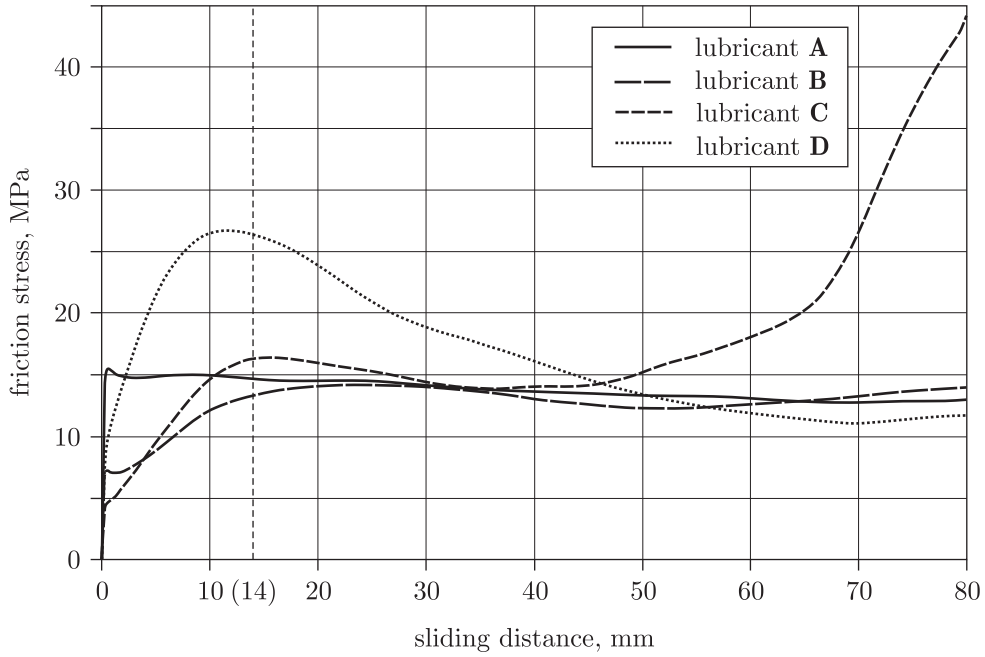

Figure 3.25: Average friction stress at one parameter set. Each curve is derived from three measurements and represents a lubricant. From a sliding distance of 14 mm, virgin lubricant layers are present.

than 20 mm, the friction stress reaches a steady state for lubricants **B** and **C**. Only in the case where lubricant **C** was tested in undiluted condition at high pressure (corresponding to the curve in Figure 3.25), lubricant break-down occurred. Using lubricant **D**, the friction stress decreases from its maximum value and reaches a steady state at a sliding distance of approximately 50 mm.

In order to show the three quantities characterising the lubricants (friction coefficient, μ, slope of regression line, γ, and standard deviation of the mean curve, σ) in a single diagram, a new quantity combining γ and σ, the progression of friction coefficient, *pfc*, was considered:

$$pfc = \frac{\gamma}{|\gamma|} \cdot \sqrt{\gamma^2 + (10 \cdot \sigma)^2}. \tag{3.11}$$

The factor 10 was introduced to make γ and σ of the same order of magnitude (to cause a balanced weighting).

Figure 3.26 shows the result of the investigation on the four lubricants. Each point in the diagram corresponds to the result of a single testing condition. The lubricants **A**-**C** show a stable behaviour (a smooth curve progression), whereas the friction coefficient is slightly decreasing with lubricant **A** and it is slightly increasing with lubricants **B** and **C** during the test. However, the outermost point of **C** indicates lubrication breakdown at the corresponding testing parameters (compare with Figure 3.25). A different behaviour

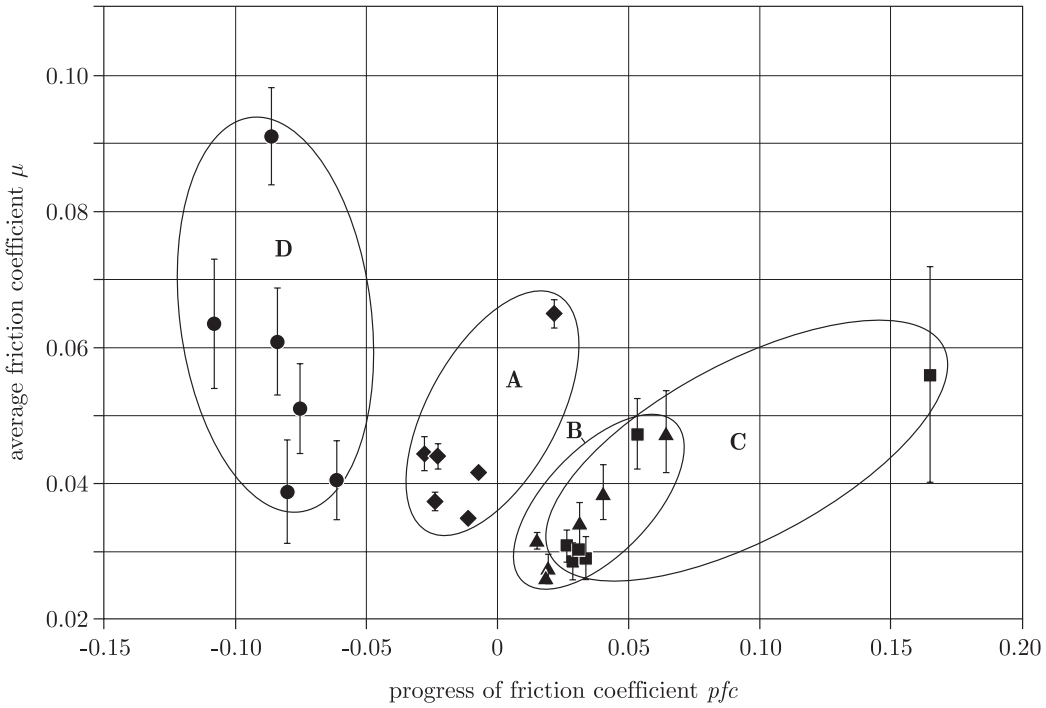

Figure 3.26: Results of the investigation of four lubricants by means of the pin-on-disc test.

is shown by the oil-based lubricant **D**: On the one hand, the friction coefficients tend to higher values than those of the lubricants on water basis, and on the other hand, the *pfc* is strongly negative what indicates a strong decrease of the friction coefficient during the test.

Figure 3.27 shows the sliding tracks on the four tools. These sliding tracks were assessed visually in terms of compactness of the lubricant layer. It was found that the oil-free lubricants **A** and **B** formed compact layers that were not worn off during the test and prevented aluminium pick-up. However, after the test, parts of the lubricant layers flaked off. In contrast, the oil-containing lubricants showed another behaviour: The water-oil-based lubricant **C** formed a very homogeneous layer, but it was worn off at high pressures and pick-up occurred in small areas. The oil-based lubricant **D** was completely abraded and heavy pick-up was present in the beginning of the sliding track (near the upset area). When sliding progressed, further pick-up occurred in small areas.

Comparing the roughness values of the tools (see Table 3.7) the following was found: Lubricant **A** gave the highest tool roughness, the roughness when applying **B** or **C** was approximately the half, and the roughness when applying lubricant **D** was in-between the roughness values of **A** and **B**, respectively.

The intention of this investigation was the assessment of lubricants with respect to their lubricating effect and their applicability in the production of parts with long flow paths.

Figure 3.27: Sliding tracks for different lubricants (sliding was performed clockwise).

This means in terms of the analysed quantities that the values of the friction coefficient, μ, the slope of regression line, γ, and the standard deviation of the mean curve, σ, should be small. The claim for a small friction coefficient in the die cavity is evident in order to achieve die filling, a small slope of regression line indicates steady state sliding conditions (no lubrication breakdown, etc.) and a small standard deviation ensures process stability. Due to these considerations, lubricant **A** or **B** would be the right choice under the investigated conditions. However, the surface roughness is much lower with lubricant **B** what leads to lower friction coefficients and a smoother workpiece surface.
The poor result of the oil-based lubricant **D** can be explained by regarding Figure 3.27. It can be clearly seen that the tool temperature was too low to evaporate the carrying agent. As a result, the lubricant was squeezed out of the tool-workpiece interface in the upsetting step, and in the beginning of the rotation, pick-up occurred. In further sliding, hydrodynamic lubrication was present and the friction coefficient decreased rapidly. However, the lubricating effect was not strong enough to prevent further pick-up completely. It is assumed, that the oil-containing lubricants **C** and **D** would give better results at higher tool temperatures.

Table 3.7: Tool roughness values.

	R_z, µm	
lubricant	sliding direction	perpendicular
A	7.58	14.19
B	3.81	7.29
C	3.72	6.54
D	5.03	9.82

3.6 Comparison of the Tests

From the results of the ring-on-disc tests, it is known that the main influence on friction in the tool-workpiece interface is exerted by the lubricant layer. As forging is an unsteady process, also the lubrication conditions are unsteady, what has to be considered in friction tests. Due to the fact that lubrication break-down is commonly caused by thinning (or abrasion) and decomposition of the lubricant layer, these mechanisms should be modeled in friction experiments.

In the ring-on-disc test with entrapped specimen, lubricant exchange is prevented and thus lubricant aging, i.e. the physical and thermal decomposition of the lubricant with sliding distance, can be investigated. The effect of aging is indicated by the steady rising friction stress in Figure 3.11.

Compared with the ring-on-disc geometry, the demands on the lubricants are obviously less severe in the pin-on-disc setup: At the beginning of the rotation, new lubricant gets into the tool-workpiece interface, and after a sliding distance of approximately 14 mm, tool and specimen are separated by a compact lubrication layer even under high initial surface expansion. Furthermore, each point of the lubricant layer is loaded just for a short time. The pin-on-disc test analyses the abrasion resistance of lubricant layers.

However, none of the tests investigates the lubricant behavior in the presence of surface expansion. In operations in which the lubricant is applied onto the specimen (e.g. cold forging), surface enlargement leads to a thinning and, when a critical value is reached, to a break-down of the lubricant layer. On the other hand, in processes, in which the lubricant is applied onto the tools (e.g. warm forging), surface expansion at the tool-workpiece interface causes lubricant abrasion. This situation is modeled by the pin-on-disc test.

From these considerations, ring-on-disc test and pin-on-disc experiment can be seen as complement methods in the investigation of friction in the tool-workpiece interface of warm forging processes.

4 New Approach to Friction Modeling

4.1 Friction Model Requirements

As already mentioned in Section 2.1, the interactions of the elements of a tribological system with the load collective are very complex. An important characteristic of the friction partners is e.g. their solubility in each other. However, this property is not constant, but depends on the interface temperature and the normal pressure. The interface temperature, on the other hand, is influenced by the sliding velocity and the number of contact points, that is again determined by the material properties, the normal pressure and the surface conditions. Of course, the yield stress of the surface asperities and therefore the real area of contact is affected by the interface temperature, and so on. An even more complex task is friction modeling in the presence of intermediate layers as oxide layers or lubricants. In this case, the break-down of the separating layers has to be considered in terms of their breaking, critical thinning, abrasion or decomposition. Of course, the mechanisms of breakdown are determined by the layer's properties and its behavior under specific loads. Furthermore, the intermediate layers affect the system in terms of their heat conductance, for example. Moreover, in discontinuous processes, the properties in the tool-workpiece interface are not constant, thus, the friction history[1] has to be considered in friction modeling [10].

Experiments by the author, in which the normal load was varied several times between a low and a high pressure level, revealed that the time dependency of friction is not only due to junction growth, but is also affected by changing loads and by the properties of the elements of the tribosystem (see Figure 4.1). The tests were performed with a toolkit similar to that shown in Figure 3.4 at room temperature, where AA6082 was used as specimen material. At the initial low pressure level, the friction stress was very small. However, as can be seen when regarding the friction coefficient, there was an asymptotic rise due to junction growth. When the pressure was raised the first time, the tool sank into the specimen and sticking occurred, the workpiece was shorn off in its bulk. As a consequence, the friction stress became equal to the shear yield stress of the workpiece, and due to strain hardening, the friction stress increased with increasing sliding distance. When the pressure was reduced to the lower level again, also the friction stress decreased, but it did not reach the initial low level. After raising the pressure the second time, sticking took place again and the friction stress increased to the shear yield stress, and so

[1] The term *friction history* indicates the time (or distance) dependent influence of the loads on friction.

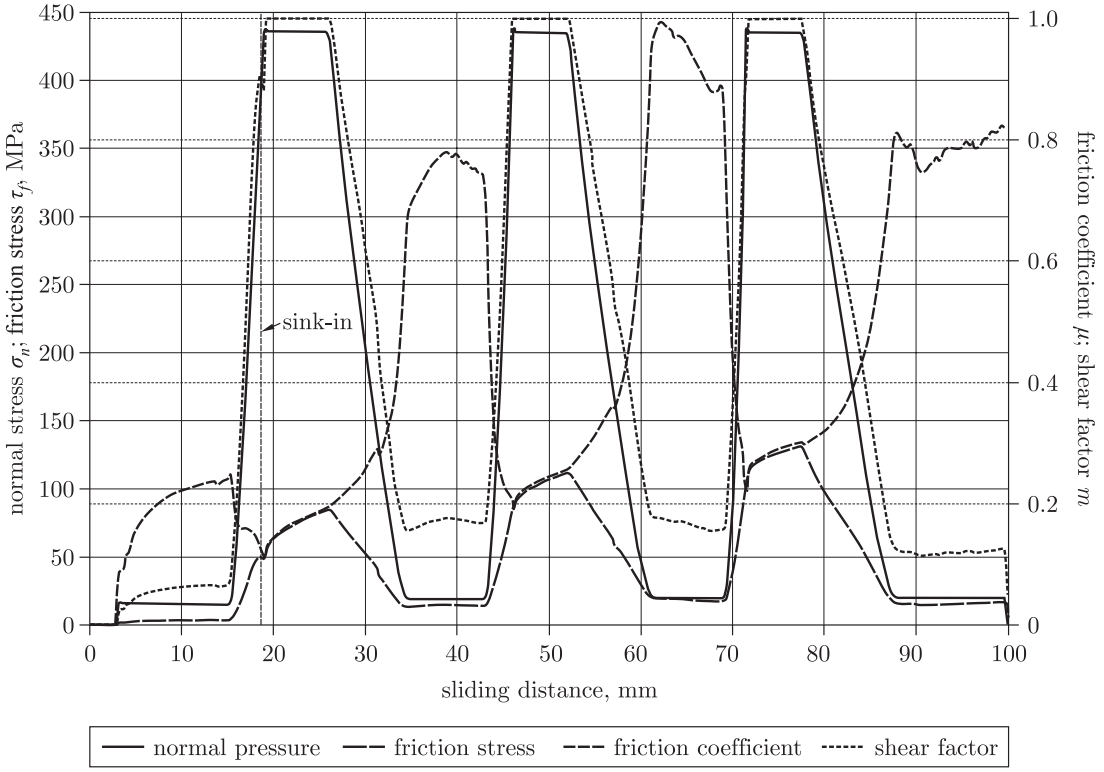

Figure 4.1: Friction experiment with two levels of normal pressure without lubrication. The fact that the friction stress at the low level raises significantly after the first compression phase compared to the initial value as well as the steadily raising friction stress under the high pressure level indicate the influence of the friction history.

on. The fact that the friction stress at the low level had significantly raised after the first compression phase compared to the initial value as well as the steadily raising friction stress under the high pressure level indicate the influence of the friction history. Further experiments with a anti-seizure paste as lubricant validated that the influence of the friction history is also present at lubricated interfaces (see Figure 4.2). The significant rise in the friction stress from the initial value at low pressure to the low pressure level after compression can be estimated by comparing the corresponding friction coefficients.
From these considerations, it is obvious that simple friction models as Amontons' law or the shear factor model cannot adequately represent the interactions in the tool-workpiece interface. For comparison, the friction coefficient and the shear factor are plotted in Figures 4.1 and 4.2. It is easily seen that neither a constant μ nor a constant m-value are suited to represent friction. Furthermore, it is shown that the shear factor law is not applicable to local friction modeling: Although the real contact area remains almost constant after the first compression stage, the friction stress varies significantly, what is obviously due to the changing normal pressure that is not considered in this model. However, when calculated from the measurements, the shear factor can indicate the correct conditions at

the interface in terms of sliding and sticking friction.

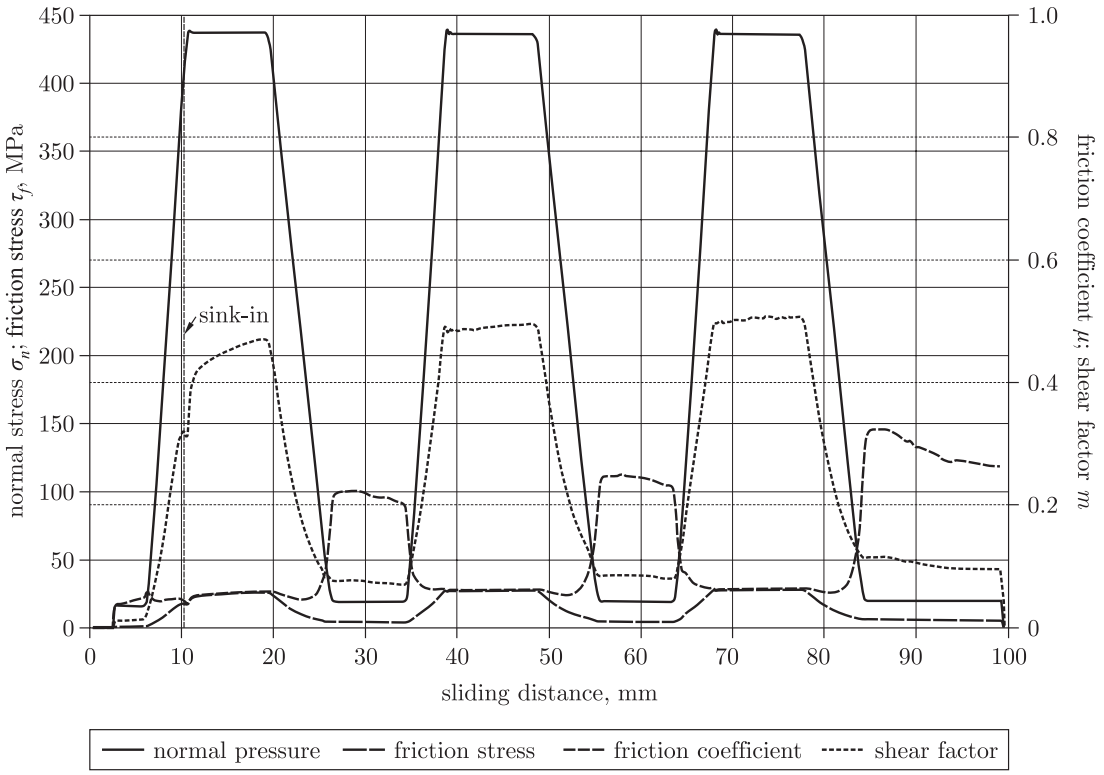

Figure 4.2: Friction experiment with two levels of normal pressure and anti-seizure paste as lubricant. From this test, the influence of friction history in the presence of lubricant is validated. The significant rise in the friction stress from the initial value at low pressure to the low pressure level after compression can be estimated by comparing the corresponding friction coefficients.

The basic requirement on a friction model should be the correct representation of the friction stress under conditions as present in the described tests. No general validity of the model is demanded, on the contrary, a customisation to the regarded application reduces the complexity of the model and thus the additional effort. Thus, for the investigated process of warm impression die forging, e.g. a rigid smooth tool and a plastic rough workpiece can be considered. Furthermore, the model can be restricted to solid lubricants applied onto the die surface. Different metals and lubricants should be considered e.g. in terms of their material properties, and a wide range of load conditions should be represented. Finally, the friction history has to be taken into account.

4.2 New Concept

4.2.1 State of the Art and Chosen Concept

Basically, two different methods are available for the formulation of friction models that take the complexity of the tribosystem into consideration: physical and empirical approaches.
In *physical approaches*, the conditions at the die-workpiece interface are described by means of contact models and local friction laws[1]. Most of the investigations of this kind are restricted to the (simpler) case of non-lubricated systems. Thus, for example, Wanheim et al. [58] calculated the real contact area from the slip-line theory and applied the constant shear factor model in the area of real contact. The time dependency of friction was only considered in terms of junction growth (comp. Figure 2.6).
Empirical approaches are based on empirical relations, that are parameterised by means of extensive friction tests. Commonly, the behaviour of a single system is investigated under various tribological loads. Of course, the results are only valid for the regarded application. Empirical models were proposed by Hemyari [112] and Doege et al. [4], for example.
However, due to the complexity of tribological systems, both approaches result in rather complex relations, especially in the presence of intermediate layers. A balance between the oversimplified but easily manageable classical friction coefficient or shear factor law and the high sophisticated approaches described above is found in the application of adaptive friction coefficients or shear factors as proposed for example by Behrens and Schafstall [131] and Bederna [122].

Regarding a scientific investigation of tribological phenomena, it was decided to utilise a physical approach to friction modeling. The exact knowledge of the real contact area is the basis for a physical friction model due to the fact that friction can only take place at the contact spots. Thus, the first task in friction modeling was the development of a robust contact model. In contrast to Wanheim's approach, real materials and surface conditions should be considered by making use of finite element analysis. Such attempts were already made by other authors in the past (see e.g. Neumaier [63]), however, their calculations were complex, time consuming and restricted to plain-strain problems and dry contact. In the present analysis, simplification should be achieved by the following considerations: On the one hand, the assumptions proposed in the previous section under

[1] Local friction models express friction in the real contact area

conditions of warm impression-die forging should be used. On the other hand, model asperities that represent the profile of real surfaces should be applied instead of whole profile traces in order to reduce the computational effort. However, the contact model had to cope with the influence of a solid lubricant on surface smoothing. The whole procedure of friction modeling was considered as follows:

1. Determination of the parameters of the tool-workpiece interface in terms of specimen roughness, material properties (tool, workpiece, lubricant) and amount of applied lubricant.

2. Simulation of the deformation of a model asperity (that represents the real workpiece surface) under various loads corresponding to the investigated process. From these calculations, the load-compliance law is determined.

3. Formulation of a local friction law regarding the demands stated in Section 4.1.

4. Calculation of the friction stress in dependence on the applied normal pressure; provision of the resulting relations in finite element codes.

Of course, this approach does not result in a general friction law but describes the frictional behaviour at the investigated interface. However, the contact model as well as the local friction model, whose development was out of the scope of the presented work and had to be performed in further investigations, should be of generality.

4.2.2 Representation of Real Surfaces

As the present analysis should consider real surfaces without extensive computational effort, model asperities that represent the shape of the original surface as well as its physical behaviour had to be found. In order to generate an experimental data base, a specimen of aluminium sheet was first sand-blasted and then compressed by a flat, polished steel punch without lubrication. The specimen's surface was inspected before and after compression by means of a confocal laser scanning microscope (LEXT OLS3100, Olympus, Japan) that is described in detail by Maass [29]. The results of surface inspection are presented in Figure 4.3 in terms of intensity images and three-dimensional profiles. From this 3D-profiles, sections were acquired at different widths (y = 48, 96 and 144 µm) and combined to a single 2D-profile for further investigations by means of a MATLAB® routine.

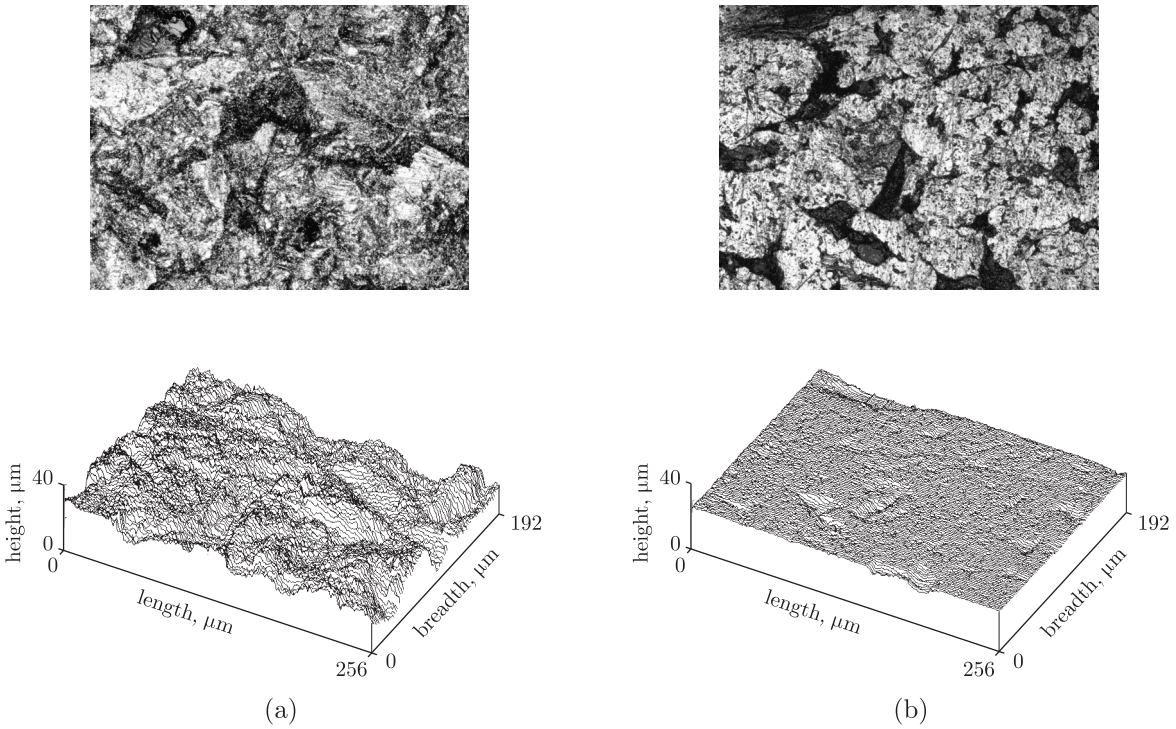

Figure 4.3: Original (a) and compressed (b) sand-blasted surfaces inspected by means of a confocal laser scanning microscope. In the intensity images (top), bright regions correspond to high areas, whereas dark regions represent valleys and cavities. From these measurements, a data base for further investigations was generated.

Figure 4.4 shows the bearing area curve and the Hansen asperities of the original and the compressed surface calculated by Equations (2.4) and (2.5), respectively. When comparing the bearing area curves, it is found that the line representing the compressed surface has not only lower values than the curve of the original profile (this follows from the obviously reduced roughness), but that also its slope is reduced. This is due to the formation of plateaus and the therefore enhanced bearing area at equal relative profile reductions[1]. When regarding the Hansen model asperities, it is apparent that the original surface has a mean asperity slope of 45 ° what is quite much compared with the values found in the literature (comp. e.g. Butler [39], Fogg [60] and Hansen [38]). However, further measurements at different areas of the specimen proofed that the mean asperity slope of the original surface was in the range of 40–45 °, and this finding is evident when regarding the undistorted 2D- or 3D-profiles of the sheet. Surprisingly, the Hansen asperity of the compressed surface is slightly flattened in the upper region, resulting in a mean asperity slope of 35–40 °. Obviously this behaviour is due to the non-ideal plastic material properties of the specimen.

[1] The relative profile reduction is the profile reduction divided by the initial peak-to-peak roughness.

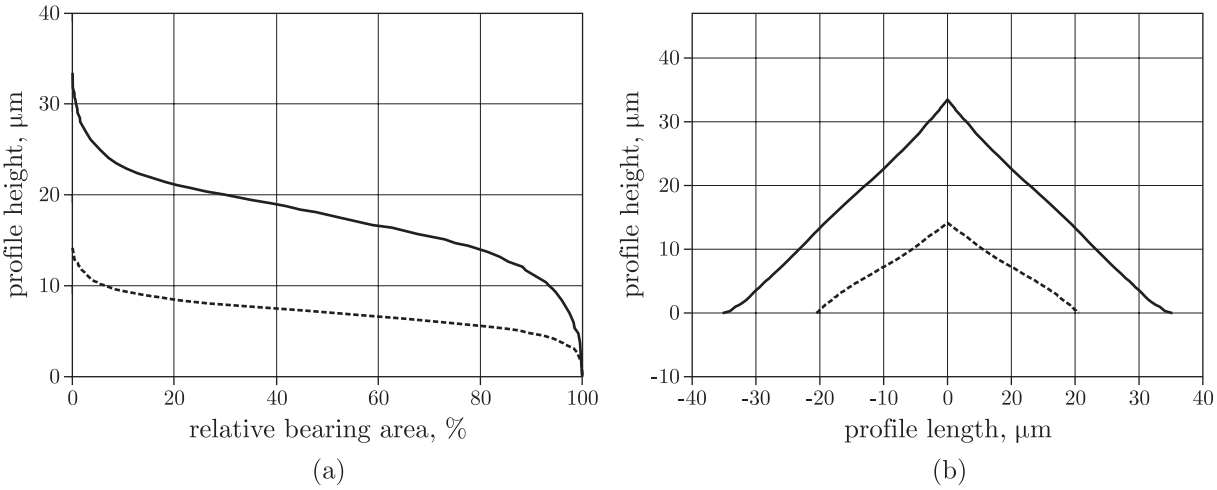

Figure 4.4: Model asperities representing the original (solid line) and compressed (dashed line) surface shown in Figure 4.3: The bearing area curve (a) and the Hansen asperity (b).

The basic demands on a model asperity that represents the behaviour of the real surface under compression are the correct prediction of the real contact area and the correct determination of the required compression force. Unfortunately, non of the described model asperities meet these demands: Of course, the bearing area curve gives a very well prediction of the real contact area, however, its width is not defined in terms of a length. Thus, no conclusions concerning the compression load can be made. On the other hand, the Hansen asperity allows the determination of the normal pressure required in order to compress the profile to a defined remaining height, but the real contact area of the original surface is not correctly predicted.

Based on these considerations, an attempt was made to determine a characteristic width (length) of the bearing area curve in order to get reliable load information when the profile was compressed. The main idea was that the new model asperity should represent the mean asperity slope at the height where the most intersections with the real profile were found. Hence, the absolute frequency of profile intersections per height, the bearing area curve and the Hansen profile were calculated for the original surface given in Figure 4.3 (see Figure 4.5). The height with the maximum number of profile intersections was determined (see Figure 4.5 (a)), and the corresponding profile sections with their slopes were determined in the model asperities. Finally, the bearing area curve was scaled in width in order to get the same slope at the considered profile section as in the Hansen asperity (see Figure 4.5 (c)). However, as can be seen, the resulting profile is narrow and has a very sharp top what complicates its use in numerical analysis. Furthermore, preliminary simulations revealed that already small variations in width caused a significant variation of the compression force. From these investigations, it was concluded that the

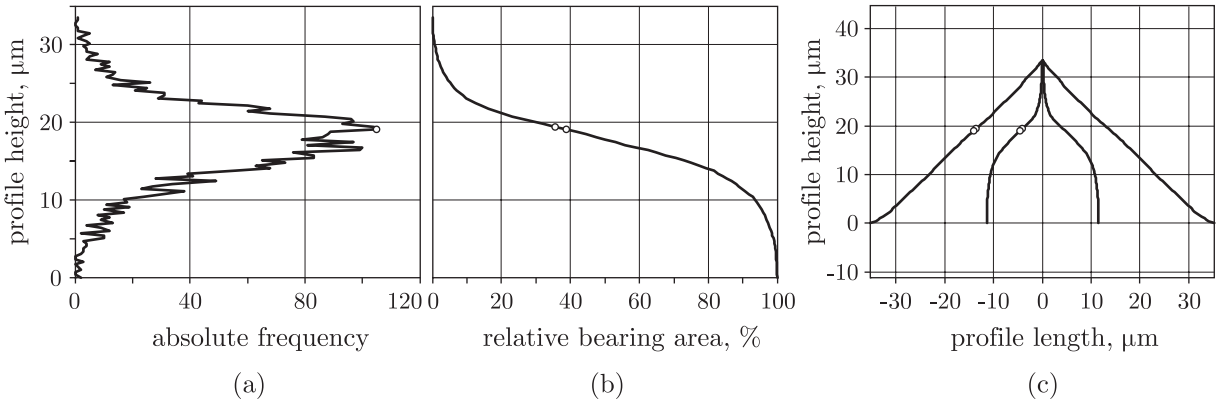

Figure 4.5: Determination of a model asperity for the correct prediction of real contact area *and* compression load: The absolute frequency of profile intersections per height (a), the bearing area curve (b) and the Hansen profile (c) were calculated for the original surface given in Figure 4.3. Then, the bearing area curve was scaled in width in order to get the same slope as the considered profile section in the Hansen asperity (c).

modeling of a real surface by a single model asperity is not possible. Hence, the new contact model should take into consideration the bearing area curve as well as the Hansen profile.

4.2.3 Analysis of Contacting Surfaces

The basics of the contact of dry metallic surfaces were already discussed in Section 2.2. This chapter aims in the practical application of the introduced theories and methods on the present investigations.

In order to understand the findings cited in the literature (see Section 2.2.4), some finite element analysis were performed. A model asperity (see Figure 4.6 (a)) with different slopes (5–60 °) was investigated using DEFORM® 2D. Makinouchi et al. [164, 165] have analysed the flattening of model asperities under plain strain deformation with plastic finite element analysis and found significant difference between the flattening with and without bulk deformation. Thus, a large amount of bulk material was considered in the actual investigation. Aluminium (Al 99.8 and AA1100), steel (AISI 1006) and lead (Pb 99.98) were used as workpiece material and constrained spreading was assumed. It was found, that the critical slope angle was for all materials in the range of 15–25 ° (see Figure 4.6 (b)). At values smaller than 15 °, complete conformation was achieved, and at slopes greater than 25 °, all materials showed remaining cracks. Of course, the maximum crack length was limited to half the initial peak-to-peak roughness.

These results are inconsistent to analysis performed by Kienzle [42], who presents pho-

tographs of an lead asperity with a slope of 40 ° before and after deformation. In contrast to the numerical results, this asperity was completely flattened. The reason for this was found to be a very well pronounced radius in the floor of the valley. Further simulations showed that – if the radius was large enough – the critical slope could be shifted to significant higher values (see Figure 4.6 (c)).

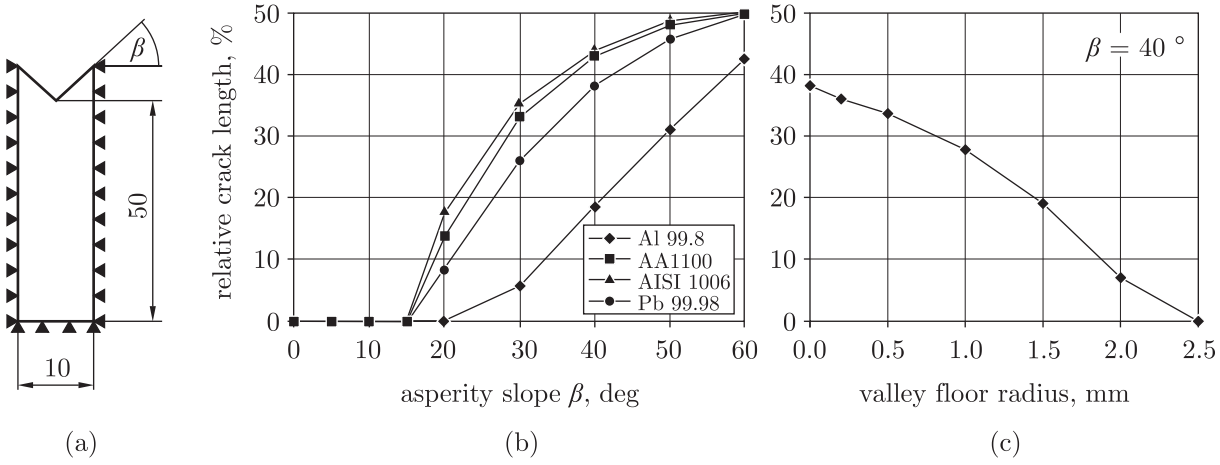

Figure 4.6: Simulation of asperity flattening: (a) shows the model asperity, where the asperity slope is varied within a range of 5–60 °, (b) presents the relative crack length in dependence on the slope and (c) gives the relative crack length in dependence on the valley floor radius for a slope of 40 °. The relative crack length is the crack length divided by the initial peak-to-valley height.

Furthermore, Heller's conclusion, that *"the final profile looks like the original profile where the amount of die stroke is removed"* could be validated at least for asperity slopes smaller than or equal to 45 °. It was found that the mean asperity slope remained almost constant during deformation and also independent on the formation of cracks (see Figure 4.7). Of course, when the slopes exceed 45 °, bulging takes place (comp. Kienzle [42]).

4.2.4 Consideration of Lubricant

In order to investigate the influence of lubricant in the die-workpiece interface on surface smoothing, tests were performed similar to that described in the previous section. On the one hand, a sand-blasted aluminium sheet was compressed by a flat, polished tool covered with graphite-based lubricant[1], and on the other hand, for comparison, a mineral

[1] The tool was lubricated at elevated temperatures, but the tests were performed at room temperature.

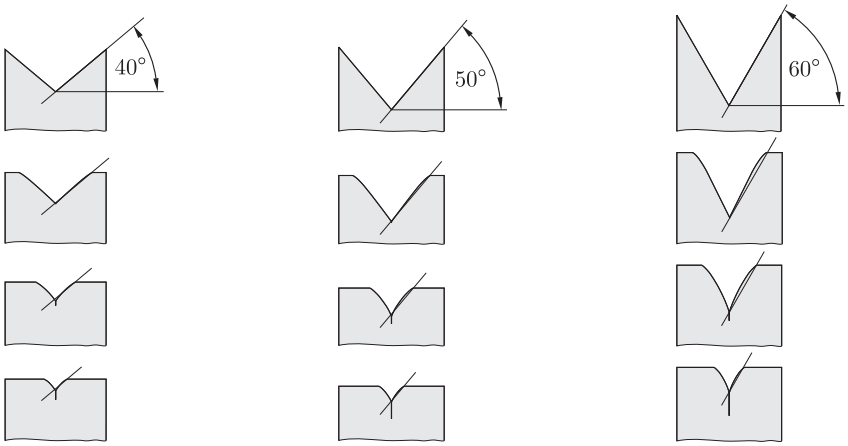

Figure 4.7: Evaluation of the asperity slope during deformation. It was found that the mean asperity slope remained almost constant during deformation also in the presence of cracks.

oil was applied onto the sheet. After the tests, the specimen were carefully cleaned and inspected by means of a confocal laser scanning microscope; the results are presented in Figure 4.8.

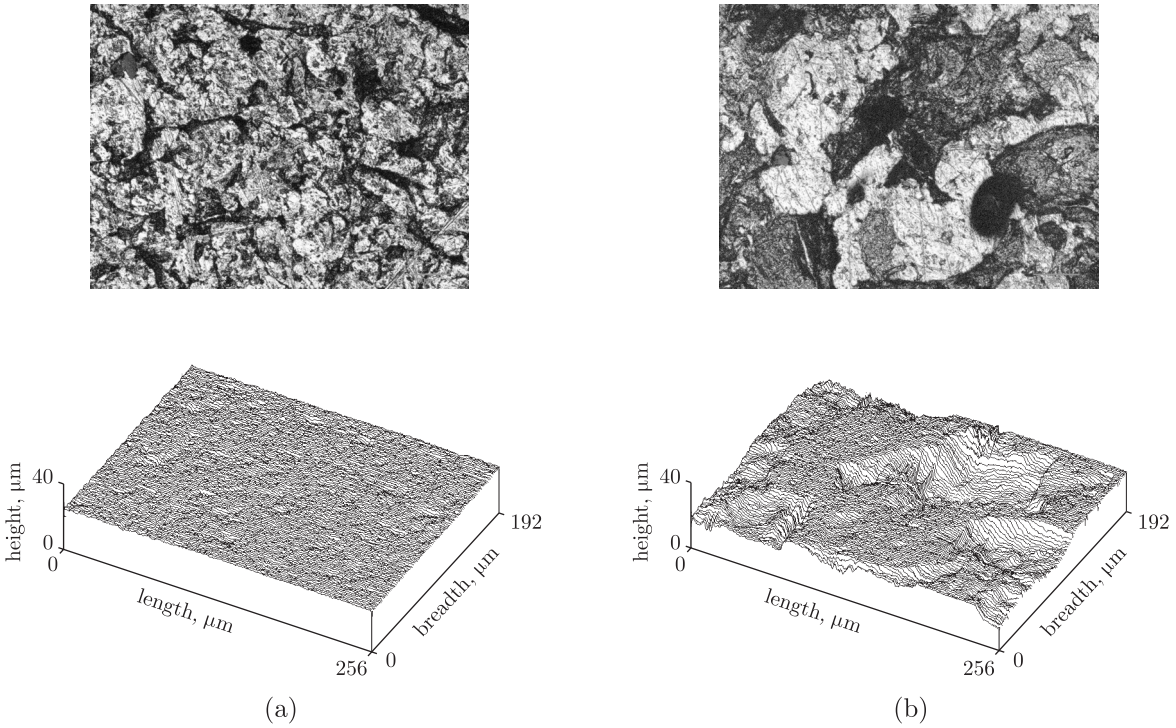

Figure 4.8: Sand-blasted aluminium sheet compressed by means of a polished, graphite-coated tool (a) and by means of fluid lubrication (b). The specimen were cleaned and inspected by means of a confocal laser scanning microscope. The original shape of the surface is presented in Figure 4.3 (a).

The different behaviour of the lubricants is apparent: While excessive liquid lubricant was squeezed out of the interface and the remaining oil formed well pronounced lubricant pockets, the solid lubricant led to a very smooth surface (comp. with Figure 4.3 (b) where no lubricant was used). From the latter surface, again three different sections were acquired at different breadths ($y = 48$, 96 and 144 µm) and evaluated in terms of a bearing area curve and a Hansen profile (see Figure 4.9). It is seen that the bearing area curve has slightly higher values than that acquired without lubrication, and the slope of the hansen profile is almost the same as that obtained from the original profile.

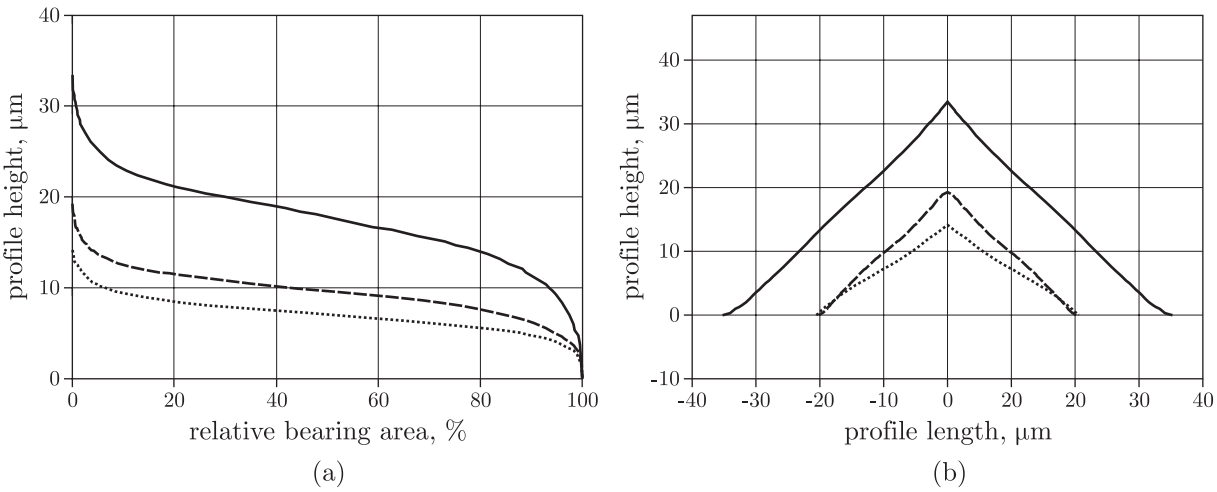

Figure 4.9: The bearing area curve (a) and the Hansen asperity (b) of the original surface (solid line), the surface compressed by means of graphite lubricant (dashed line) and the surface compressed without lubrication (dotted line).

In the further investigations, graphite-based lubricants were decided to have the same fundamental behaviour as porous materials because of their composition of fine graphite particles and polymeric binders. Thus the numerical analysis presented in the previous section was repeated, where the valley between the asperities was filled with a wedge of 30 % relative density, what was a realistic value regarding virgin, graphite-based lubricant films. However, the results revealed that the lubricant film had no significant influence on the asperity smoothing. In fact, the cracks started to form at the same strokes as they did in the absence of lubricant; the only exception was found at asperity slopes smaller than 40 ° where the relative density of the lubricant became 100 % and thus restricted the maximum real contact area before a crack was initiated in the unlubricated case.
For a estimation of the maximum real contact area in the application of porous lubricants, an analytic approach was developed assuming a constant asperity slope β during

deformation[1]. Furthermore, it was assumed that the best representation of an isotropic surface was a cone (see Figure 4.10 (a)) with the same mean slope as the Hansen profile and an asperity volume of

$$V_a = \frac{r^3 \cdot \pi \cdot \tan(\beta)}{3} \ . \tag{4.1}$$

When the lubricant layer is assumed to fill at least the surface valleys, the initial lubricant volume follows with

$$V_{l,in} = \frac{2 \cdot r^3 \cdot \pi \cdot \tan(\beta)}{3} \ , \tag{4.2}$$

and when the relative density of the layer is indicated by ρ_{rel}, its final volume is given by

$$V_{l,f} = \frac{2 \cdot r^3 \cdot \pi \cdot \tan(\beta)}{3} \cdot \rho_{rel} \ . \tag{4.3}$$

From the final total volume $V_f = V_a + V_{l,f}$, the final height can be calculated as

$$h_f = \frac{r \cdot \tan(\beta)}{3} \cdot \left(1 + 2 \cdot \rho_{rel}\right) \ . \tag{4.4}$$

When regarding the situation in Figure 4.10, the volume of the deformed asperity is expressed by

$$V_{a,d} = r^2 \cdot \pi \cdot \Delta r \cdot \tan(\beta) + \frac{\pi \cdot \tan(\beta) \cdot \left(r^3 - \left(r_x + \Delta r\right)^3\right)}{3} \ , \tag{4.5}$$

and when remembering that the asperity's volume must not change during deformation (e.g $V_a = V_{a,d}$), the following relation is determined:

$$r^2 \cdot \Delta r - \frac{\left(r_x + \Delta r\right)^3}{3} = 0 \ . \tag{4.6}$$

Now, the value of r_x at the final height h_f can be easily calculated with

$$r_x = \frac{r \cdot \tan(\beta) - h_f}{\tan(\beta)} \ , \tag{4.7}$$

[1] This assumption was based on the findings of other authors (comp. [40, 41, 61, 104]) and on own investigations (see Figures 4.7 and 4.9 (b)).

and when inserting in Equation 4.6, Δr can be determined. Finally, the value of the maximum real contact area is given by

$$\alpha = \frac{\left(r_x \cdot \Delta r\right)^2}{r^2} \ . \tag{4.8}$$

Figure 4.10 (b) presents the load-compliance relation for the compression of a 45 °-cone shaped asperity with graphite-based lubricants of different relative density determined by numerical simulation and the analytically determined maximum relative contact areas.

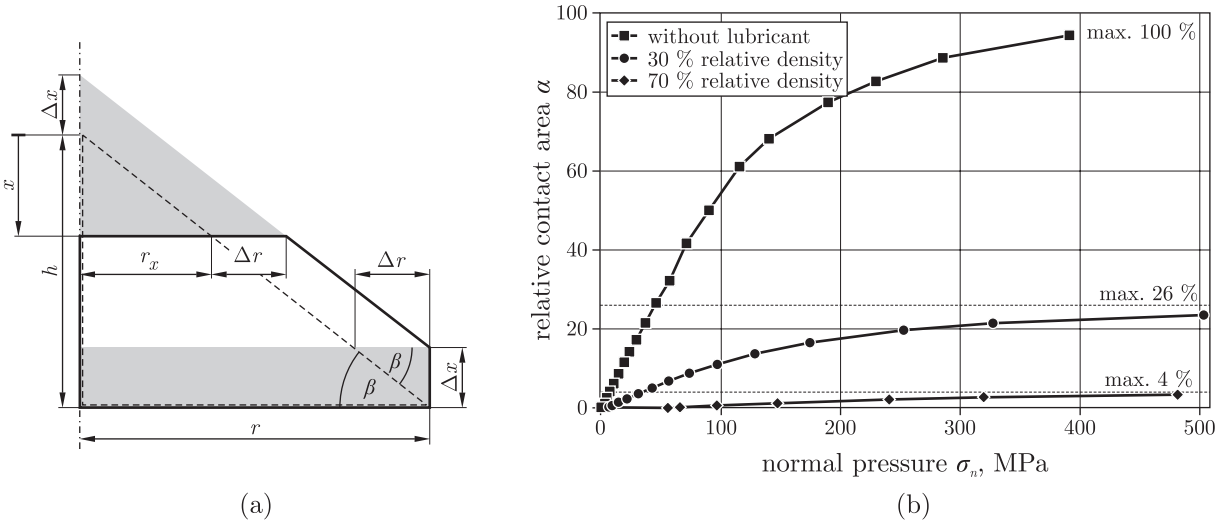

Figure 4.10: Analytical determination of the maximum contact area in the application of porous lubricants: geometrical model (a) and results (b). When the original cone ((a), dashed line) is compressed by the amount x, the displaced material (gray cone at the top) reappears as a uniform rise at the bottom of the asperity (gray disc at the bottom side). As a consequence, the radius r_x at stroke x is enlarged by the amount Δr. The load-compliance relation (b) for the compression of a 45 °-cone shaped asperity with graphite-based lubricants of different relative density as found by a DEFORM® 2D simulation. The radius at the base of the cone was $r = 5$ mm, the asperity was modeled with aluminium AA1100. The maximum relative contact areas determined by Equation (4.8) are indicated by dashed lines.

4.3 New Surface Contact Model

4.3.1 Basic Idea

The main idea of the new concept was now to obtain the real contact area-load relation by combining the bearing area curve and the Hansen profile as follows (see Figure 4.11):

1. The deformation of both profiles to a remaining height y(j) is simulated using a commercial finite element code (The simulation with the bearing area curve is necessary in order to take the real material flow and rising material due to volume conservation into consideration).

2. The real area of contact at step j, $A_{r,j}$, is determined from the deformed bearing area curve:
$$A_{r,j} = a_j \cdot \frac{A_a}{100}, \tag{4.9}$$
where a_j is the contact area with the die and A_a is the apparent area.

3. The corresponding total load $F_{t,j}$ is derived by relating the load $F_{H,j}$ (necessary to deform the Hansen profile to y(j)) to the real contact area determined from the bearing area curve:
$$F_{t,j} = F_{H,j} \cdot \frac{a_j}{b_j}, \tag{4.10}$$
where F_j (N) is the compression force at the remaining height y(j), and a_j (%), b_j (%) are the contact areas with the dies.

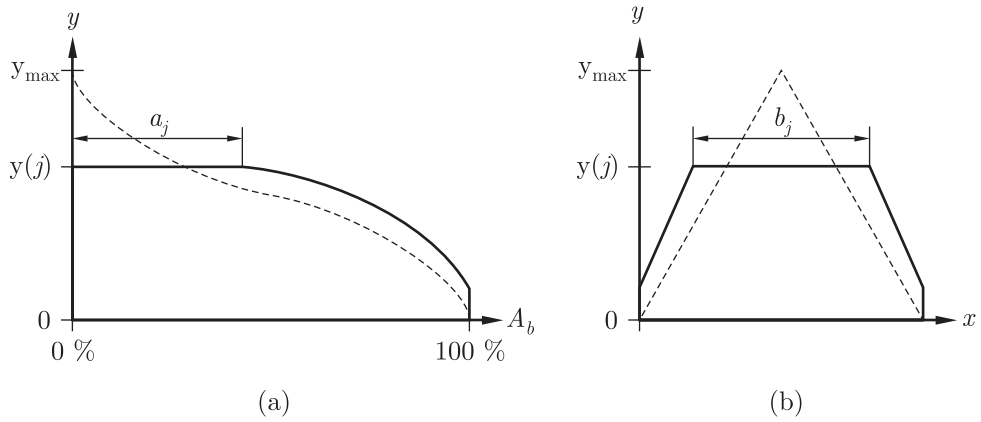

Figure 4.11: The main idea of the new concept: The deformation of the bearing area curve (a) and the Hansen profile (b) are calculated by finite element analysis. For a given remaining height y(j), the real contact area and total normal force are determined by Equations (4.9) and (4.10), respectively.

4.3.2 Numerical Simulation

4.3.2.1 Geometrical Input Parameters

In a first step, a surface profile was obtained from a ground aluminium specimen. Then, the bearing area curve and the Hansen profile were calculated by means of Equations (2.4) and (2.5), respectively. Figure 4.12 gives the original profile and the model asperities for the investigated surface.

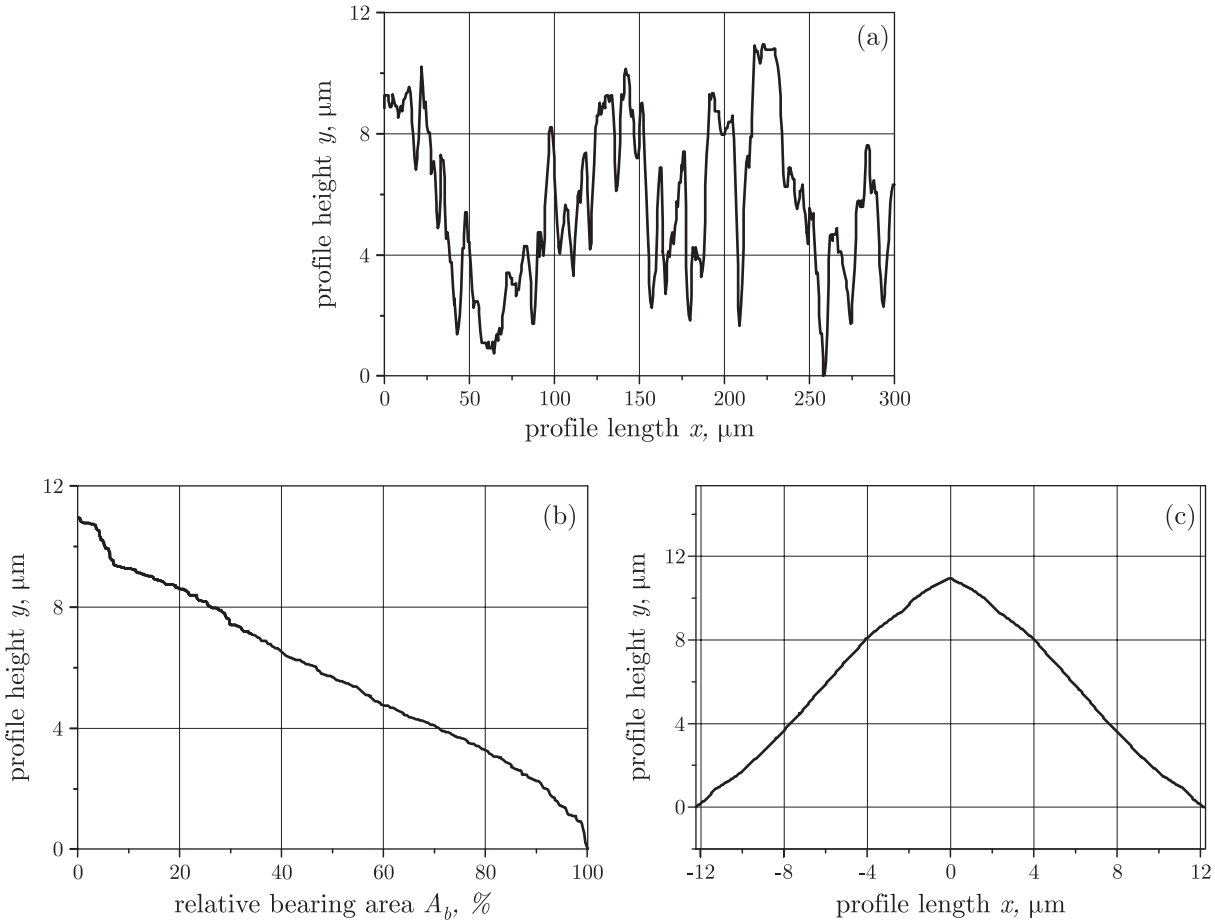

Figure 4.12: Surface profile (a), bearing area curve (b) and Hansen profile (c) of aluminum AA6016 as used for the numerical calculation.

4.3.2.2 Numerical Modeling

For the geometrical model, metal forming conditions were assumed, i.e. the tool surface was decided to be much smoother than workpiece surface and therefore plane dies were employed.

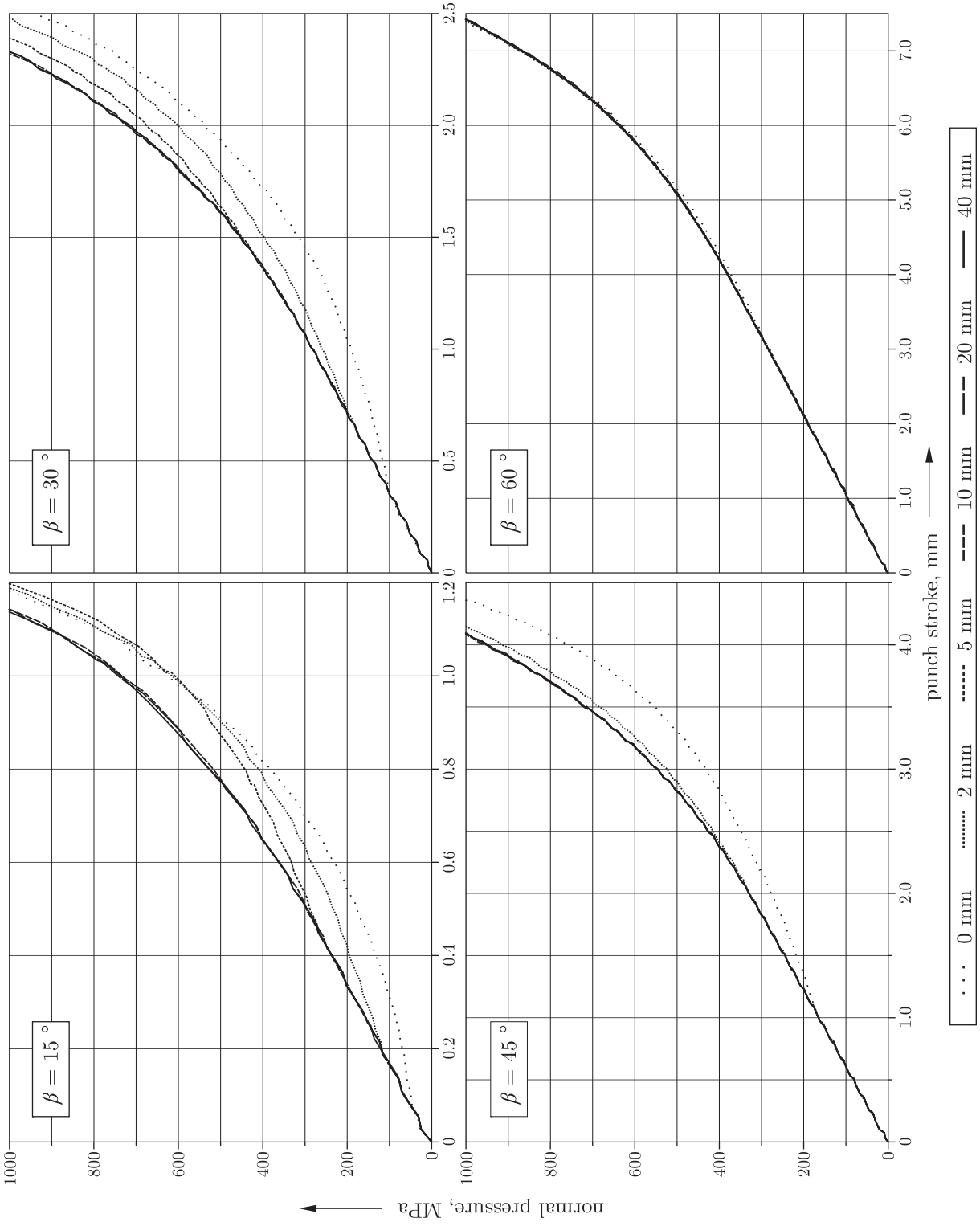

Figure 4.13: Determination of the influence of bulk material: It is seen that the influence of bulk material decreases with increasing asperity slope. The minimum height of bulk material to be considered in the simulation is half the profile width of 20 mm.

As Makinouchi et al. [164, 165] have found significant difference between the flattening with and without bulk deformation, preliminary simulations were performed aiming in the identification of the minimum bulk height leading to correct load calculations. The model asperity made of AA1100 was similar to that shown in Figure 4.6 (a), where the breadth was 20 mm, the asperity slope was varied from 15–60 ° and a bulk height of 0–40 mm was considered. The results are presented in Figure 4.13; it is easily seen that the influence of bulk material decreases with increasing asperity slope. The minimum height of bulk material to be considered in the simulation was identified to be half the profile width (higher bulks had no further effect on the load calculation).
In the modeling of the Hansen profile, further simplification was achieved by making use of the symmetry of the asperity. The geometrical models used for the simulation are shown in Figure 4.14.

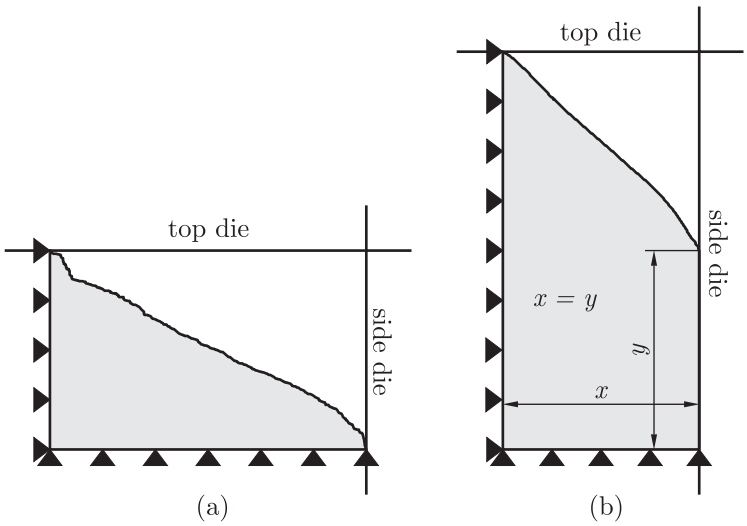

Figure 4.14: Geometrical model of the bearing area profile (a) and the Hansen profile (b) for the finite element analysis. In the simulation of the Hansen profile, bulk material had to be considered in order to calculate the correct loads.

The simulation was performed as plain-strain calculation in DEFORM^{TM} 2D, and the results are presented as solid line in Figure 4.15 (a); the corresponding flow chart is presented in Figure 4.15 (b).

4.3.2.3 Numerical Validation of the Concept

The principal correctness of the proposed concept was validated by comparing the real contact area-load curves of the simulation described above and a simulation of upsetting

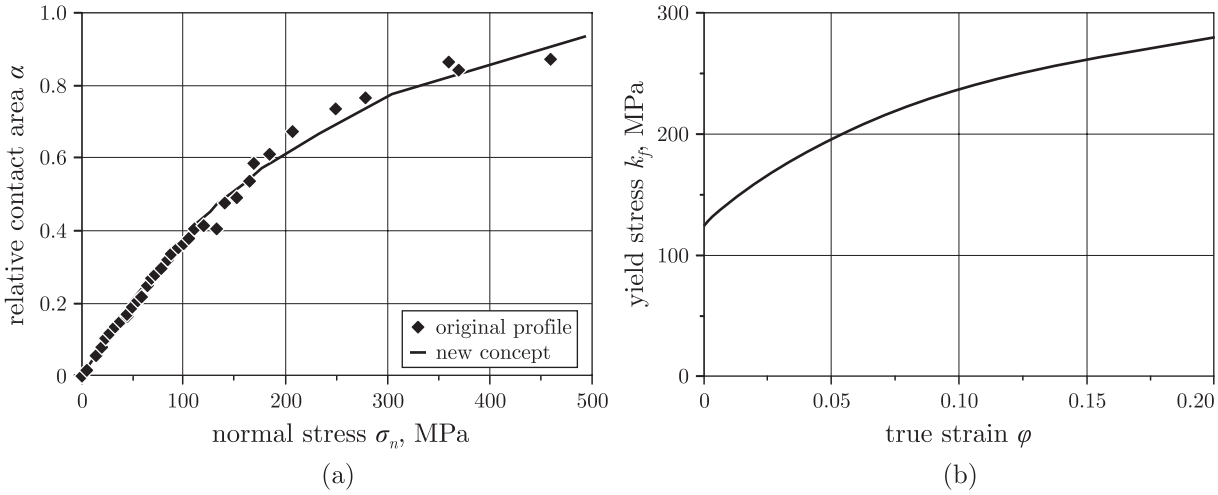

Figure 4.15: Numerically validated results of the new concept (a) and flow curve of aluminium (AA6016) at room temperature (b). The line in (a) was calculated by means of the new method, the points were determined from the simulation of the original profile (see Figure 4.12 (a)).

the original profile.

For the simulation with the original profile, the same parameters were used as before. The height of bulk material under the original profile was set to half the profile width (150 µm), as correct forces had to be considered. The results of this simulation are shown in Figure 4.15 (a) as diamonds, and the good correspondence with the results obtained by the new concept is obvious. From this, it could be stated that the new concept with its simplifications represents the original system very well.

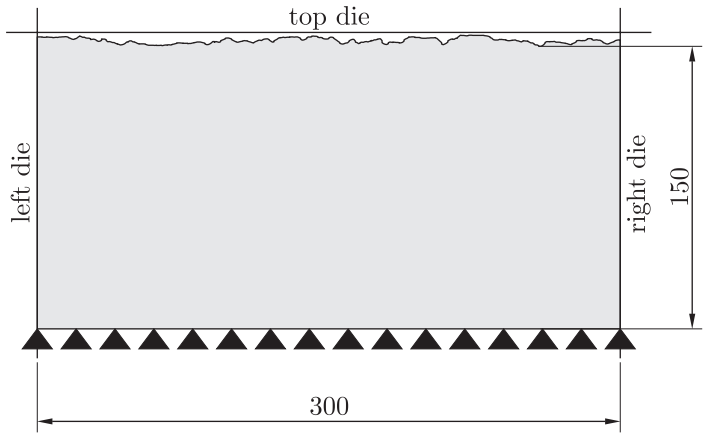

Figure 4.16: Geometrical model of the original profile for numerical validation.

4.3.3 Experimental Verification of the Concept

In order to investigate if the new concept is suitable to model real forming conditions, additional to the numerical validation an experimental validation was performed.

4.3.3.1 Experimental Setup

As Greenwood and Rowe [159] have pointed out, deformation of surface asperities can only be achieved by coining operation or when the deformation of the bulk material is prevented. Due to the problem of determining flow curves of sheet metals (especially at elevated temperatures), it was decided to perform closed die upsetting experiments similar to that proposed by other authors (see e.g. [41, 61]). Cylindrical specimen made of AA7075 were placed into a container and compressed by a hardened steel tool at different normal loads (see Figure 4.17). The specimen end faces were ground with sandpaper (220 grit) and the tool surface was polished with 3 µm diamond suspension. Before each experiment, tool and specimen were carefully cleaned with acetone.

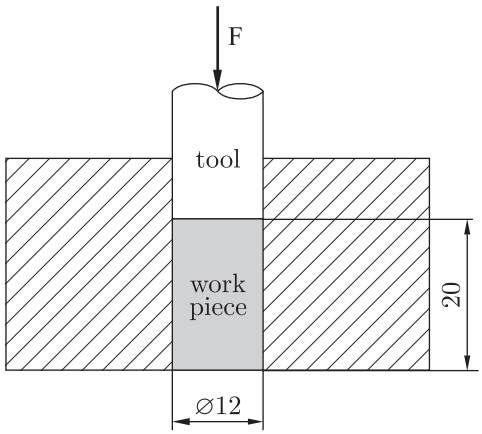

Figure 4.17: Experimental setup: Cylindrical specimen made of AA7075 were placed into a container and compressed by a hardened steel tool at different normal loads.

4.3.3.2 Evaluation of the Tests

After the experiments, the specimens were carefully removed from the container and again cleaned with acetone. Then, the upset end faces were inspected by means of a confocal laser scanning microscope. The 3D-surfaces measured with the microscope were saved as images (where the color of each pixel corresponded to a certain height) and opened in

MATLAB® for further processing.
In MATLAB®, the calculation of the real contact area was performed as follows (see Figure 4.18): At first, the hight distribution of the inspected surface region was calculated. The next step was the computation of a 1 % right-side interval (corresponding to the highest values) in order to remove outliers. From the remaining 99 % of the values, the real area of contact was decided to consist of the points with a maximum difference of 4 µm to the highest value. The threshold of 4 µm follows from the tool surface that was polished to an average roughness of 3 µm. The results of the experiments are plotted as diamonds in Figure 4.19 (a).

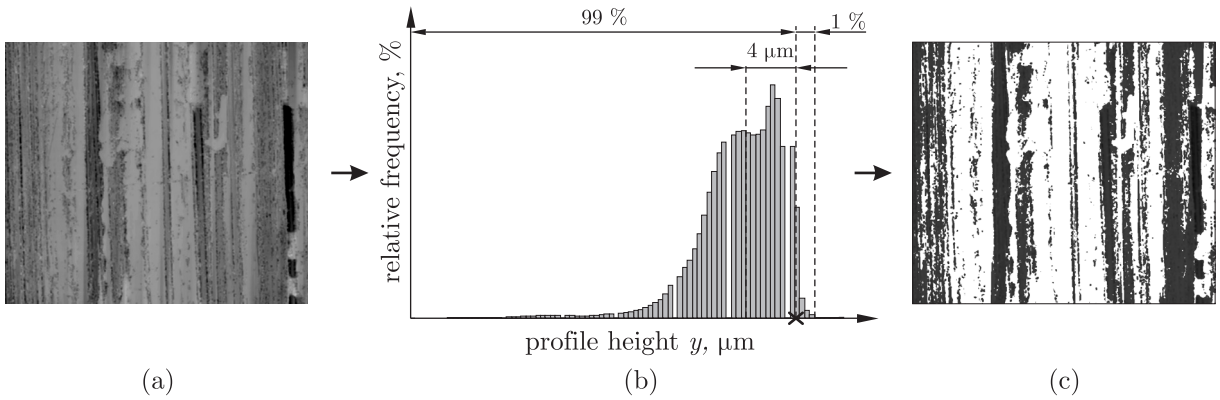

Figure 4.18: Determination of the real contact area from a height image (the color of each pixel corresponds to a certain height, (a)): The real area of contact was decided to consist of the points with a maximum difference of 4 µm to the highest value (see the height distribution, (b)). The result (c) shows the determined contact area in white.

4.3.3.3 Numerical Simulation of the Tests

The most important task in the simulation of the experiments was the exact determination of the material data. Since the specimen were heated by grinding and upsetting, it was not sufficient to consider just the virgin condition of the material, but the real conditions had to be modeled as close as possible. The heat generation during grinding is obvious, however, it was nearly impossible to get any data of the amount of local temperature rise. Thus, the temperature of the contact layer was assumed to rise to 250 °C. Cylinder compression tests showed that this temperature rise caused significant weakening of the specimen (the specimens were heated to 250 °C for 30 min, then cooled on air to room temperature, and then compressed; the flow curves are given in Figure 4.19 (b)). Due to this, the material data of the heat treated material had to be used in the simulation. In or-

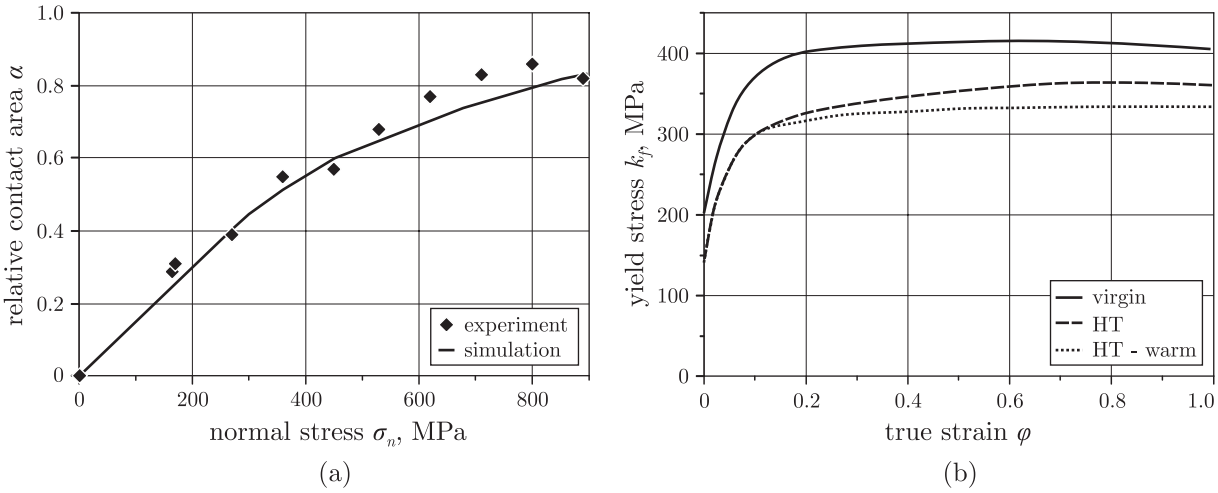

Figure 4.19: Experimentally validated results of the new concept (a) and flow curves of AA7075 (b). In order to take the heat treatment due to grinding and warming due to deformation into consideration, heat treated specimens were tested at room temperature (HT) and 105 °C (HT-warm).

der to take into consideration also heating due to deformation (Hofmann and Kirsch [166] stated that this temperature rise can be up to 90 °C), flow curves had also to be acquired at elevated temperatures.

The principal procedure of numerical modeling was equal to that described in the Sections 4.3.2.1 and 4.3.2.2. The original profile and the model asperities are shown in Figure 4.20. However, there were two differences: At first, the area bearing curve and the Hansen profile were not calculated from a single surface profile, but from a series of seven profiles in order to get a solid statistical basis. Furthermore, heat generation due to deformation was considered during the analysis. The results of the simulation are compared with the experimental data in Figure 4.19 (a), and the correspondence is very good.

4.4 Results and Future Work

The new concept based on the combination of the bearing area curve and a model asperity representing the average asperity slope of the original surface profile shows very good correspondence with experimentally obtained data and the results of the calculation can be easily integrated e.g. in numerical friction models. The proceeding is advantageous compared to up-to-date methods because no limiting assumptions are made in terms of material properties (e.g. strain hardening) or geometry (the concept is independent on the asperity slope). On the other hand, the new approach allows the determination of the

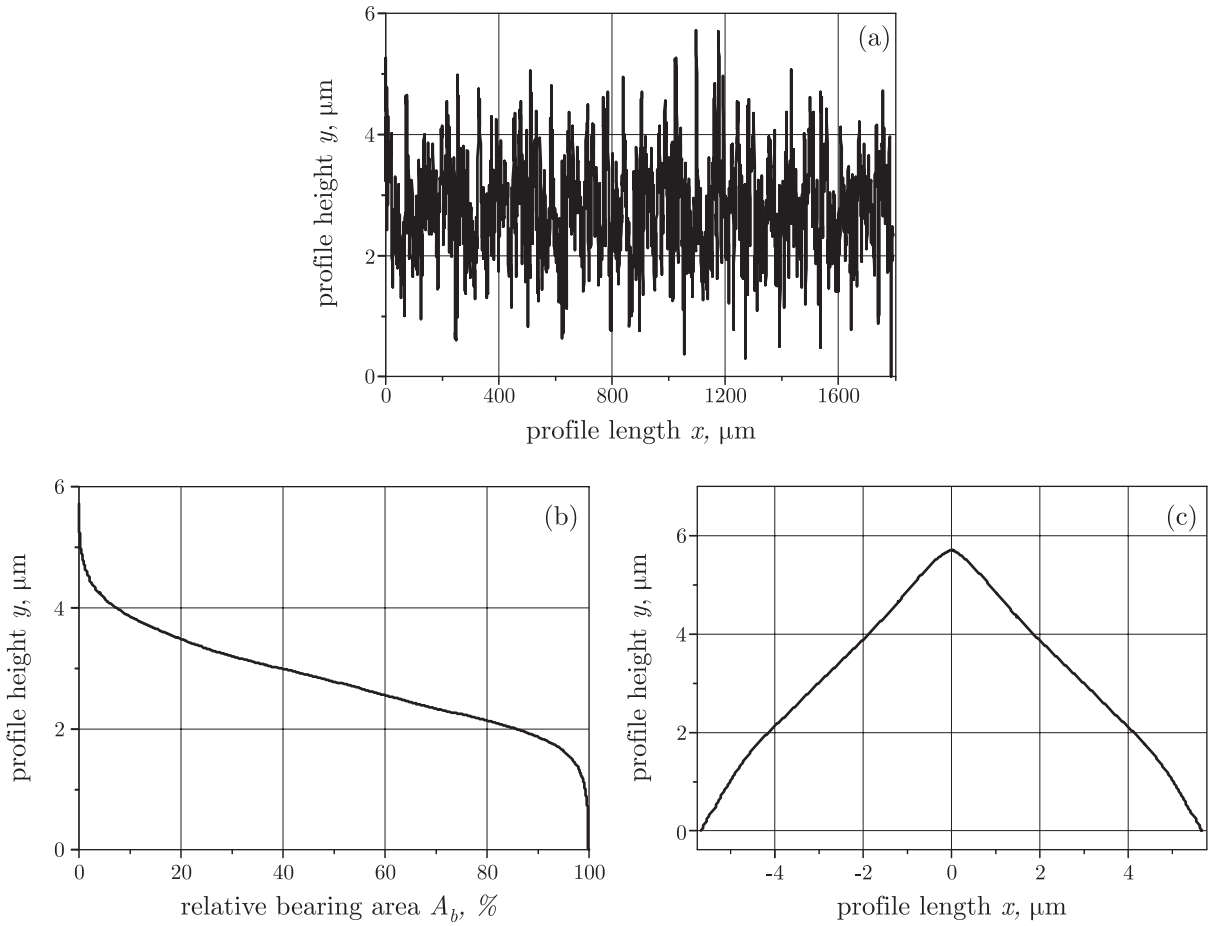

Figure 4.20: Surface profile (a), bearing area curve (b) and Hansen profile (c) of AA7075 as used for the numerical simulation of the tests.

real contact area-load relation for any surface compressed by a flat tool without excessive effort. In fact, the new concept gives a better statistical representation of the surface than Neumaier's [63] approach because much longer surface profiles can be considered. Additionally, the time consumption of the new method is much lower than that of simulating the compression of the original profile. Besides, the proposed concept allows simply theoretical analysis of interface problems by use of Hansen asperities. The calculation of the real forming conditions can then be easily performed by making use of the bearing area curve.

However, there are still many problems to be solved in future investigations: A serious problem present also in the simple case of dry contact is the commonly used constitutive material laws. The elastic and plastic material parameters are only valid for a macroscopic scale. The single roughness asperities, however, have a microscopic scale in which the parameters have completely different magnitudes [64]. In fact, this was the reason why

ground instead of sand-blasted surfaces were used in the validation of the new concept: The changed local material properties due to sandblasting could not be described by the author.

The next step of the procedure of friction modeling proposed in Section 4.2.1 would be the consideration of a lubricant layer of certain height in the tool-workpiece interface. However, the constitutive material laws cause again serious problems. In contrast to liquid lubricants, whose properties can be easily described in terms of their viscosity and their bulk modulus, solid graphite-based layers have to be characterised in terms of their flow curves. Moreover, the layers have to be considered as porous materials, thus their initial relative density and the behaviour of the polymeric binders have to be taken into account.

Finally, a local friction model has to be developed taking into consideration the normal pressure, material properties and lubricant breakdown. Thus, the friction history has not only to be expressed in terms of the contact model, but also in terms of the local friction law.

5 Conclusion

Two new approaches for the investigation of friction in the die-workpiece interface under aluminium forging conditions have been presented: In the ring-on-disc test with entrapped specimen, lubricant exchange is prevented and thus lubricant aging can be studied, whereas the pin-on-disc test analyses the abrasion resistance of lubricant layers, what is of interest in processes in which the lubricant is applied onto the tools. From these considerations, ring-on-disc test and pin-on-disc experiment can be seen as complement methods in the investigation of friction in the tool-workpiece interface of warm forging processes. Both tests are appropriate approaches for friction testing under aluminium forging conditions when the toolkits are adapted to the flow behaviour of aluminium alloys and the demands of bulk metal forming, respectively. Moreover, a physical interpretation of the interactions at the tool-workpiece interface is permitted due to the independent variation of the main influencing parameters. However, none of the tests investigates the lubricant behaviour in the presence of surface expansion.
Regarding the complexity of tribological systems present at warm forging processes, the reproducibility of the results is good, and due to the stationary conditions during the tests, the results are representative. Certainly, the deficiency of missing surface expansion restrains the characterisation of lubricants, but it does not affect the validity of the investigation. However, there are two remaining problems to be solved in future analysis: On the one hand, a setup has to be designed that allows a defined surface expansion of the specimen, and on the other hand, the investigations should be performed at even higher loads and relative velocities in order to study the limits of the lubricants.

The experiments performed without lubrication clearly validated the asymptotic friction model proposed by Finnie and Shaw [28]. The fact that the results obtained by using different lubricants showed a similar – but much smoother – development of friction stress allows the assumption that the asymptotic friction law can be also applied to this case, where the yield shear stress of the lubricant has to be considered as the maximum friction stress. Regarding the friction coefficient, its value is very high at very low normal loads and sliding velocities irrespective of the presence and type of lubricant. However, negative effects are only found in unlubricated systems where extensive welding takes place.
As in solid lubricated interfaces (nearly) all shearing is done in the lubricant layer, the lubricant itself and the surface conditions of the friction partners are the dominating parameters of the tribological system. Considering the influence of the load collective, the effect of the contact pressure is clearly more pronounced than that of the sliding velocity.

Because of the complexity of tribological systems, models with just one parameter as the classical friction laws can present at best rough approximations of the interactions at the interface. However, due to the roughly asymptotic behaviour of the friction stress when lubricants are applied, a constant friction stress (corresponding to the shear yield stress of the lubricant layer) may be used as simplest representation of friction in the tool-workpiece interface. Moreover, when regarding the absolute values of the friction coefficient and considering the high contact loads, even the assumption of a constant μ seems possible, although this approach is not physically correct. Nevertheless, when applying Amontons' law in numerical analysis, the friction will be overestimated and concerning force calculations, the simulation will be on the "safe side". Of course, such a crude approach can not model the breakdown of the lubrication, that represents the limit of the process, due to aging and thinning or abrasion of the lubricant.

In order to take into consideration these influences, a new procedure to friction modeling was suggested based on a physical approach, i.e. a contact model and a local friction law. Although only a new contact model could be realised in the scope of this thesis, a clear advance could be obtained compared to state-of-the-art methods. The only possibility to enhance the quality of contact models consisted in representing the actual conditions in the die-workpiece interface as closely as possible. This means, that the evolution of the real contact area had to be determined for all mating surfaces in dependence on the contacting materials, their surface conditions and the lubricant layer. The new contact model based on the combination of the bearing area curve and a model asperity representing the average asperity slope of the original surface profile shows very good correspondence with experimentally obtained data and the results of the calculation. No other approach is able to describe the contact of a smooth tool with a rough workpiece in dry contact better in terms of real materials and surfaces and with less computational effort than the new model.

Of course, there are several remaining problems to be solved in future investigations. On the one hand, procedures for determining the microscopic properties of surfaces and lubricants as well as the limits of lubricant layers have to be developed, and on the other hand, a local friction model has to be formulated.

List of Figures

List of Tables

Bibliography

[1] T. Altan and V. Vazquez: "Status of process simulation using 2D and 3D finite element method 'What is practical Today? What can we expect in the future?' ", *Journal of Materials Processing Technology* **71**:49–63, 1997.

[2] P. Groche and B. Kappes: "Tribologie der Massivumformung – Modellprüfstände der Tribologie", in: "Tribologie und Schmierung bei der Massivumformung", (W. J. Bartz, ed.), vol. 13, pp. 1–14, expert verlag, Renningen-Malmsheim (Germany), 2004.

[3] E. Doege and M. Alasti: "Ergebnisbericht des Sonderforschungsbereiches 489-A2 (2000–2002): Erweiterte Simulationsmodelle für das Präzisionsschmieden", Tech. rep., Institut für Umformtechnik und Umformmaschinen, Universität Hannover (Germany), 2002.

[4] E. Doege, M. Alasti, and R. Schmidt-Jürgensen: "An innovative procedure for the numerical identification of accurate friction and heat transfer laws for precision forging processes", in: "9th ISPE International Conference on Concurrent Engineering: Research and Application – Advances in Concurrent Engineering (CE2002)", (R. Jardim-Goncalves, R. K. Roy, and A. Steiger-Garcao, eds.), pp. 199–207, Ashgate Pub Co, Cranfield (UK), 2002.

[5] U. Weiss: *Numerische Simulation von Präzisionsschmiedeprozessen mit der Finite-Elemente-Methode*, vol. 146 of *Fortschritt-Berichte VDI: Reihe 2, Fertigungsstechnik*, VDI Verlag, Düsseldorf (Germany), 1988.

[6] P. Groche and U. Weiss: "Numerical identification of forging parameters", in: "Modelling of Metal Forming Processes: Proceedings of the Euromech 233 Colloquium", (J.-L. Chenot and E. Onate, eds.), pp. 237–244, Kluwer Academic Publishers, Sophia Antipolis (France), 1988.

[7] R. G. Snape, S. E. Clift, A. N. Bramley, and A. N. McGilvray: "Forging modelling – sensitivity to input parameters using FEA", in: "12th National Conference on Manufacturing Research – Advances in Manufacturing Technology X", pp. 51–55, Bath (UK), 1996.

[8] R. Kopp and F.-D. Philipp: "Physical parameters and boundary conditions for the numerical simulation of hot forming processes", *Steel Research International* **63**(9):392–398, 1992.

[9] R. Kopp, R. Bünten, K. Karhausen, F.-D. Philipp, and R. Schneiders: "Maßnahmen zur Steigerung der Genauigkeit bei der Simulation und Optimierung umformtechnischer Prozesse", *Umformtechnik* **26**(5):318–325, 1992.

[10] R. Herbertz and M.-L. Cho: "Reibungsmechanismen in der Grenzfläche Werkstück/Werkzeug bei Umformverfahren und daraus resultierende Probleme für theoretische Berechnungen", *Archiv für das Eisenhüttenwesen* **54**(12):499–502, 1983.

[11] C. Kaminsky: *Numerische Modellierung der Oberflächenwandlung von Feinblechen*, vol. 528 of *Fortschritt-Berichte VDI: Reihe 2, Fertigungstechnik*, VDI Verlag, Düsseldorf (Germany), 1999.

[12] DIN50323-1: *Tribologie; Begriffe*, 1988.

[13] H. P. Jost: "Lubrication (Tribology) – A Report of the Present Position and Industry's Needs", Tech. rep., Department of Education and Science, H. M. Stationarey Office, London (UK), 1966.

[14] E. Dannenmann, R. Geiger, and T. Gräbener: "Tribologische Grundlagen; Oberflächenwandlung", in: "Umformtechnik: Handbuch für Industrie und Wissenschaft", (K. Lange, ed.), vol. Band 1, Springer-Verlag, Berlin (Germany), 2nd ed., 1984.

[15] M. Gariety and G. Ngaile: "Friction and Lubrication", in: "Cold and hot forging: fundamentals and applications", (T. Altan, G. Ngaile, and G. Shen, eds.), pp. 341–407, ASM International Materials Park, Ohio (USA), 2005.

[16] H. Czichos and K.-H. Habig: *Tribologie-Handbuch: Reibung und Verschleiß*, Friedr. Vieweg & Sohn Verlag / GVW Fachverlag GmbH, Wiesbaden (Germany), 2nd ed., 2003.

[17] C. Messner, E. A. Werner, and H. Grass: *Reibung und Wärmeübergang beim Schmieden*, vol. 604 of *Fortschritt-Berichte VDI: Reihe 2, Fertigungstechnik*, VDI Verlag, Düsseldorf (Germany), 2002.

[18] DIN50320: *Verschleiß; Begriffe; Systemanalyse von Verschleißvorgängen; Gliederung des Verschleißgebietes*, 1979.

[19] DIN50323-3: *Tribologie; Reibung; Begriffe, Arten, Zustände, Kenngrößen*, 1993.

[20] E. Doege, R. Melching, and G. Kowallik: "Investigations into the behaviour of lubricants and the wear resistance of die materials in hot and warm forging", *Journal of Mechanical Working Technology* **2**(2):129–143, 1978.

[21] R. Melching: *Verschleiß, Reibung und Schmierung beim Gesenkschmieden*, PhD Thesis, Universität Hannover (Germany), 1980.

[22] R. Schneider: *Untersuchung der Einflußgrößen des tribologischen Systems Werkzeug-Schmierstoff-Schmiedestück*, vol. 78 of *Fortschritt-Berichte VDI, Reihe 2: Betriebstechnik*, VDI Verlag, Düsseldorf (Germany), 1984.

[23] H. Westheide: *Einfluß von Oberflächenbeschichtungen auf den Werkzeugverschleiß bei der Massivumformung*, vol. 87 of *Berichte aus dem Institut für Umformtechnik der Universität Stuttgart*, Springer-Verlag, Berlin (Germany), 1986.

[24] F. Fischer and A. Cron: "Festschmierstoffe, insbesondere Graphit für die Warmumformung", in: "Tribologie und Schmierung in der Umformtechnik", (W. J. Bartz, ed.), pp. 564–600, expert verlag, Sindelfingen (Germany), 1987.

[25] J. A. Schey: *Tribology in Metalforming. Friction, Lubrication and Wear*, American Society for Metals, Ohio (USA), 1983.

[26] T. Tsukizoe and T. Hisakado: "On the Mechanics of Contact Between Metal Surfaces. Part 2: The Real Area and the Number of the Contact Points", *Transactions of the American Society of Mechanical Engineers: Series F - Journal of Lubrication Technology* **2**(1):81–88, 1968.

[27] R. Holm and E. Holm: *Electric Contacts – Theory and Application*, Springer-Verlag, Berlin (Germany), 4th ed., 1967.

[28] I. Finnie and M. C. Shaw: "The Friction Process in Metal Cutting", *Transactions of the American Society of Mechanical Engineers* **78**:1649–1657, 1956.

[29] M. Maass: "LEXT – Konfokales Laserscanningmikroskop für die Oberflächenanalytik", *Inspect (Sonderdruck)* **5**(1), 2005.

[30] J. Dyson and W. Hirst: "The True Contact Area Between Solids", *Proceedings of the Physical Society. Section B* **67**(4):309–312, 1954.

[31] M. Pfestorf, U. Engel, and M. Geiger: "Three-dimensional characterization of surfaces for sheet metal forming", *Wear* **216**:244–250, 1998.

[32] A. Azushima, S. Kuba, S. Tani, and D. D. Olsson: "Direct observation of asperity deformation of specimens with random rough surfaces in upsetting and indentation processes", *Wear* **260**(3):258–264, 2006.

[33] J. S. McFarlane and D. Tabor: "Relation between friction and adhesion", *Proceedings of the Royal Society of London. Series A, Mathematical and Physical Sciences* **202**:244–253, 1950.

[34] E. Rabinowicz: *Friction and wear of materials*, John Wiley & Sons, Inc., New York (USA), 2nd ed., 1995.

[35] D. Semwogerere and E. R. Weeks: "Confocal Microscopy", *Encyclopedia of Biomaterials and Biomedical Engineering* pp. 1–10, 2005. doi: 10.1081/E-EBBE-120024153.

[36] E. J. Abbott and F. A. Firestone: "Specifying Surface Quantity – A Method Based on Accurate Measurement and Comparison", *Mechanical Engineering (American Society of Mechanical Engineers)* **55**:569–572, 1933.

[37] E. D. Brown, R. S. Owens, and E. R. Booser: "Chapter 2 – Friction of Dry Surfaces", in: "Boundary Lubrication. An Appraisal of World Literature", (F. Ling, E. Klaus, and R. Fein, eds.), pp. 7–18, ASME American Society of Mechanical Engineers, New York (USA), 1969.

[38] N. Hansen: "Der Böschungswinkel von Rauheitsprofilen", *Maschinenmarkt* **73**(86):1790–1791, 1967.

[39] L. H. Butler: "Surface Conformation of Metals Under High Nominal Contact Pressures", *Metallurgia* **61**(366):167–174, 1960.

[40] W. Heller: *Einebnungsvorgänge in werkzeuggebundenen Metalloberflächen bei bildsamer Formgebung*, PhD Thesis, Technische Hochschule Aachen (Germany), 1970.

[41] J. Pullen and J. B. P. Williamson: "On the plastic contact of rough surfaces", *Proceedings of the Royal Society of London. Series A, Mathematical and Physical Sciences* **327**:159–173, 1972.

[42] O. Kienzle: "Zur Typologie umgeformter metallischer Oberflächen", *Microtecnic* **XIV**(3):134–140, 1960.

[43] H. Mühlenweg: "Die Oberflächenrauheit bei warm und kalt gezogenen Stahlrohren", *Stahl und Eisen* **79**(24):1792–1800, 1959.

[44] H. Hertz: "Ueber die Berührung fester elastischer Körper", *Journal für die reine und angewandte Mathematik* **XCII**(2):156–171, 1882.

[45] H. Hertz: *Schriften vermischten Inhalts*, vol. 1 of *Gesammelte Werke von Heinrich Hertz*, Barth, Leipzig (Germany), 1895.

[46] F. P. Bowden and D. Tabor: "The area of contact between stationary and between moving surfaces", *Proceedings of the Royal Society of London. Series A, Mathematical and Physical Sciences* **169**(938):391–413, 1939.

[47] J. F. Archard: "Elastic deformation and laws of friction", *Proceedings of the Royal Society of London. Series A, Mathematical and Physical Sciences* **243**(1233):190–205, 1957.

[48] Y. H. Li and C. M. Sellars: "Modelling deformation behaviour of oxide scales and their effects on interfacial heat transfer and friction during hot steel rolling", in: "2nd International Conference on Modelling of Metals Rolling Processes", pp. 192–201, The Institute of Materials, London (UK), 1996.

[49] M. S. Longuet-Higgins: "The statistical analysis of a random, moving surface", *Philosophical Transactions of the Royal Society of London. Series A, Mathematical and Physical Sciences* **249**(966):321–387, 1957.

[50] J. A. Greenwood and J. B. P. Williamson: "The contact of nominally flat surfaces", in: "International Symposium on Electronic Contact Phenomena", pp. 24–38, Graz (Austria), 1964.

[51] J. Greenwood and J. Williamson: "Contact of Nominally Flat Surfaces", *Proceedings of the Royal Society of London. Series A, Mathematical and Physical Sciences* **295**(1442):300–319, 1966.

[52] A. W. Bush, R. D. Gibson, and T. R. Thomas: "The elastic contact of a rough surface", *Wear* **35**(1):87–111, 1975.

[53] J. I. McCool and S. S. Gassel: "The contact of two surfaces having anisotropic roughness geometry", *ASLE Special Publication SP-7* pp. 29–38, 1981. Proceedings of the ASLE Energy Sources Technology Conference.

[54] P. R. Nayak: "Random process model of rough surfaces in plastic contact", *Wear* **26**(3):305–333, 1973.

[55] J. Greenwood: "The Real Area of Contact Between Rough Surfaces and Flats", *Transactions of the American Society of Mechanical Engineers: Series F - Journal of Lubrication Technology* **1**(1):81–91, 1967.

[56] I. V. Kragelsky and N. B. Demkin: "Contact area of rough surfaces", *Wear* **3**(3):170–187, 1960.

[57] R. Hill: "Some special problems of indentation and compression in plasticity", in: "7th International Congress for Applied Mechanics", vol. 1, pp. 365–377, 1948.

[58] T. Wanheim, N. Bay, and A. S. Petersen: "A theoretically determined model for friction in metal working processes", *Wear* **28**(2):251–258, 1974.

[59] F. F. Ling and N. Y. Troy: "Some Factors Influencing the Area-Load Characteristics for Semismooth Contiguous Surfaces Under "Static" Loading", *Transactions of the American Society of Mechanical Engineers* **80**:1113–1120, 1958. Paper Nr. 57 - A 246.

[60] B. Fogg: "The Relationship Between the Blank and Product Surface Finish and Lubrication in Deep-drawing and Stretching Operations", *Sheet Metal Industries* **44**(2):95–112, 1967.

[61] T. Wanheim: "Friction at high normal pressures", *Wear* **25**(2):225–244, 1973.

[62] W. Johnson: "Extrusion through square dies of large reduction", *Journal of the Mechanics and Physics of Solids* **4**(3):191–198, 1956.

[63] T. Neumaier: *Zur Optimierung der Verfahrensauswahl von Kalt-, Halbwarm- und Warmmassivumformverfahren*, vol. 637 of *Fortschritt-Berichte VDI: Reihe 2, Fertigungstechnik*, VDI Verlag, Düsseldorf (Germany), 2003.

[64] E. Doege, C. Kaminsky, and A. Bagaviev: "A new concept for the description of surface friction phenomena", *Journal of Materials Processing Technology* **94**:189–192, 1999.

[65] S. Stupkiewicz and Z. Mroz: "Phenomenological model of real contact area evolution with account for bulk plastic deformation in metal forming", *International Journal of Plasticity* **19**(3):323–344, 2003.

[66] R. Holm: "Über die auf die wirkliche Berührungsfläche bezogene Reibungskraft", *Mitteilungen aus dem Forschungslaboratorium I der Siemens-Werke zu Siemensstadt* **XVII**:400–404, 1938.

[67] H. Ernst and M. E. Merchant: "Surface friction of clean metals – A basic factor in the metal cutting process", in: "The Special Summer Conference on Friction and Surface Finish", pp. 76–101, M.I.T. Press, MIT, Cambridge (USA), 1940.

[68] F. P. Bowden and D. Tabor: *The friction and lubrication of solids*, The international series of monographs on physics, Clarendon Press, Oxford (UK), 2nd ed., 1958.

[69] F. P. Bowden and D. Tabor: *Reibung und Schmierung fester Körper*, Springer-Verlag, Berlin (Germany), 1959.

[70] I. Ming-Feng: "Metal Transfer and Wear", *Journal of Applied Physics* **23**(9):1011–1019, 1952.

[71] I. W. Kragelski: *Reibung und Verschleiß*, VEB Verlag Technik, Berlin (Germany), 1971.

[72] B. Avitzur and Y. Nakamura: "Analytical determination of friction resistance as a function of normal load and geometry of surface irregularities", *Wear* **107**(4):367–383, 1986.

[73] R. Geiger: "Reibung und Schmierung beim Fließpressen von Stahl", in: "Neuere Entwicklungen in der Massivumformung", Forschunggesellschaft Umformtechnik m.b.H., Stuttgart (Germany), 1981. Printed in German.

[74] J. H. Beynon: "Tribology of hot metal forming", *Tribology International* **31**(1–3):73–77, 1998.

[75] R. Bernhardt: *Ein Beitrag zur experimentellen und numerischen Analyse lokaler Kontaktspannungen und Kontakttemperaturen in der Wirkfuge von Gesenkgravuren unter besonderer Beachtung des Randreibungsproblems*, Freiberger Forschungshefte: B; 286: Werkstoffwissenschaft, Werkstoffertigungstechnologie, TU Bergakademie Freiberg (Germany), 1998.

[76] E. Nehl: "Tribologische Aspekte in der Umformtechnik - Teil 1", in: "Tribologie und Schmierung in der Umformtechnik", (W. J. Bartz, ed.), pp. 71–112, expert verlag, Sindelfingen (Germany), 1987.

[77] R. Geiger: "Reibung und Schmierung beim Kaltfließpressen von Stahl", in: "Tribologie und Schmierung in der Umformtechnik", (W. J. Bartz, ed.), pp. 283–318, expert verlag, Sindelfingen (Germany), 1987.

[78] O. Pawelski: "Gelöste und ungelöste tribologische Probleme in der Umformtechnik", *Schmiertechnik + Tribologie* **25**(4):137–140, 1978.

[79] Y. Kasuga and K. Yamaguchi: "Friction and Lubrication in the Deformation Processing of Metals (1st Report: Quantitative Assessment of the Surface Texture of Materials being deformed under Rigid Tool)", *Bulletin of the Japan Society of Mechanical Engineers* **11**(44):344–353, 1968.

[80] U. Engel: "Tribology in microforming", *Wear Tribology in Manufacturing Processes* **260**(3):265–273, 2006.

[81] J. Bech, N. Bay, and M. Eriksen: "Entrapment and escape of liquid lubricant in metal forming", *Wear* **232**(2):134–139, 1999.

[82] T. Sobis, U. Engel, and M. Geiger: "A theoretical study on wear simulation in metal forming processes", *Journal of Materials Processing Technology* **34**(1–4):233–240, 1992.

[83] M. Geiger, M. Pfestorf, and U. Engel: "Dreidimensionale Oberflächenanalyse bei Feinblechen", *Stahl und Eisen* **115**(7):47–53, 1995.

[84] M. Pfestorf, U. Engel, and M. Geiger: "3D-Surface Parameters and their Application on Deterministic Textured Metal Sheets", *International Journal of Machine Tools and Manufacture* **38**(5–6):607–614, 1998.

[85] N. Bay and T. Wanheim: "Contact Phenomena under Bulk Plastic Deformation Conditions", *Advanced Technology of Plasticity* **4**:1677–1691, 1990.

[86] R. Shivpuri and S. Kini: "Lubricants and Their Applications in Forging", in: "ASM Handbook", (S. L. Semiatin, ed.), vol. 14A; Metalworking: Bulk Forming, pp. 84–92, ASM International, Ohio (USA), 2005.

[87] R. H. Savage: "Graphite Lubrication", *Journal of Applied Physics* **19**(1):1–10, 1948.

[88] L. Anand: "A constitutive model for interface friction", *Computational Mechanics* **12**:197–213, 1993.

[89] E. Doege, M. Alasti, and R. Schmidt-Jürgensen: "Accurate friction and heat transfer laws for enhanced simulation models of precision forging processes", *Journal of Materials Processing Technology* **150**:92–99, 2004.

[90] J. H. Li: *Untersuchung der Wirkflächenreibung für die Finite-Elemente-Simulation der Massivumformung*, vol. 374 of *Fortschritt-Berichte VDI: Reihe 2, Fertigungstechnik*, VDI Verlag, Düsseldorf (Germany), 1996.

[91] D. Nolte and H. Valberg: "The Effect of Die Geometry on Forging Conditions in Axisymmetric Hot Aluminium Forging – An Example", *International Journal of Forming Processes* **9**(2):189–213, 2006.

[92] P. A. Petrov: "Generalized approach to the choice of lubricant for hot isothermal forging of aluminuim alloys", *Computer Methods in Materials Science* **7**(1):106–111, 2007.

[93] A. Nádai: "The Forces Required for Rolling Steel Strip Under Tension", *Journal of Applied Mechanics* **6**:A–54–A–62, 1939.

[94] C. C. António, C. F. Castro, and L. C. Sousa: "Eliminating Forging Defects Using Generic Algorithms", *Materials and Manufacturing Processes* **20**(3):509–522, 2005.

[95] A. I. Baltov and A. G. Nedev: "An approach to the modelling of contact friction during rolling", *Journal of Materials Processing Technology* **53**(3–4):695–711, 1995.

[96] N. Bontcheva and G. Petzov: "Microstructure evolution during metal forming processes", *Computational Materials Science* **28**(3–4):563–573, 2003.

[97] H. Gläser, H. Franeck, and H. Wulf: "Universelles Kontaktreibgesetz und Verschleißsimulation", *Tribologie + Schmierungstechnik* **45**(6):19–27, 1998.

[98] O. Mahrenholtz, N. Bontcheva, and M. Brzozowski: "Influence of friction and geometry on plastic spread", *Mechanics Research Communications* **24**(4):351–358, 1997.

[99] X. Tan: "Comparisons of friction models in bulk metal forming", *Tribology International* **35**(6):385–393, 2002.

[100] E. Siebel: "Formänderungswiderstand und Werkstoffffluß beim Walzen", *Stahl und Eisen* **50**(51):1769–1775, 1930.

[101] E. Orowan: "The Calculation of Roll Pressure in Hot and Cold Flat Rolling", *Proceedings of the Institution of Mechanical Engineers* **150**:140–167, 1943.

[102] M. C. Shaw, A. Ber, and P. A. Mamin: "Friction Characteristics of Sliding Surfaces Undergoing Subsurface Plastic Flow", *Transactions of the American Society of Mechanical Engineers: Series D - Journal of Basic Engineering* **82**:342–346, 1960.

[103] M. C. Shaw: "The role of friction in deformation processing", *Wear* **6**:140–158, 1963.

[104] N. Bay and T. Wanheim: "Real area of contact and friction stress at high pressure sliding contact", *Wear* **38**:201–209, 1976.

[105] N. Bay and T. Wanheim: "Real area of contact between a rough tool and a smooth workpiece at high normal pressures", *Wear* **38**:225–234, 1976.

[106] N. Bay: "Friction stress and normal stress in bulk metal-forming processes", *Journal of Mechanical Working Technology* **14**(2):203–223, 1987.

[107] T. Nellemann, N. Bay, and T. Wanheim: "Real area of contact and friction stress – The role of trapped lubricant", *Wear* **43**(1):45–53, 1977.

[108] J. Hallström: "Influence of friction on die filling in counterblow hammer forging", *Journal of Materials Processing Technology* **108**(1):21–25, 2000.

[109] D. A. Stephenson: "Friction in cold strip rolling", *Wear* **92**(2):293–311, 1983.

[110] E. Doege, C. Bederna, T. El-Dsoki, D. Seibert, and N. Werner: "Struktur zur Beschreibung lokaler, geschichtsabhängiger Zwischenschichtgesetze", in: "Abschlußkolloquium des PSU-Projektes", (K. Lange, ed.), vol. 4 of *Prozeßsimulation in der Umformtechnik*, pp. 87–102, Springer-Verlag, Stuttgart (Germany), 1993.

[111] J. Betten: "Bemerkungen zum Versuch von Hohenemser", *Zeitschrift für Angewandte Mathematik und Mechanik (ZAMM)* **55**:149–158, 1975.

[112] D. Hemyari: *Methode zur Ermittlung von Konstitutivmodellen für Reibvorgänge in der Massivumformung bei erhöhten Temperaturen*, vol. 43 of *Berichte aus Produktion und Umformtechnik*, Shaker Verlag, Aachen (Germany), 1999.

[113] E. Ceretti and C. Giardini: "Development of an Analytical Model for Evaluation of Friction Coefficient in Cold Forming", *International Journal of Forming Processes* **10**(3):317–335, 2007.

[114] E. Doege, M. Alasti, and R. Schmidt-Jürgensen: "Ein innovatives Verfahren zur Charakterisierung der Reibung und des Wärmeübergangs beim Präzesionsschmieden", *UTF science* **IV**:4–8, 2002.

[115] J. A. Schey: "The validity of various friction concepts in deformation processing", in: "North American Metalworking Research Conference (NAMRC 4)", (T. Altan, ed.),

vol. 4, pp. 108–114, American Society of Mechanical Engineers (SME), Columbus, OH (USA), 1976.

[116] S. B. Petersen, P. A. F. Martins, and N. Bay: "Friction in bulk metal forming: a general friction model vs. the law of constant friction", *Journal of Materials Processing Technology* **66**:186–194, 1997.

[117] S. Kobayashi, S.-I. Oh, and T. Altan: *Metal forming and the finite-element method*, vol. 4 of *Oxford series on advanced manufacturing*, Oxford University Press, New York (USA), 1989.

[118] J. Löwen: *Ein Beitrag zur Bestimmung des Reibungszustandes beim Gesenkschmieden*, PhD Thesis, Technische Universität Hannover (Germany), 1971.

[119] A. T. Male: "The Relative Validity of the Concepts of Coefficient of Friction and Interface Friction Shear Factor for Use in Metal Deformation Studies", *ASLE Transactions* **16**(3):177–184, 1973.

[120] D. R. Hayhurst and M. W. Chan: "Determination of friction models for metallic die-workpiece interfaces", *International Journal of Mechanical Sciences* **47**(1):1–25, 2005.

[121] H. Bühler and J. Löwen: "Verfahren zum Messen des Reibungswiderstandes für die instationären Umformverfahren", *Stahl und Eisen* **92**(14):698–704, 1972. Printed in German and Spain.

[122] C. Bederna: *Bestimmung des lokalen Zwischenschichtzustandes in der Massivumformung*, vol. 416 of *Fortschritt-Berichte VDI: Reihe 2, Fertigungstechnik*, VDI Verlag, Düsseldorf (Germany), 1997.

[123] G. T. van Rooyen and W. A. Backofen: "Friction in Cold Rolling", *Journal of the Iron and Steel Institute* **186**:235–244, 1957.

[124] G. T. van Rooyen and W. A. Backofen: "Distribution of interface stress in plane strain and axial symmetric compression", *Journal of the Mechanics and Physics of Solids* **7**:163–168, 1959.

[125] W. Voelkner: "Experimentelle Methoden der örtlichen Normal- und Schubspannungsermittlung beim Umformen", *Fertigungstechnik und Betrieb* **26**(2):92–96, 1976.

[126] R. Ebrahimi and A. Najafizadeh: "A new method for evaluation of friction in bulk metal forming", *Journal of Materials Processing Technology* **152**:136–143, 2004.

[127] M. Kunogi: "On Plastic Deformation of Hollow Cylinder under Axial Compression", *Reports of the Scientific Research Institute (Kagaku Kenkyujo Hokoku)* **30**(2):63–92, 1954. Printed in Japanese.

[128] M. Kunogi: "A New Method of Cold Extrusion", *Journal of the Scientific Research Institute* **50**(1437):215–246, 1956.

[129] A. T. Male and M. G. Cockcroft: "A Method for Determination of the Coefficient of Friction of Metals under Conditions of Bulk Plastic Deformation", *Journal of the Institute of Metals* **93**:38–46, 1965.

[130] A. T. Male: "Friction Measurement Using the Ring Compression Test", in: "7th International Conference on Technology of Plasticity (ICTP) – Advanced Technology of Plasticity", vol. 1, pp. 321–325, Yokohama (Japan), 2002.

[131] A. Behrens and H. Schafstall: "2D and 3D simulation of complex multistage forging processes by use of adaptive friction coefficient", *Journal of Materials Processing Technology* **80–81**:298–303, 1998.

[132] R. E. Dutton, V. Seetharaman, R. L. Goetz, and S. L. Semiatin: "Effect of flow softening on ring test calibration curves", *Materials Science and Engineering A* **270**(2):249–253, 1999.

[133] K. Pöhlandt, D. Banabic, and K. Lange: "On the determination of friction coefficients by ring compression", *UTF science* **III**, 2004.

[134] J. A. Schey and A. H. Lonn: "Durability of Graphite Films in Plastic Deformation", *Journal of Lubrication Technology* pp. 289–295, 1975.

[135] H. Sofuoglu and J. Rasty: "On the measurement of friction coefficient utilizing the ring compression test", *Tribology International* **32**:327–335, 1999.

[136] R. Volles, M. Wolske, and R. Kopp: "Determination of friction coefficient by use of conical tube upsetting tests", in: "IV Conferência Internacional de Forjamento (XX SENAFOR)", Porto Allegre (Brasil), 2000.

[137] W. R. D. Wilson and S. Lak: "The Transport and Breakdown of Solid Lubricants in a Simple Forging Operation.", *Transactions of the American Society of Mechanical Engineers: Series F - Journal of Lubrication Technology* **99**(2):230–235, 1977.

[138] R. K. Uyyuru: "Plane Strain Compression Test as a Friction-Measuring Test", *International Journal of Forming Processes* **7**(3):301–319, 2004.

[139] S. Sheljaskow: "Tool lubricating systems in warm forging", *Journal of Materials Processing Technology* **113**(1–3):16–21, 2001.

[140] H. Sofuoglu and H. Gedikli: "Determination of friction coefficient encountered in large deformation processes", *Tribology International* **35**:27–34, 2002.

[141] D. M. Kok and H. Gankema: "Entwicklungen bei den Gesenkschmierstoffen sowie mögliche Synergien in Verbindung mit Applikationstechniken", in: "Sommerschule Schmiedetechnik", Chair of Metal Forming, University of Leoben, Teichalm (Austria), 2005.

[142] H. Kim, S. Padwad, and T. Altan: "Evaluation of New Lubricants for Cold Forging Without Zinc Phosphate Coating", in: "37th Plenary Meeting of the International Cold Forging Group (ICFG)", Istanbul (Turkey), 2004. Paper No. 525-1.

[143] M. Gariety, G. Ngaile, and T. Altan: "Evaluation of new cold forging lubricants without zinc phosphate precoat", *International Journal of Machine Tools and Manufacture* **47**(3-4):673–681, 2007.

[144] S. L. Wang and J. A. H. Ramaekers: "Measurement of friction and material flow-stress by a plane-strain compression tribometer", *Journal of Materials Processing Technology* **57**(3–4):345–350, 1996.

[145] N. Kawai and K. Dohda: "A New Lubricity Evaluation Method for Metal Forming by a Compression-Twist Type Friction Testing Machine", *Journal of Tribology* **109**:343–350, 1987.

[146] A. Attanasio, A. Fiorentino, E. Ceretti, and C. Giardini: "Experimental Device to Study Surface Contacts in Forming Processes", in: "10th ESAFORM Conference on Material Forming", (E. Cueto and F. Chinesta, eds.), pp. 275–278, American Institute of Physics, Zaragoza (Spain), 2007.

[147] C. Vergne, C. Boher, C. Levaillant, and R. Gras: "Analysis of the friction and wear behaviour of hot work tool scale: application to the hot rolling process", *Wear* **250**:322–333, 2001.

[148] C. Bruni, A. Forcellese, F. Gabrielli, M. Simoncini, and L. Montelatici: "Evaluation of Friction Coefficient in Tube Drawing Processes", in: "10th ESAFORM

Conference on Material Forming", (E. Cueto and F. Chinesta, eds.), pp. 552–557, American Institute of Physics, Zaragoza (Spain), 2007.

[149] E. Daouben, L. Dubar, M. Dubar, R. Deltombe, A. Dubois, N. Truong-Dinh, and L. Lazzarotto: "Friction and wear in hot forging of steels", in: "10th ESAFORM Conference on Material Forming", (E. Cueto and F. Chinesta, eds.), pp. 505–508, American Institute of Physics, Zaragoza (Spain), 2007.

[150] J. D. Guérin, H. Bartys, A. Dubois, and J. Oudin: "Finite element implementation of a generalized friction model: application to an upsetting-sliding test", *Finite Elements in Analysis and Design* **31**:193–207, 1999.

[151] O. Pawelski: "Ein neues Gerät zum Messen des Reibungsbeiwertes bei plastischen Formänderungen", *Stahl und Eisen* **84**(20):1233–1243, 1964.

[152] G. Ngaile, H. Saiki, L. Ruan, and Y. Marumo: "A tribo-testing method for high performance cold forging lubricants", *Wear* **262**(5-6):684–692, 2007.

[153] L. Anand and W. Tong: "A Constitutive Model for Friction in Forming", *Annals of the CIRP* **42**(1):361–366, 1993.

[154] N. Bay and B. G. Hansen: "Simulation of friction and lubrication in cold forging", in: "7th International Cold Forging Congress", pp. 55–62, Birmingham (UK), 1985.

[155] U. Klafs: *Ein Beitrag zur Bestimmung der Temperaturverteilung in Werkzeug und Werkstück beim Warmumformen*, PhD Thesis, Technische Universität Hannover (Germany), 1969.

[156] M. Tajdari and M. Javadi: "A new experimental procedure of evaluating the friction coefficient in elastic and plastic regions", *Journal of Materials Processing Technology Proceedings of the 11th International Conference on Metal Forming 2006* **177**(1-3):247–250, 2006.

[157] B. G. Hansen and N. Bay: "Two new methods for testing lubricants for cold forging", *Journal of Mechanical Working Technology* **13**(2):189–204, 1986.

[158] E. Doege, C. Kaminsky, and R. Schmidt-Jürgensen: "Numerischer Vergleich der Reibzustände zwischen Modellversuch und Präzisionsschmiedeversuch", *Umformtechnik* (3):36–40, 1998.

[159] J. A. Greenwood and G. W. Rowe: "Deformation of Surface Asperities During Bulk Plastic Flow", *Journal of Applied Physics* **36**:667–668, 1965.

[160] K. Markut: *Design and Commissioning of a Rotational Forging Tribometer*, Master Thesis, University of Leoben (Austria), 2006.

[161] B. Buchner, K. Markut, and B. Buchmayr: "Bestimmung der Reibzahl unter Schmiedebedingungen mithilfe des Rotationsreibversuches", in: "XXV. Verformungskundliches Kolloquium", (B. Buchmayr and O. Harrer, eds.), pp. 101–117, Chair of Metal Forming, University of Leoben, Planneralm/Donnersbach (Austria), 2006.

[162] D. A. Rigney and J. P. Hirth: "Plastic deformation and sliding friction of metals", *Wear* **53**(2):345–370, 1979.

[163] I. N. A. Oguocha: *Characterization of Aluminum Alloy 2618 and Its Composites Containing Alumina Particles*, PhD Thesis, University of Saskatchewan (Canada), 1999.

[164] A. Makinouchi, H. Ike, M. Murakawa, K. Koga, and L. Ciupik: "Finite Element Analysis of Flattening of Surface Asperities by Rigid Dies in Metal Working Processes", in: "2nd International Conference on Advanced Technology of Plasticity", (K. Lange, ed.), vol. 1, pp. 59–66, Springer-Verlag, Stuttgart (Germany), 1987.

[165] A. Makinouchi, H. Ike, M. Murakawa, and N. Koga: "A finite element analysis of flattening of surface asperities by perfectly lubricated rigid dies in metal working processes", *Wear* **128**(2):109–122, 1988.

[166] W. Hofmann and J. Kirsch: "Zur Frage der Platzwechsel bei der Kaltpreßschweißung der Metalle", *Zeitschrift für Metallkunde* **57**:305–311, 1966.

A Author's Publications

2004

B. Buchner and P. O'Leary: "Real-time stereo for industrial inspection", in: "Machine Vision Applications in Industrial Inspection XII", (J. R. Price and F. Meriaudeau, eds.), pp. 22–30, San Jose, CA (USA), 2004.

2006

B. Buchner, K. Markut, and B. Buchmayr: "Bestimmung der Reibzahl unter Schmiedebedingungen mithilfe des Rotationsreibversuches", in: "XXV. Verformungskundliches Kolloquium", (B. Buchmayr and O. Harrer, eds.), pp. 101–117, Chair of Metal Forming, University of Leoben, Planneralm/Donnersbach (Austria), 2006.

2007

B. Buchner, A. Umgeher, and B. Buchmayr: "Estimation of friction under forging conditions by means of the ring-on-disc test", in: "10th ESAFORM Conference on Material Forming", (E. Cueto and F. Chinesta, eds.), pp. 505–508, Zaragoza (Spain), 2007.

B. Buchner, G. Maderthoner, and B. Buchmayr: "Charakterisierung unterschiedlicher Schmierstoffe hinsichtlich des Reibzahlverlaufes beim Schmieden von Aluminiumlegierungen", in: "XXVI. Verformungskundliches Kolloquium", (B. Buchmayr and O. Harrer, eds.), pp. 255–265, Chair of Metal Forming, University of Leoben, Planneralm/Donnersbach (Austria), 2007.

C. Monetti, B. Buchner, I. Schiester, F. Tonnerer, and G. Hering: "Oils for Internal Thread Molding Description of a Test-Methodology", in: "XXVI. Verformungskundliches Kolloquium", (B. Buchmayr and O. Harrer, eds.), pp. 243–254, Chair of Metal Forming, University of Leoben, Planneralm/Donnersbach (Austria), 2007.

C. Monetti, F. Novotny-Farkas, G. Hering, B. Buchner, I. Schiester, and F. Tonnerer: "Description of a test-methodology for the formulation and selection of components of thread-molding oils", in: "ECOTRIB 2007 - Joint European Conference on Tribology

and Final Conference of COST 532 action: Triboscience and Tribotechnology", (Joze Vižintin, ed.), pp. 15–23, Slovenian Society for Tribology, Ljubljana (Slovenia), 2007.

2008

B. Buchner, G. Maderthoner, and B. Buchmayr: "Characterisation of different lubricants concerning the friction coefficient in forging of AA2618", *Journal of Materials Processing Technology* **198**(1–3):41–47, 2008.

B. Buchner, A. Weber, and B. Buchmayr: "Investigation of friction in warm forging of AA6082", in: "11th ESAFORM Conference on Material Forming", Lyon (France), 2008, in press.

M. Buchner, B. Buchner, B. Buchmayr, H. Kilian, and F. Riemelmoser: "Investigation of different parameters on roll bonding quality of aluminium and steel sheets", in: "11th ESAFORM Conference on Material Forming", Lyon (France), 2008, in press.